Electronic Theses and Dissertations

Theses, Dissertations, and Major Papers

10-19-2015

The Effects of Uncertainty in Engineering Data on the Design and Performance of Automotive Thermal Systems

Ashley Nicole Lehman
University of Windsor

Follow this and additional works at: https://scholar.uwindsor.ca/etd

The Effects of Uncertainty in Engineering Data on the Design and Performance of Automotive Thermal Systems

By

Ashley Nicole Lehman

A Thesis
Submitted to the Faculty of Graduate Studies
through the Department of **Mechanical, Automotive, and Materials Engineering**
in Partial Fulfillment of the Requirements for
the Degree of **Master of Applied Science**
at the University of Windsor

Windsor, Ontario, Canada

2015

The Effects of Uncertainty in Engineering Data on the Design and Performance of Automotive Thermal Systems

by

Ashley Nicole Lehman

APPROVED BY:

_____
Dr. D. Green
Engineering Materials

_____
Dr. J. Johrendt
Mechanical Engineering

_____
Dr. V. Stoilov, Co-Advisor
Mechanical Engineering

_____
Dr. A. Sobiesiak, Co-Advisor
Mechanical Engineering

September 16, 2015

DECLARATION OF ORIGINALITY

I hereby certify that I am the sole author of this thesis and that no part of this thesis has been published or submitted for publication.

I certify that, to the best of my knowledge, my thesis does not infringe upon anyone's copyright nor violate any proprietary rights and that any ideas, techniques, quotations, or any other material from the work of other people included in my thesis, published or otherwise, are fully acknowledged in accordance with the standard referencing practices. Furthermore, to the extent that I have included copyrighted material that surpasses the bounds of fair dealing within the meaning of the Canada Copyright Act, I certify that I have obtained a written permission from the copyright owner(s) to include such material(s) in my thesis and have included copies of such copyright clearances to my appendix.

I declare that this is a true copy of my thesis, including any final revisions, as approved by my thesis committee and the Graduate Studies office, and that this thesis has not been submitted for a higher degree to any other University or Institution.

ABSTRACT

This study has two purposes: (1) to investigate the effects of uncertainty on thermal design and performance (2) to establish a process to couple the results from uncertainty analysis with Design for Six Sigma (DFSS) to improve robustness. The research was conducted with support from FCA group. The analysis was applied to a component selected by FCA group; however, it is applicable to any system.

The effects of uncertainty were investigated using the Fourier Amplitude Sensitivity Test (FAST). The analysis was run on MATLAB software package using estimated uncertainty ranges for each parameter. The parameters with the greatest influence on thermal performance uncertainty were identified.

These parameters were used as control factors in a DFSS study. The thermal performance was simulated on RadTherm software package with several settings for the critical parameters. The settings which allowed the performance to remain consistent, regardless of noise, were determined. Thus, robustness was improved.

DEDICATION

This thesis is dedicated to my parents, who have always supported me, and took care of Scooby while I was away for the year.

I would also like to dedicate this thesis to my boyfriend, Thomas, for always being there for me and making me laugh in the stressful times.

And finally, I would like to dedicate this thesis to Scott, Yvette, & Leto, for providing me with the greatest inspiration to complete this work while I was in Italy; to come home and spend time with my beautiful nephew.

ACKNOWLEDGEMENTS

There are many people who I would like to sincerely thank for making this thesis possible.

First, I would like to sincerely thank my University of Windsor advisor, Dr. Stoilov, for teaching me and making sure I had everything I needed to be successful. I definitely could not have completed this thesis without the extra effort and time you put in to help me and I am very thankful to you.

I would also like to thank my industrial advisors, Alaa El-Sharkawy, Richard Sun & Enrico Ribaldone, for your kindness and helpfulness throughout the past two years. I learned a great deal from you and I appreciate everything you did to help me complete this thesis.

I would like to thank my supervisors from the Politecnico di Torino, Professor Ezio Spessa and Professor Daniela Misul, for taking the time to meet with me and review my progress while I was in Italy. You helped me to stay on track and gave me helpful advice for improving this thesis.

Finally, I would like to sincerely thank the Mitacs-Accelerate Program for providing the financial support which made this research project possible. The Mitacs-Accelerate Program provided me with a truly exceptional learning experience and I am very grateful that I was able to be part of it.

TABLE OF CONTENTS

LIST OF TABLES

LIST OF FIGURES

LIST OF APPENDICES

LIST OF ABBREVIATIONS/SYMBOLS

FAST   Fourier Amplitude Sensitivity Test

DFSS   Design for Six Sigma

c_{st} Specific heat capacity of spare tire tub

c_{hs_o} Specific heat capacity of outer layers of heat shield

$D1_m$ Diameter 1 of muffler

$D2_m$ Diameter 2 of muffler

ε_m Emissivity of muffler

ε_{st} Emissivity of spare tire tub

ε_{hs} Emissivity of heat shield

h_{st} Heat transfer coefficient for air flow over spare tire tub

h_{hsl} Heat transfer coefficient for air flow over lower surface of heat shield

h_{hsu} Heat transfer coefficient for air flow over upper surface of heat shield

k_{hs_i} Thermal conductivity of inner layer of heat shield

L_{st} Length of spare tire tub

L_{hs} Length of heat shield

L_{hs_st} Clearance between heat shield and spare tire tub

L_{m_hs} Clearance between muffler and heat shield

ρ_{st} Density of spare tire tub

ρ_{hs_o}	Density of outer layers of heat shield
T_m	Temperature of muffler surface
$T_{a_{hsu}}$	Temperature of air flow over upper surface of heat shield
$T_{a_{hsl}}$	Temperature of air flow over lower surface of heat shield
$T_{a_{st}}$	Temperature of air flow over spare tire tub
t_{st}	Thickness of spare tire tub
t_{hs_o}	Thickness of outer layers of heat shield
t_{hs_i}	Thickness of inner layer of heat shield
W_{st}	Width of spare tire tub
W_{hs}	Width of heat shield
S/N	Signal-to-noise ratio
r	Sum of squares of the input (signal factor levels)
β	Slope of best-fit line
S_β	Sum of squares of distance between zero and the least square best fit line (Forced through zero) for each data point
S_e	Sum of squares of distance between individual data point to the least square best fit line
S_T	Sum of squares of distance between zero to each data point
V_e	Variance
M_i	Input signal

y_i Output response

CHAPTER 1

PURPOSE AND SIGNIFICANCE OF THE STUDY

Purpose

The objective of this project is to study the effects of uncertainty on the thermal design process. This project is focused on the uncertainty in design parameters which affect heat transfer to the underbody components which are in the direct radiation view path of the exhaust system. However, the goal of this investigation is to produce an uncertainty analysis method which is applicable to any system.

Through this analysis, a greater understanding of uncertainty with respect to thermal protection will be achieved. Once the uncertainty in the design parameters has been studied, the Fourier Amplitude Sensitivity Test (FAST) will be applied to understand which parameter's uncertainty has the greatest influence on the uncertainty in the thermal performance of the system. Thus, the most critical design parameters can be identified.

Another objective of this project is to develop a method to interface the results from uncertainty analysis with Design for Six Sigma (DFSS). This method should allow for the determination of the best settings for the most influential design parameters to improve system robustness. In this specific case study, the goal is to improve thermal performance of vehicle components which are exposed to high thermal loads. In the future, this methodology may be applied to other systems to improve robustness in the early design stages. The main advantage of this process is that it can be used to pinpoint potential issues and determine optimal solutions prior to experimental testing.

Significance

Uncertainty analysis has not been widely used in the study of computational model uncertainty in the automotive industry (El-Sharkawy A. , Sensitivity and Uncertainty Analysis in Computational Thermal Models, 2014). This study aims to analyze the uncertainty in computational models and develop a method so that it may be further applied to other automotive applications.

CHAPTER 2

LITERATURE REVIEW

Uncertainty is an inherent part of the design process. Every measurement, experiment, and simulation depends on parameters which are uncertain; therefore, they provide uncertain results. Engineers conduct uncertainty analysis to understand how uncertainty affects the performance of products and processes. In *"Experimentation and Uncertainty Analysis for Engineers"* (Coleman & Steele, 1999) an interesting example of uncertainty analysis is highlighted involving lignite samples. In this example, an experiment is conducted using a bomb calorimeter to find the heating value of a one gram sample of lignite. The experimenters are able to find the heating value of this sample with uncertainty less than two percent. However, there is a significant amount of variation within a sample of lignite and even more variation between different samples of lignite. Thus, the uncertainty arises not from the measurement technique but rather from the variation within the physical variable itself. Coleman & Steele pose the question, "What is the uncertainty in the lignite heating value?" They conclude that the uncertainty estimate depends on what the question is. Uncertainty analysis traditionally focuses on

the accuracy of a particular measurement; however, it can also be used to investigate the entire range of potential values which may exist for a parameter.

Sensitivity and uncertainty analysis allow the engineer to understand the sources of uncertainty in the input parameters and discover ways to reduce the amount of uncertainty in the performance of the product or system. For example, after performing an uncertainty analysis, an engineer may find that the variation in the thickness of a heat shield for a component causes the temperature of that component to vary significantly and to frequently exceed the specification. With this information, the engineer can evaluate whether the tolerances for the heat shield should be tightened or if the nominal value of the thickness of the heat shield should be increased. Both of these methods will cause the component temperature to become more robust, meaning that it will remain consistent regardless of variation in other parameters. By improving robustness, the engineer ensures that the component remains within the specifications and therefore will always meet the customer requirements.

An example of the benefits of uncertainty analysis is shown in the SAE paper, "Analysis of Thermocouple Temperature Response under Actual Vehicle Test Conditions" (El-Sharkawy A. E., Analysis of Thermocouple Temperature Response under Actual Vehicle Test Conditons, 2008). In this case, the uncertainty in temperature measurements made by thermocouples during vehicle testing is investigated. These temperature measurements are used as a basis for design decisions; therefore, it is very important that they are accurate.

The uncertainty in these temperature measurements is due to radiation from the exhaust, ambient temperature, and air flow. To combat these sources of uncertainty, El-Sharkawy points out that the method of thermocouple installation must be carefully controlled. Installing the thermocouple on the outer surface of the component risks errors due to the difference in emissivity between the thermocouple and the component. The disparity in emissivity may cause a difference between the amount of radiation heat transfer which occurs between the surroundings and the component and the surrounding and the thermocouple. Installing the thermocouple too far within the component may cause the thermocouple to measure a lower temperature than the surface temperature if the component is made of a material with low thermal conductivity. To understand exactly where the thermocouple should be installed to obtain accurate temperature measurements, an uncertainty analysis must be applied.

The uncertainty analysis begins with the development of an analytical model for the transient response of the thermocouple. El-Sharkawy applies an energy balance to the thermocouple junction.

Equation 1

$$m_c c_p \frac{\partial T_c}{\partial t} = hA(T_{air} - T_c) + \sigma \varepsilon F A\left(T_{exh}^{4} - T_c^{4}\right) - k_c A \frac{\partial T_c}{\partial r}$$

Where:

m_c: mass of thermocouple junction

c_p: specific heat capacity of thermocouple junction

T_c: temperature of thermocouple junction

T_{air}: temperature of ambient air

h: heat transfer coefficient between air flow and thermocouple junction

A: surface area of thermocouple junction (available for heat exchange with ambient)

k_c: thermal conductivity of thermocouple junction

r: radius of thermocouple junction

This energy balance considers convection from air flow, conduction through the thermocouple junction, and radiation from the exhaust surface.

Next, the conduction is neglected based on the transient response time of a spherical thermocouple which is calculated to be approximately ten seconds. In typical automotive testing procedures, the sampling time is five to ten seconds. Therefore, this response time is considered fast enough to neglect the conduction resistance. Under steady-state conditions, the energy balance becomes:

Equation 2

$$0 = hA(T_{air} - T_c) + \sigma\varepsilon FA(T_{exh}^4 - T_c^4)$$

Equation 3

$$(T_c - T_{air}) = \frac{\sigma\varepsilon F(T_{exh}^4 - T_c^4)}{h}$$

Therefore, El-Sharkawy defines the error between the actual temperature and the temperature read by the thermocouple in the following form.

Equation 4

$$Error = \left(\frac{\sigma \varepsilon F}{h}\right)(T_{exh}{}^4 - T_c{}^4)$$

Based on this equation, it can be concluded that the error is strongly dependent on the heat source temperature and inversely proportional to the heat transfer coefficient. Therefore, El-Sharkawy concludes that when the vehicle is not heavily loaded and there is high air flow, the thermocouple error will be lower. Contrastly, when the vehicle is heavily loaded, the error will be high. Also, the emissivity of the thermocouple has a direct impact on the error. Typically, the emissivity of the thermocouple junction is between 0.2 and 0.3. However, if the surface of the junction is oxidized or if carbon or soot accumulates on the surface, the emissivity will increase to 0.9 or 1. In this case, the error will be much higher.

El-Sharkawy explains that thermal testing is usually conducted at high loads and speeds, where radiation can be very significant, and therefore the error in the thermocouple reading can reach up to 40%. Based on this approximation of the error, a plot of the percent error versus air flow velocity is provided for four different heat source temperatures. For each heat source temperature curve, the error percentage begins very high and then asymptotically approaches zero. The higher source temperature curve shows a higher error percentage for an equal amount of air velocity. Also, given the same source temperature, a higher air velocity will reduce the error percentage.

To further understand the effects of uncertainty on thermocouple measurements, El-Sharkawy set up an experimental test on an actual vehicle. Thermocouples were placed before the muffler and after the muffler to determine the effect of airflow on the

measurements. Some of the thermocouples were shielded from the muffler to understand how radiation affects the temperature measurements. It is noted that the air flow at the rear of the muffler is significantly lower than the front. The experiment was a 4% grade test with a speed of eighty kilometers per hour.

First, a comparison is made between two thermocouples installed at the rear of the muffler. One of these thermocouples was unshielded and the other was shielded. The difference between the two thermocouple measurements was significant and increased over time due to the grade. The error reached a maximum value of 50 °C (323.15 K). This test confirmed the analytical observation that a high load will increase the error in the thermocouple measurements.

Next, a comparison is made between two thermocouples at the front of the muffler. Once again, one of the thermocouples was shielded from the radiation from the muffler and one was unshielded. At the front of the muffler, the airflow is higher; therefore, the heat transfer coefficient is greater. At this location, the maximum error in thermocouple measurements was limited to ten degrees Celsius. This test confirmed that the heat transfer coefficient is inversely proportional to the error in the thermocouple measurements.

This analysis clearly identified the effects of radiation and heat transfer coefficients on the error in a thermocouple measurement. This information can be used to improve the accuracy of the thermocouple measurements; therefore, the design decisions which are based on this information will be improved. In this way, the components can be designed to be thermally protected and issues can be avoided further along in the design process.

In the automotive field, there are a significantly high number of sources of uncertainty to be analyzed. Thus, sensitivity and uncertainty analysis can offer many benefits in terms of improvement of robustness. However, El-Sharkawy pointed out that there are very few authors which have discussed the application of uncertainty analysis to computational thermal models for automotive applications (El-Sharkawy A. , Sensitivity and Uncertainty Analysis in Computational Thermal Models, 2014).

Sensitivity analysis can be conducted locally or globally. Local sensitivity analysis is based on making small incremental changes to a parameter and observing the change in another parameter. For this type of analysis, it is helpful to make use of the Taylor series, shown below.

Equation 5

$$f(x) = f(x_0) + f'(x_0)(x - x_0) + \frac{f''(x_0)}{2!}(x - x_0)^2 + \frac{f'''(x_0)}{3!}(x - x_0)^3$$

$$+ \frac{f''''(x_0)}{4!}(x - x_0)^4 + \cdots = \sum_{n=0}^{\infty} \frac{f^{(n)}(x_0)}{n!}(x - x_0)^n$$

To find the sensitivity of output, $f(x)$, to input parameter, x, the first order approximation of the Taylor Series is often applied and only the first two terms in Equation 5 are considered. To find the sensitivity, the Taylor Series first-order approximation can be rearranged as follows:

Equation 6

$$f'(x_0) = \frac{f(x) - f(x_0)}{(x - x_0)}$$

Therefore, the output parameter must be evaluated at x and x_0 to find the sensitivity. The

disadvantage of this technique is that it assumes that output function has a linear

dependence on the input parameter. Therefore, this calculation should only be applied in

small gradients around the input parameter. Furthermore, the sensitivity may need to be

calculated at many different points to obtain an accurate understanding of the sensitivity

over the entire range of the input parameter.

Application of global sensitivity methods can overcome the disadvantages of the local

techniques. One global sensitivity method which offers significant potential for

application in the automotive field is the Fourier Amplitude Sensitivity Test (FAST)

method suggested by Cukier, Levine, and Schuler (Cukier, Levine, & Shuler, 1974). This

method can be used to study the effects of multiple input parameter uncertainties on a

performance parameter. It is a global sensitivity method which can calculate the average

variance of the performance parameter over the entire input parameter uncertainty ranges.

The equations used in the FAST analysis, shown below, were described in the SAE

International paper, "Sensitivity and Uncertainty Analysis in Computational Thermal

Models" (El-Sharkawy A. , Sensitivity and Uncertainty Analysis in Computational

Thermal Models, 2014).

The variance is calculated by:

Equation 7

$$\sigma_f{}^2 = \langle f^2 \rangle - \langle f \rangle^2$$

The average variance over the entire input parameter range is calculated by a multiple

integral:

Equation 8

$$\langle f \rangle = \int \cdots \int f(p_1, p_2, \ldots p_n) P(p_1, p_2, \ldots p_n) dp_1 dp_2 \ldots dp_n$$

FAST requires the transformation of the multi-dimensional integral to a one-dimension integral by:

Equation 9

$$p_l = G_l[\sin(\omega_l s)], \ldots l = 1, 2, \ldots n$$

Equation 10

$$\sum_{l=1}^{n} \gamma \omega_l = 0$$

FAST calculates the partial variance of each of the input parameters by:

Equation 11

$$S = \frac{\frac{1}{2} \sum_{p=1}^{\infty} (a_{p\omega_l}{}^2 + b_{p\omega_l}{}^2)}{\sigma^2}$$

$a_{p\omega_l}, b_{p\omega_l}$: Fourier series coefficients

FAST allows for the ranking of input variables based on contribution to output parameter variance. This ranking identifies the input parameters which offer the greatest opportunities for improvement to system robustness. Application of FAST in the early design phases may identify solutions to mitigate thermal issues which may not have otherwise been discovered until experimental testing.

In the SAE paper, "Sensitivity and Uncertainty Analysis in Computational Thermal Models", El-Sharkawy applied the FAST method to a component which is exposed to

radiation from a heat source and underbody airflow. A heat shield is located between the component and the heat source. Six input parameters were examined; insulation thickness, ambient temperature, exhaust surface temperature, clearance between the component and the exhaust, heat shield thickness, and heat shield thermal conductivity. For the FAST analysis, these parameters were fluctuated ten percent above and below the nominal value. The FAST analysis was conducted at four different vehicle speeds. It was found that at low speeds, the exhaust surface temperature and heat source emissivity were the most influential. At high speeds, the ambient temperature and heat shield properties became more influential. However, as highlighted by El-Sharkawy, the heat source emissivity can vary much more than 10% during vehicle life (El-Sharkawy A. , Sensitivity and Uncertainty Analysis in Computational Thermal Models, 2014). Therefore, it is possible that heat source emissivity may have an even stronger influence than calculated by this analysis. There exists a need to run the FAST analysis with representative uncertainty values to determine exactly how strong this influence may be. With this information, the system can be designed to perform robustly against the sources of uncertainty regardless of the operating condition.

The FAST method has also been applied to other types of system designs. In the SAE paper, "Sensitivity/Uncertainty Analysis of Automotive Heat Exchanger Designs", El-Sharkawy applied the FAST method to a simple model of a heat exchanger (El-Sharkawy A. E., Sensitivity/Uncertainty Analysis of Automotive Heat Exchanger Designs, 2001). The purpose of this application was to investigate the uncertainties in the heat exchanger design and determine how they affect performance. Specifically, the goal was to find the confidence level that a heat exchanger will meet its design goals. To apply the FAST

method, the uncertainty in the design parameters must be estimated. In this example, all of the design parameters were varied 1%, 2%, and then 3% around their nominal values to see how increasing the uncertainty affects the confidence level. It was found that for 1% uncertainty, the confidence level was high and reached nearly 100% once the excess area of the heat exchanger reached approximately 10%. For an uncertainty of 2%, the confidence level did not reach near 100% until the excess area was roughly 15%. For an uncertainty of 3%, the confidence level did not reach near 100% until the excess area was about 20%. Application of the FAST method to reduce the uncertainty in the most influential parameters is clearly beneficial when trying to reach a specific confidence level. However, the amount of uncertainty in the design parameters must be known to apply this method which can be difficult in some scenarios.

The FAST method has also been used in the automotive industry to investigate thermal degradation. One example of this is shown in the SAE paper, "Sensitivity/Uncertainty Analysis of Material Thermal Degradation Models" (El-Sharkawy & Kamrad, Sensitivity/Uncertainty Analysis of Material Thermal Degradation Models, 2012). In this paper, the concept of time-temperature analysis is introduced as a method to determine the useful life of an automotive component. As with every analysis, there are sources of uncertainty which affect the results. In this case, the authors point out four major factors which contribute to the uncertainty in this analysis. These factors include measured component temperatures, material temperature limits, material activation energy, and vehicle duty cycle. In this case, a constant amount of uncertainty of 1% was assumed for the component temperatures while the uncertainty in the material temperature limits, material activation energy, and vehicle duty cycle were placed at 1%, 2%, 3%, 4%, and

5%. It was found that increasing the uncertainty in these three input parameters from 1% to 5% only caused a 1% increase to the overall uncertainty in the time-temperature analysis. The analysis was then applied to natural rubber as well as high density polyethylene and it was found that for both cases, the component temperature was the most influential parameter followed by the temperature goal, the activation energy, and the exposure time.

In all of the cases highlighted above, a constant amount of uncertainty was assumed for all input parameters. However, not all design parameters have an equal amount of uncertainty. There are design parameters, such as the thickness of the heat shield, which vary depending on the manufacturing process. There are instances in which an unintentional gap may occur between the heat shield layers. Since the heat shield is very thin to begin with, these small variations can cause the nominal value to vary by 20%. Other parameters, such as the length of the heat shield, cannot possibly vary 20% above or below the nominal value because the nominal value is relatively high. If the length were to vary by even 5%, this component would not fit in the proper location. Therefore, these parameters should not be assigned an equal amount of uncertainty because it is not realistic.

Therefore, uncertainty ranges should be more carefully evaluated. However, this can be difficult to accomplish, especially for design parameters which depend on multiple measurements. For these cases, Kline and McClintock suggested an improved method to determine a possible range of uncertainty (Kline & McClintock, Mechanical Engineering). Consider a value, F, which is a function of multiple measured values.

Equation 12

$$F = F(x_1, x_2, x_3 \dots)$$

This method requires the specification of the uncertainties in the measurements (x_1, x_2, x_3,…) which were used to calculate the result. Once these are specified, the following equation can be used to calculate the uncertainty in the calculated value.

Equation 13

$$\partial F = \sqrt{\left(\frac{\partial F}{\partial x_1} \partial x_1\right)^2 + \left(\frac{\partial F}{\partial x_2} \partial x_2\right)^2 + \left(\frac{\partial F}{\partial x_3} \partial x_3\right)^2 + \cdots}$$

For example, one method to determine the volume of a cube is to measure the length, width, and height and multiply these three measurements. To find the uncertainty in the volume of the cube, this method requires that the uncertainty in the measurement of the length, width, and height is specified.

El-Sharkawy recommended the coupling of the thermal analysis process with techniques for robust design such as Design for Six Sigma (DFSS) (El-Sharkawy A. , Sensitivity and Uncertainty Analysis in Computational Thermal Models, 2014). DFSS is a business philosophy which aims to achieve six sigma quality. Six sigma quality means that there are six standard deviations between the mean value and the specification. Therefore, producing a value which is outside of the specification will only happen approximately 3.4 times per million. In the book, "Design for Six Sigma: The Revolutionary Process for Achieving Extraordinary Profits" Chowdhury points out that this level of quality may seem unattainable; however, there are many companies that are consistently achieving between five and six sigma quality (Chowdhury, 2003). DFSS allows a company to

reduce the number of last-minute design changes required by improving the original design process. The goal of DFSS is to design the product or process right the first time so that less changes are needed later on. Chowdhury highlights many examples in which companies applied DFSS with very successful results. One of these examples is highlighted through General Electric's 1999 annual report in which they stated that they introduced seven products in 1999 using DFSS and planned to release 20 more in 2000. They confirmed that the DFSS products are unique because they meet the customer requirements better and can be brought to market faster. These are clear indicators that DFSS is a tool which will improve the design process and create more robust products and processes.

CHAPTER 3

SELECTION OF CASE STUDY OF A SPECIFIC UNDERBODY COMPONENT WHICH HAS SIGNIFICANT INTEREST TO THE COMPANY AND AERO/THERMAL ORGANIZATION

Underbody vehicle components are subjected to extremely high temperatures due to their proximity to the exhaust system. Subsequently, these underbody components are constructed to endure elevated temperatures. However, the temperature of these underbody components may fluctuate based on changes in environmental conditions, wear and ageing, and/or variation in the manufacturing process.

One particular source of uncertainty, wear and ageing, has a significantly strong effect on the emissivity of the exhaust surface due to oxidation. The emissivity of a component is a measure of the amount of radiation that a component can emit. Therefore, the FAST

uncertainty technique can offer significant benefits in the study of underbody components which are within the direct radiation view path of the exhaust surface.

This particular type of uncertainty is due to wear and ageing, but in particular, it is caused by oxidation which occurs over a long period of time. The *"Introduction to High Temperature Oxidation and Corrosion"* explains that oxidation is the most significant high temperature reaction (Khanna, 2002). Oxidation will occur when a metal is at an elevated temperature in the presence of air. Therefore, the metal underbody components, such as the muffler, are highly susceptible to this reaction. The reactants for this process are the metal and oxygen and the products are oxides.

Equation 14

$$M(s) + O_2(g) = MO_2(s)$$
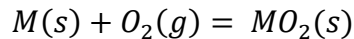
From experience, it is known that oxidation occurs on the muffler. However, to predict the occurrence of oxidation, it must be determined if the oxygen potential in the environment is greater than the oxygen partial pressure in equilibrium with the oxide (Khanna, 2002).

The oxygen partial pressure in equilibrium with the oxide can be found by calculating the standard free energy of formation of the oxide.

Equation 15

$$\Delta G^\circ = -RTln(\frac{a_{MO_2}}{a_M p_{(O_2)}})$$

16

Where:

a_{MO_2} is the activity of the oxide

a_M is the activity of the metal

$p_{(O_2)}$ is the partial pressure of the oxygen gas

In *"Introduction to High Temperature Oxidation and Corrosion"* the activity of the oxide and the metal are assumed to be equal resulting in the following equation.

Equation 16

$$\Delta G° = RT ln(p_{(O_2)})$$

Equation 17

$$p_{(O_2)} = exp(\frac{°\Delta G}{RT})$$

Therefore, to obtain the partial pressure of the oxygen gas in equilibrium with the oxide, the standard free energy of formation must be found from the Ellingham/Richardson diagrams.

There are four steps involved in the oxidation process:

1) Adsorption of oxygen molecules from the air
2) Nucleation of oxides
3) Development of thin oxide layer
4) Growth of oxide layer into thicker scale

When oxidation occurs, the oxide layer changes the surface condition of the component; therefore, the emissivity of the component will change. This variation in emissivity creates uncertainty in the temperature of the surrounding components because it affects the amount of radiation emitted by the exhaust surface. Therefore, the variation in emissivity must be studied to determine how strongly it degrades the robustness of the system and if design solutions should be implemented to reduce its variability.

Considering all of the possible sources of uncertainty that affect the vehicle underbody components, it is clear that predicting the underbody thermal performance is difficult.

$$k = f(T)$$

UNPREDICTABLE THERMAL SYSTEM
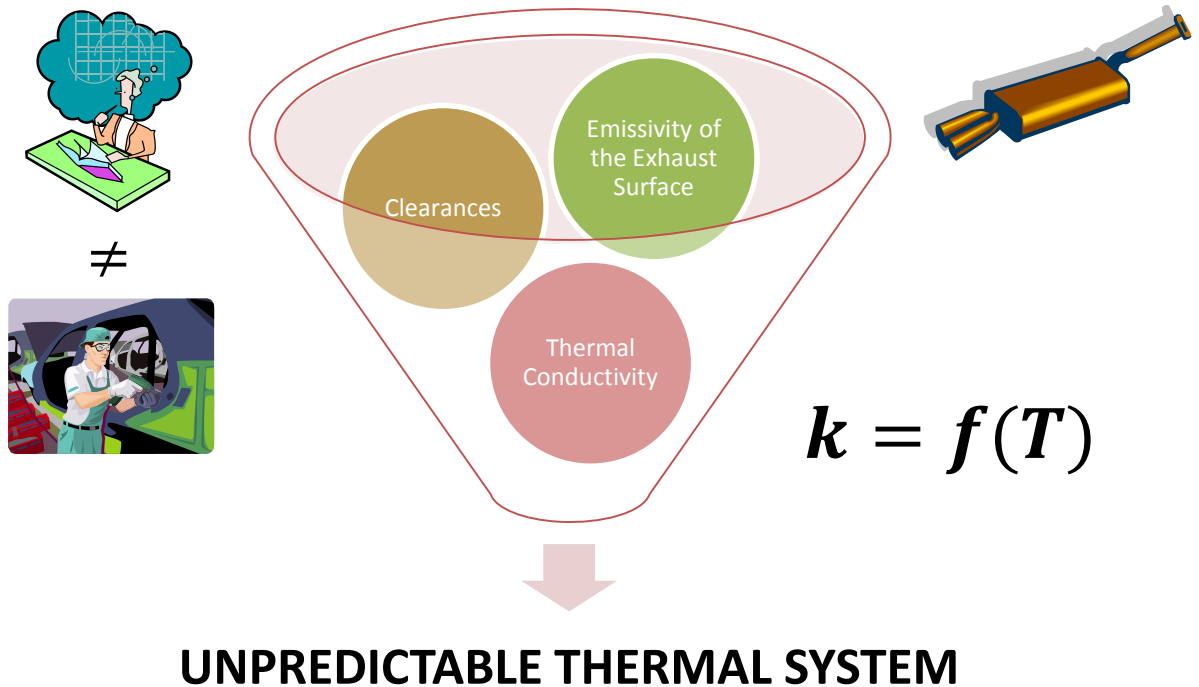
Figure 1 - Many Sources of Uncertainty Exist for the Thermal Performance of Underbody Components Resulting in an Unpredictable Thermal System

On a number of vehicle architectures, the spare tire tub is an underbody component which is directly above the muffler and therefore can be strongly affected by the variation

in the emissivity of the exhaust surface. This underbody component has significant interest to the aero/thermal organization and was therefore selected as a case study for the application of the FAST method coupled with DFSS.

CHAPTER 4

APPLICATION OF THE FOURIER AMPLITUDE SENSITIVITY TEST (FAST) METHOD TO AN UNDERBODY COMPONENT

Fourier Amplitude Sensitivity Test (FAST)

For this case study, the FAST method was used to investigate the effect of uncertainty in design parameters on thermal system performance of the spare tire tub. The results from this study will pinpoint the design parameters which offer the greatest opportunity for improvement of thermal system performance and reliability. In turn, this method can save engineering time and resources.

The first step required to apply the FAST method is to form an analytical model for the system to be studied. For this case study, the vehicle underbody system consists of a muffler, a three-layer heat shield, and spare tire tub. The output of interest from this model is the temperature of the spare tire tub. The majority of the input parameters in this model deviate from their nominal values due to environmental factors, wear and ageing, and/or variation in the manufacturing process. Using MATLAB software package, the model was simulated with input parameters which were simultaneously and sinusoidally varied at distinct frequencies over their respective uncertainty ranges.

Finally, the Fourier transform was applied to the output of the model to convert the response into the frequency domain to allow the amplitude of each of the distinct

frequencies to be recognized. The amplitude of each frequency was used as an indication of the strength of the effect of the corresponding parameter's variation on the temperature of the spare tire tub. Reducing the partial variance of the most influential input parameters by decreasing the system's sensitivity to these parameters and/or decreasing the uncertainty of these parameters will have the greatest improvement on the overall thermal performance of the system.

Analytical Model Development

The analytical model is developed to represent the thermal system containing the underbody component of interest. For this case study, the component of interest is the spare tire tub. A configuration in which this component is located directly above the muffler was considered. In vehicles with this particular configuration, there is usually a heat shield located between the muffler and the underbody component to protect the component from the radiation energy emitted by the muffler. This model considered the heat shield to consist of three layers; two aluminum layers with a layer of fiberglass in between.

The components within this system exchange heat by three modes; conduction,

convection, and radiation.
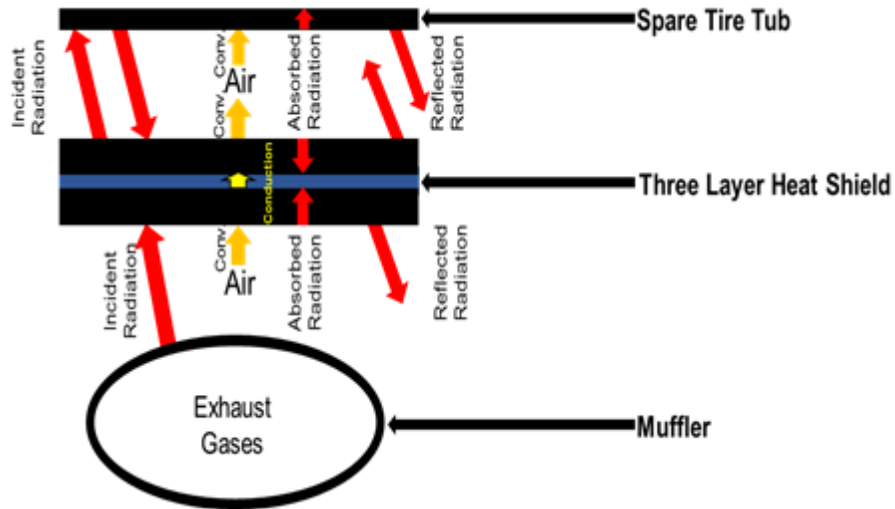
Figure 2 - Sketch of Underbody Components Considered in the Analytical Model

Energy Balance Equations

The following section explains the steps followed to develop the analytical model. To

begin, the definition of the parameters used within the model are presented in Table 1.

The fifth column in this table provides the nominal values approximated for each of these

parameters. A brief description of the determination of these values is shown in the

section, "Approximation of Nominal Values of Input Parameters" on page 46.

Table 1 - Input Parameters for the Analytical Model Developed to Implement the FAST

Method

No.	Parameter	Component(s)	Matlab Definition	Nominal Value	Unit	Uncertainty	
1	Convection Heat Transfer Coefficients	Air to Spare Tire Tub	h_{st}	10	W/(m^2 K)	-31.0%	31.0%
2		Air to Heat Shield Lower Surface	h_{hsl}	13	W/(m^2 K)	-76.0%	76.0%
3		Air to Heat Shield Upper Surface	h_{hsu}	7	W/(m^2 K)	-29.0%	29.0%
4	Temperatures	Muffler Surface	T_m	603	K	-30.0%	30.0%
5		Air Flow Over Heat Shield Upper Surface	$T_{a_{hsu}}$	320	K	-20.0%	20.0%
6		Air Flow Over Heat Shield Lower Surface	$T_{a_{hsl}}$	333	K	-20.0%	20.0%
7		Air Flow Over Spare Tire Tub	$T_{a_{st}}$	317	K	-20.0%	20.0%
8	Emissivities	Muffler	ε_m	0.2	-	0.0%	350.0%
9		Spare Tire Tub	ε_{st}	0.9	-	0.0%	0.0%
10		Heat Shield	ε_{hs}	0.45	-	0.0%	100.0%
11	Densities	Spare Tire Tub	ρ_{st}	7769	kg/m^3	-10.0%	10.0%
12		Heat Shield (Outer Layer)	ρ_{hs_o}	2770	kg/m^3	-10.0%	10.0%
13	Specific Heat Capacities	Spare Tire Tub	c_{st}	461	J/(kg K)	-7.0%	7.0%
14		Heat Shield (Outer Layer)	c_{hs_o}	884	J/(kg K)	-7.0%	7.0%
15	Thermal Conductivities	Heat Shield (Inner Layer)	k_{hs_i}	0.3	W/(m K)	-7.0%	7.0%
16	Thicknesses	Spare Tire Tub	t_{st}	0.002	m	-13.33%	13.33%
17		Heat Shield (Outer Layer)	t_{hs_o}	0.00025	m	-78.74%	78.74%
18		Heat Shield (Inner Layer)	t_{hs_i}	0.004	m	-5.00%	5.00%
19	Lengths	Spare Tire Tub	L_{st}	0.456	m	-0.044%	0.044%
20		Heat Shield	L_{hs}	0.456	m	-0.044%	0.044%
21	Widths	Spare Tire Tub	W_{st}	0.811	m	-0.025%	0.025%
22		Heat Shield	W_{hs}	0.811	m	-0.025%	0.025%
23	Diameters	Muffler Diameter 1	$D1_m$	0.180	m	-0.111%	0.111%
24		Muffler Diameter 2	$D2_m$	0.230	m	-0.087%	0.087%
25	Clearances	Heat Shield to Spare Tire Tub	L_{hs_st}	0.002	m	-10.20%	10.20%
26		Muffler to Heat Shield	L_{m_hs}	0.105	m	-0.19%	0.19%

To develop the analytical model for this case study, the first law of thermodynamics was applied. The first law of thermodynamics is also referred to as the principle of conservation of energy (Cengel & Ghajar, 2014). This law states that energy cannot be created or destroyed; however, it can change forms. This law can be expressed as the following.

Equation 18

$$(Total\ Energy\ Entering\ the\ System) - (Total\ Energy\ Leaving\ the\ System)$$
$$= (Change\ in\ the\ Total\ Energy\ of\ the\ System)$$

For a general system undergoing any process, this law can be expressed in the following terms.

Equation 19

$$\dot{E}_{in} - \dot{E}_{out} = \frac{\Delta E_{system}}{dt}$$

When the system is not subject to substantial surface tension, gravity, magnetic, or electric effects, the term on the right side of this equation can be expressed as the change in internal energy, as written below.

Equation 20

$$\Delta E_{system} = \Delta U_{system}$$

When conducting heat transfer analysis, the focus is placed on energy transfer due to a temperature difference, known as thermal energy. In this case, the electrical, chemical,

and nuclear energies are placed in to one term of heat generation and the first law can be written as shown below.

Equation 21

$$\dot{Q}_{in} - \dot{Q}_{out} + \dot{E}_{gen} = \frac{\Delta E_{thermal,system}}{dt}$$

In this specific analysis, the components include the muffler, heat shield, and spare tire tub. These components have a fixed mass; therefore, they are considered to be closed systems. In this case, the equation can be further simplified, as depicted below.

Equation 22

$$\dot{Q}_{in} - \dot{E}_{out} = \Delta\dot{U} = mc_v\frac{dT}{dt}$$

One final simplification can be made because there are no work interactions across the boundaries of the components in this system. Therefore, all of the energy in and out of the system is transferred by heat. With this understanding, the equation can be written as below.

Equation 23

$$\dot{Q}_{in} - \dot{Q}_{out} = mc_v\frac{dT}{dt}$$

The terms on the left side of this equation represent the net amount of heat transfer across the boundary of the component. A component may have heat transferred across the boundary through conduction, convection, and/or radiation.

Conduction

Conduction can occur in any phase of a substance. This form of heat transfer takes place when heat is transferred from particles with more energy to particles with less energy. It depends upon the thermal conductivity of the substance, the dimensions of the substance, and the temperature difference from one side of the substance to the other. Fourier's Law of heat conduction governs this mode of heat transfer and is shown below.

Equation 24

$$\dot{Q}_{cond} = kA\frac{dT}{dx}$$

In this analytical model, the heat shield and spare tire tub are modelled as plane walls. The equation for heat transfer by conduction through a plane wall is shown below.

Equation 25

$$\dot{Q}_{cond} = kA\frac{\Delta T}{\Delta x}$$

Where:

k is the thermal conductivity of the substance

A is the cross-sectional area of the substance

ΔT is the temperature difference across the thickness of the substance

Δx is the thickness of the substance

Convection

The second mode of heat transfer to be discussed is convection. This mode of heat transfer is conduction in the presence of fluid motion. Thus, this form of heat transfer occurs between a solid and liquid or a solid and gas. This form of heat transfer is governed by Newton's Law of cooling, shown below.

Equation 26

$$\dot{Q}_{conv} = hA_s(T_s - T_\infty)$$

Where:

h is the heat transfer coefficient (determined experimentally)

A_s is the surface area of the solid

T_s is the temperature of the solid surface

T_∞ is the temperature of the fluid flowing over the solid surface

Radiation

Radiation is a form of heat transfer which occurs due to variations in the electronic arrangements of atoms and/or molecules. This form of heat transfer occurs as electromagnetic waves and does not require a medium. The equation which governs this form of heat transfer is the Stefan-Boltzmann law, shown below.

Equation 27

$$\dot{Q}_{emitted\ rad} = \varepsilon\sigma A_s T_s^{\ 4}$$

Where:

ε is the emissivity of the surface

σ is the Stefan-Boltzmann constant ($5.67 \times 10^{-8} \frac{W}{m^2 K^4}$)

A_s is the surface area

T_s is the temperature of the surface

When radiation strikes a surface, the radiation can be absorbed, reflected, and/or transmitted. The incident radiation, also known as irradiation, G, can be written in the form shown below.

$$G = G_{abs} + G_{ref} + G_{tra}$$

The fraction of radiation which is absorbed, reflected, and transmitted depends on the absorptivity of the surface, α, the reflectivity of the surface, ρ, and the transmissivity of the surface, τ.

Equation 28

$$\alpha = \frac{G_{abs}}{G}$$

Equation 29

$$\rho = \frac{G_{ref}}{G}$$

Equation 30

$$\tau = \frac{G_{tra}}{G}$$

Substituting these three relationships into Equation 27 results in the following equation.

Equation 31

$$\alpha + \rho + \tau = 1$$

For the three components in this analysis (lower layer of heat shield, upper layer of heat shield, and spare tire tub), the transmitted radiation is assumed to be negligible because these surfaces are opaque. Therefore, a portion of the incident radiation is absorbed, which will increase the thermal energy of the component and another portion is reflected away from the component.

In the following three sections, Equation 23 will be used to develop an energy balance for the lower layer of the heat shield, the upper layer of the heat shield, and the component of interest (the spare tire tub). These energy balances will include conduction, convection, and radiation terms to describe the energy transfer across the boundaries of these three components which will result in a change in thermal energy of the components. The purpose of developing these equations is to identify the design parameters which affect the temperature of the spare tire tub so that uncertainty analysis can be conducted on these parameters.

Energy Balance for the Lower Layer of the Heat Shield

The lower layer of the heat shield is modelled as a closed system with no work interactions; thus, the energy balance for the lower layer of the heat shield can be expressed by the equation below.

Equation 32

$$\dot{Q}_{in} - \dot{Q}_{out} = mc_v \frac{dT}{dt}$$

The left side of the equation is the net heat transfer to this layer and the right side

provides the corresponding increase in temperature. Therefore, the sources of heat

transfer to and away from this component need to be identified. This layer experiences

heat transfer by conduction, convection, and radiation. A diagram which shows these

modes of heat transfer is given below.
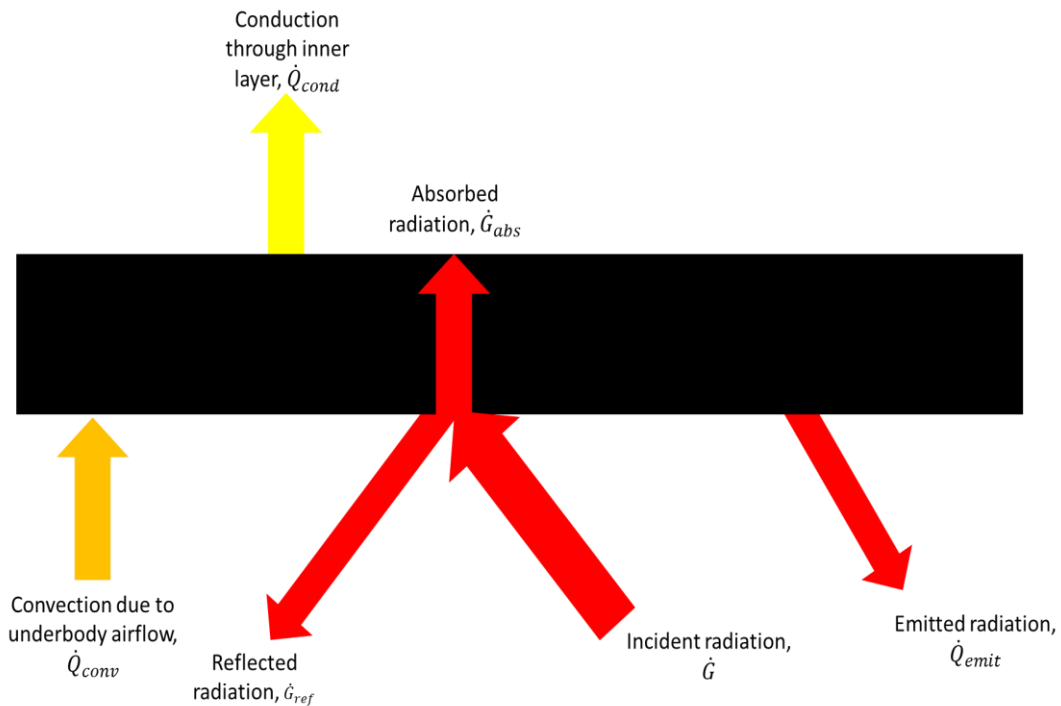
Figure 3 - Energy Balance of Lower Layer of Heat Shield

Conduction

Conduction occurs at the upper boundary of this component through the inner layer of the

heat shield. This heat transfer is driven by the temperature difference between the lower

layer of the heat shield and the upper layer of the heat shield. The equation for this

conduction heat transfer, based on Fourier's Law of heat conduction, is given below.

Equation 33

$$\dot{Q}_{cond} = k_{hsi} A_{hs} \frac{(T_{hsu} - T_{hsl})}{t_{hsi}}$$

Convection

Convection occurs at the lower boundary of this component due to the underbody

airflow. The equation, based on Newton's Law of cooling, is given below.

Equation 34

$$\dot{Q}_{conv} = h_{hsl} A_{hs} (T_{a_{hsl}} - T_{hsl})$$

Radiation

To simplify the analysis of the radiation heat transfer to this component, the lower layer

of the heat shield was assumed to be gray, opaque, and diffuse. A gray surface is one

whose emissivity is equal to its absorptivity. An opaque surface does not transmit any of

the incident radiation; thus, it is not transparent. A diffuse surface emits and reflects

radiation in a manner which is independent of the wavelength of the radiation and is

isothermal.

The majority of the incident radiation to this component, $\dot{G}$, will come from the surface of

the muffler because it is at a highly elevated temperature. The fraction of radiation

emitted by the muffler which actually strikes the heat shield will depend upon the view

factor from the muffler to the heat shield, F_{m-hsl}. The equation for the incident radiation,

based on the Stefan-Boltzmann law, is shown below.

Equation 35

$$\dot{G} = \varepsilon_m \sigma A_m F_{m-hsl} T_m{}^4$$

The calculation of the view factor from a cylinder to a plane wall is more complex than the view factor from a plane wall to a cylinder. To reduce the complexity of the view factor calculation, the reciprocity relation was applied. This relation is show below.

Equation 36

$$A_i F_{i-j} = A_j F_{j-i}$$

Applying the reciprocity relation to the muffler and lower surface of the heat shield renders the following.

Equation 37

$$A_m F_{m-hsl} = A_{hs} F_{hsl-m}$$

Thus, to simplify the calculations, the irradiation was expressed by the equation below.

Equation 38

$$\dot{G} = \varepsilon_m \sigma A_m F_{m-hsl} T_m{}^4 = \varepsilon_m \sigma A_{hs} F_{hsl-m} T_m{}^4$$

A portion of this irradiation will be reflected away from the heat shield and the rest will be absorbed, increasing the thermal energy of the component. The amount of reflected radiation depends on the reflectivity of the surface, ρ, as shown in the equation below.

Equation 39

$$\dot{G}_{ref} = \rho \dot{G} = \rho_{hsl} \varepsilon_m \sigma A_{hs} F_{hsl-m} T_m{}^4$$

Since this surface was assumed to be gray ($\varepsilon = \alpha$) and opaque ($\tau = 0$), the reflected radiation can also be expressed by the following equation.

Equation 40

$$\dot{G}_{ref} = \rho\dot{G} = (1 - \varepsilon_{hsl})\varepsilon_m\sigma A_{hs}F_{hsl-m}T_m{}^4$$

The amount of radiation which is absorbed can also be expressed as the difference between the amount of incident radiation and the amount of reflected radiation.

Equation 41

$$\dot{G}_{abs} = \dot{G} - \dot{G}_{ref} = \varepsilon_m\sigma A_{hs}F_{hsl-m}T_m{}^4 - (1 - \varepsilon_{hsl})\varepsilon_m\sigma A_{hs}F_{hsl-m}T_m{}^4$$

Radiation will also be emitted from the lower layer of the heat shield's surface to the surroundings.

Equation 42

$$\dot{Q}_{rad\ emit} = \varepsilon_{hs}\sigma A_{hs}T_{hsl}{}^4$$

Substituting the conduction, convection, and radiation terms into the energy balance, Equation 32, yields the following.

Equation 43

$$m_{hsl}c_{hs}\frac{dT_{hsl}}{dt} = \dot{Q}_{cond} + \dot{Q}_{conv} + \dot{G}_{abs} - \dot{Q}_{rad\ emit}$$

Substituting the equations for convection, conduction, radiation emitted, and radiation absorbed provides the equation below.

Equation 44

$$m_{hsl} c_{hs\_o} \frac{dT_{hsl}}{dt}$$

$$= k_{hsi} A_{hs} \frac{(T_{hsu} - T_{hsl})}{t_{hsi}} + h_{hsl} A_{hs} (T_{a_{hsl}} - T_{hsl}) + \varepsilon_m \sigma A_{hs} F_{hsl-m} T_m^4$$

$$- (1 - \varepsilon_{hsl}) \varepsilon_m \sigma A_{hs} F_{hsl-m} T_m^4 + \varepsilon_{hsl} \sigma A_{hs} T_{hsl}^4$$

In this form of the equation, there are parameters which are dependent on one another. These parameters are the view factor from the lower layer of the heat shield to the muffler, the surface area of the heat shield, and the mass of the heat shield. These interactions are not ideal for DFSS analysis. Therefore, the view factor, surface area, and mass terms were substituted with equations which are functions of the geometric properties of the system.

The view factor from the heat shield to the muffler was found by approximating the muffler as an infinitely long cylinder and the heat shield as an infinitely long flat plate. The formula for this view factor was found from the ASME paper, "Compilation of Radiation Shape Factors for Cylindrical Assemblies" (Leuenberger & Person, 1994).

Equation 45

$$F_{2 \to 1} = \frac{2R}{T} tan^{-1} \frac{T}{2S}$$

Where:

2 is the flat plate

1 is the cylinder

R is the radius of the cylinder

T is the length of the plate

S is the distance between the cylinder axis and the plate

Substituting the variables being used in this model, the formula for the view factor from the heat shield to the muffler becomes:

Equation 46

$$F_{hsl-m} = \frac{2(D1_m + D2_m)}{4L_{hs}} tan^{-1} \frac{L_{hs}}{2Lm\_hs}$$

The surface area of the lower surface of the heat shield was put in to terms of the dimensions of the heat shield by approximating it as a flat plate; thus, the surface area was simply calculated by multiplying the length and width. The mass of the lower layer of the heat shield was calculated by multiplying the density of the lower layer of the heat shield by the volume. The volume was calculated as the product of length, width, and thickness. Therefore, the final energy balance equation for the lower layer of the heat shield was formed.

Equation 47

$$\rho_{hs\_o} L_{hs} W_{hs} t_{hs\_o} c_{hs\_o} \frac{dT_{hsl}}{dt}$$

$$= k_{hs\_i}(L_{hs}W_{hs})\frac{(T_{hsu} - T_{hsl})}{t_{hs\_i}} + h_{hsl}(L_{hs}W_{hs})(T_{a_{hsl}} - T_{hsl})$$

$$+ \varepsilon_m \sigma(L_{hs}W_{hs})(\frac{2(D1_m + D2_m)}{4L_{hs}} tan^{-1} \frac{L_{hs}}{2L_{m\_hs}})T_m^4 - (1$$

$$- \varepsilon_{hs})\varepsilon_m\sigma(L_{hs}W_{hs})(\frac{2(D1_m + D2_m)}{4L_{hs}} tan^{-1} \frac{L_{hs}}{2L_{m\_hs}})T_m^4$$

$$+ \varepsilon_{hs}\sigma(L_{hs}W_{hs})T_{hsl}^4$$

Energy Balance for the Upper Layer of the Heat Shield

The same method used for the lower surface of the heat shield was used to develop the energy balance equation for the upper surface of the heat shield. To begin, the general form of the energy balance equation for a closed system with no work interactions was applied.

Equation 48

$$\dot{Q}_{in} - \dot{Q}_{out} = mc_v\frac{dT}{dt}$$

To determine the net heat transfer to this component, the modes of heat transfer were identified as shown in the figure below.
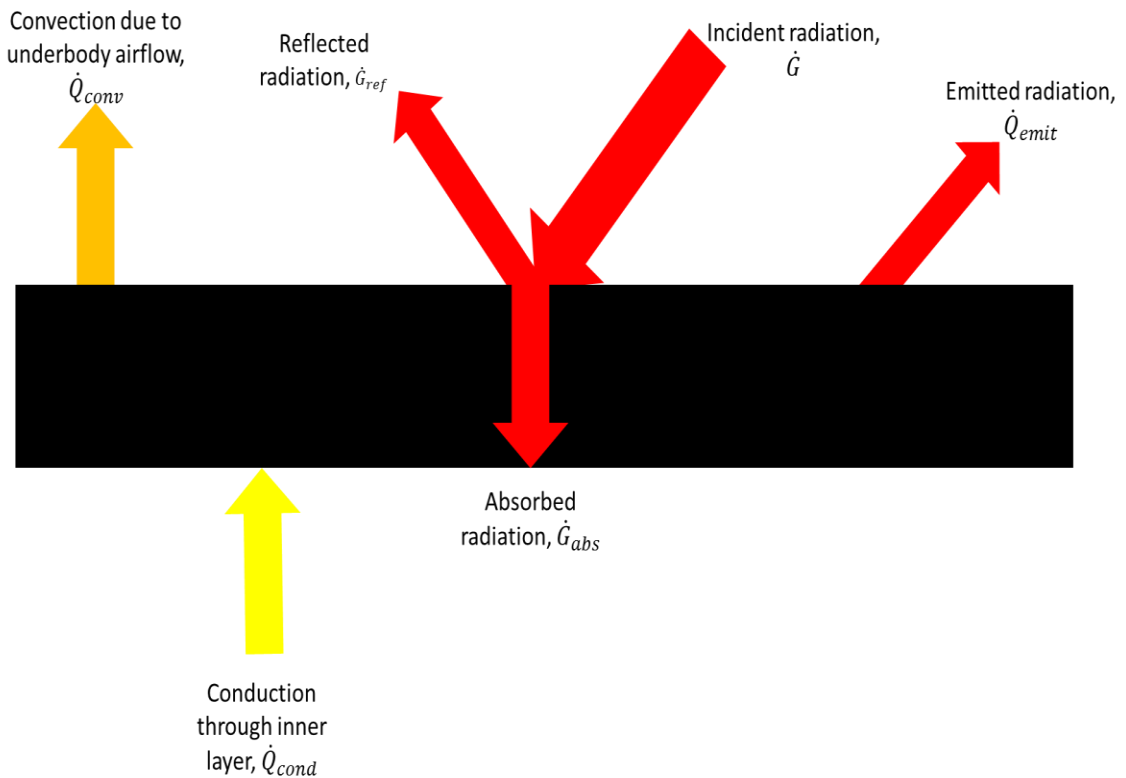
Figure 4 - Energy Balance of Upper Layer of Heat Shield

Conduction

Conduction occurs at the lower boundary of this component through the inner layer of the heat shield. This heat transfer is driven by the temperature difference between the lower layer of the heat shield and the upper layer of the heat shield. The equation for this conduction heat transfer, based on Fourier's Law of heat conduction, is given below.

Equation 49

$$\dot{Q}_{cond} = k_{hsi} A_{hs} \frac{(T_{hsl} - T_{hsu})}{t_{hsi}}$$

Convection

Convection occurs at the upper boundary of this component due to the underbody airflow. The equation, based on Newton's Law of cooling, is shown here.

Equation 50

$$\dot{Q}_{conv} = h_{hsu} A_{hs} (T_{a_{hsu}} - T_{hsu})$$

Radiation

As discussed during the development of the energy balance for the lower layer of the heat shield, the analysis was simplified by assuming that the upper layer of the heat shield is gray, opaque, and diffuse.

The incident radiation to the upper layer of the heat shield, $\dot{G}$, will come from the surface of the spare tire tub. The fraction of radiation emitted by the spare tire tub which strikes the heat shield will depend upon the view factor from the spare tire tub to the upper surface of the heat shield, F_{st-hsu}. The equation for the incident radiation, based on the Stefan-Boltzmann law, is shown below.

Equation 51

$$\dot{G} = \varepsilon_{st}\sigma A_{st}F_{st-hsu}T_{st}{}^{4}$$

A portion of this irradiation will be reflected away from the heat shield and the rest will be absorbed, increasing the thermal energy of the component. The amount of reflected radiation depends on the reflectivity of the surface, ρ, as shown in the equation below.

Equation 52

$$\dot{G}_{ref} = \rho\dot{G} = \rho_{hsu}\varepsilon_{st}\sigma A_{st}F_{st-hsu}T_{st}{}^{4}$$

Since this surface was assumed to be gray ($\varepsilon = \alpha$) and opaque ($\tau = 0$), the reflected radiation can also be expressed by the following equation.

Equation 53

$$\dot{G}_{ref} = \rho\dot{G} = (1 - \varepsilon_{hs})\varepsilon_{st}\sigma A_{st}F_{st-hsu}T_{st}{}^{4}$$

The amount of radiation which is absorbed can also be expressed as the difference between the amount of incident radiation and the amount of reflected radiation.

Equation 54

$$\dot{G}_{abs} = \dot{G} - \dot{G}_{ref} = \varepsilon_{st}\sigma A_{st}F_{st-hsu}T_{st}{}^{4} - (1 - \varepsilon_{hs})\varepsilon_{st}\sigma A_{st}F_{st-hsu}T_{st}{}^{4}$$

Radiation will also be emitted from the upper layer of the heat shield's surface to the surroundings.

Equation 55

$$\dot{Q}_{rad\ emit} = \varepsilon_{hs}\sigma A_{hs}T_{hsu}{}^{4}$$

Substituting the conduction, convection, and radiation terms into the energy balance, Equation 48, yields the following.

Equation 56

$$m_{hsu} c_{hs} \frac{dT_{hsu}}{dt} = \dot{Q}_{cond} + \dot{Q}_{conv} + \dot{G}_{abs} - \dot{Q}_{rad\ emit}$$

Substituting the equations for convection, conduction, radiation emitted, and radiation absorbed provides the equation below.

Equation 57

$$m_{hs} c_{hs\_o} \frac{dT_{hsu}}{dt}$$

$$= k_{hsi} A_{hs} \frac{(T_{hsl} - T_{hsu})}{t_{hsi}} + h_{hsu} A_{hs} \left(T_{a_{hsu}} - T_{hsu} \right) + \varepsilon_{st} \sigma A_{st} F_{st-hsu} T_{st}^{4}$$

$$- (1 - \varepsilon_{hs}) \varepsilon_{st} \sigma A_{st} F_{st-hsu} T_{st}^{4} - \varepsilon_{hs} \sigma A_{hs} T_{hsu}^{4}$$

As described in the previous section, the view factors, surface areas, and masses were written in terms of dimensional properties to avoid using parameters which depend on one another. The equation for the view factor from the spare tire tub to the upper surface of the heat shield was found by approximating the heat shield and spare tire tub as parallel flat plates of the same dimensions. The formula for this configuration was found from the textbook, "Heat and Mass Transfer: Fundamentals and Applications" (Cengel & Ghajar, 2014).

Equation 58

$$F_{i \to j} = \frac{2}{\pi \bar{X} \bar{Y}} \left\{ ln \left[\frac{(1 + \bar{X}^2)(1 + \bar{Y}^2)}{1 + \bar{X}^2 + \bar{Y}^2} \right]^{1/2} + \bar{X}(1 + \bar{Y}^2)^{1/2} tan^{-1} \frac{\bar{X}}{(1 + \bar{Y}^2)^{1/2}} \right.$$

$$\left. + \bar{Y}(1 + \bar{X}^2)^{1/2} tan^{-1} \frac{\bar{Y}}{(1 + \bar{X}^2)^{\frac{1}{2}}} - \bar{X} tan^{-1} \bar{X} - \bar{Y} tan^{-1} \bar{Y} \right\}$$

Where:

X is the length of the plates

Y is the width of the plates

L is the distance between the plates

$\bar{X}$ is equal to X/L

$\bar{Y}$ is equal to Y/L

Substituting the variables being used in this model, the formula for the view factor from the heat shield to the spare tire tub becomes:

Equation 59

$$F_{st \to hsu} = \frac{2}{\pi \dfrac{L_{hs}}{Lhs\_st} \dfrac{W_{hs}}{Lhs\_st}} \left\{ ln \left[\frac{(1 + L_{hs}^2)(1 + W_{hs}^2)}{1 + L_{hs}^2 + W_{hs}^2} \right]^{1/2} \right.$$

$$+ L_{hs}(1 + W_{hs}^2)^{\frac{1}{2}} tan^{-1} \frac{L_{hs}}{(1 + W_{hs}^2)^{\frac{1}{2}}}$$

$$+ W_{hs}(1 + L_{hs}^2)^{\frac{1}{2}} tan^{-1} \frac{W_{hs}}{(1 + L_{hs}^2)^{\frac{1}{2}}} - (L_{hs}) tan^{-1}(L_{hs})$$

$$\left. - (W_{hs}) tan^{-1}(W_{hs}) \right\}$$

The mass was written as the density multiplied by the length, width, and thickness of the layer. Therefore, this equation was written as shown here.

Equation 60

$$\rho_{hs\_o} L_{hs} W_{hs} t_{hs\_o} c_{hs\_o} \frac{dT_{hsu}}{dt}$$

$$= k_{hs_i}(L_{hs}W_{hs})\frac{(T_{hsl} - T_{hsu})}{t_{hs_i}} + h_{hsu}(L_{hs}W_{hs})(T_{a_{hsu}} - T_{hsu})$$

$$+ \varepsilon_{st}\sigma(L_{hs}W_{hs})(\frac{2}{\pi \frac{L_{hs}}{L_{hs_{st}}}\frac{W_{hs}}{L_{hs_{st}}}}\left\{ ln\left[\frac{(1 + L_{hs}^2)(1 + W_{hs}^2)}{1 + L_{hs}^2 + W_{hs}^2}\right]^{\frac{1}{2}}\right.$$

$$+ L_{hs}(1 + W_{hs}^2)^{\frac{1}{2}}tan^{-1}\frac{L_{hs}}{(1 + W_{hs}^2)^{\frac{1}{2}}}$$

$$+ W_{hs}(1 + L_{hs}^2)^{\frac{1}{2}}tan^{-1}\frac{W_{hs}}{(1 + L_{hs}^2)^{\frac{1}{2}}} - (L_{hs})tan^{-1}(L_{hs})$$

$$\left. - (W_{hs})tan^{-1}(W_{hs})\right\})T_{st}^4$$

$$- (1 - \varepsilon_{hs})\varepsilon_{st}\sigma(L_{hs}W_{hs})(\frac{2}{\pi \frac{L_{hs}}{L_{hs\_st}}\frac{W_{hs}}{L_{hs\_st}}}\left\{ ln\left[\frac{(1 + L_{hs}^2)(1 + W_{hs}^2)}{1 + L_{hs}^2 + W_{hs}^2}\right]^{\frac{1}{2}}\right.$$

$$+ L_{hs}(1 + W_{hs}^2)^{\frac{1}{2}}tan^{-1}\frac{L_{hs}}{(1 + W_{hs}^2)^{\frac{1}{2}}}$$

$$+ W_{hs}(1 + L_{hs}^2)^{\frac{1}{2}}tan^{-1}\frac{W_{hs}}{(1 + L_{hs}^2)^{\frac{1}{2}}} - (L_{hs})tan^{-1}(L_{hs})$$

$$\left. - (W_{hs})tan^{-1}(W_{hs})\right\})T_{st}^4 - \varepsilon_{hs}\sigma(L_{hs}W_{hs})T_{hsu}^4$$

Energy Balance for the Spare Tire Tub

The final energy balance was for the component of interest in this study, the spare tire tub. To begin, the general equation for energy balance of a closed system with no work interactions is stated below.

Equation 61

$$\dot{Q}_{in} - \dot{Q}_{out} = mc_v \frac{dT}{dt}$$

The net heat transfer to the spare tire tub is due to convection heat transfer caused by the underbody airflow, radiation absorbed by the spare tire tub, and radiation emitted from the spare tire tub.
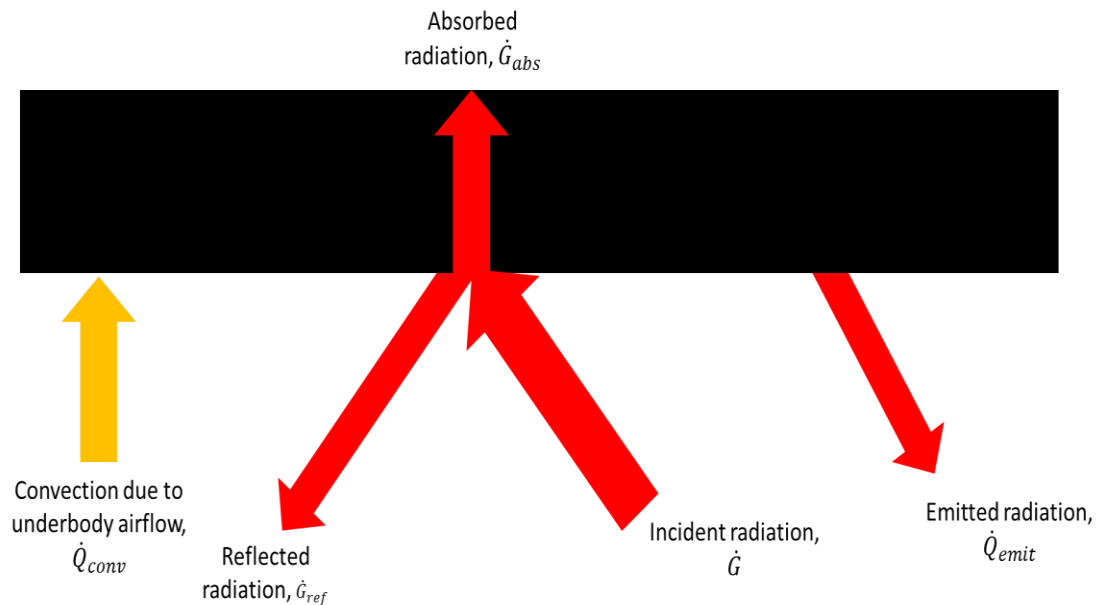
Figure 5 - Energy Balance of Spare Tire Tub

Convection

Convection occurs at the lower boundary of this component due to the underbody airflow. The equation, based on Newton's Law of cooling, is given here.

Equation 62

$$\dot{Q}_{conv} = h_{st}A_{st}(T_{a_{st}} - T_{st})$$

Radiation

The spare tire tub was assumed to be gray, opaque, and diffuse (for the same considerations discussed in the development of the energy balances for the upper and lower layers of the heat shield). The incident radiation to the spare tire tub, $\dot{G}$, will come from the upper surface of the heat shield. The fraction of radiation emitted by the upper surface of the heat shield which strikes the spare tire tub will depend upon the view factor from the upper surface of the heat shield to the spare tire tub, F_{hsu-st}. The equation for the incident radiation, based on the Stefan-Boltzmann law, is shown below.

Equation 63

$$\dot{G} = \varepsilon_{hs}\sigma A_{hs}F_{hs-st}T_{hsu}{}^4$$

A portion of this irradiation will be reflected away from the spare tire tub and the rest will be absorbed, increasing the thermal energy of the component. The amount of reflected radiation depends on the reflectivity of the surface, ρ, as shown in the equation below.

Equation 64

$$\dot{G}_{ref} = \rho\dot{G} = \rho_{st}\varepsilon_{hs}\sigma A_{hs}F_{hs-st}T_{hsu}{}^4$$

Since this surface was assumed to be gray ($\varepsilon = \alpha$) and opaque ($\tau = 0$), the reflected radiation can also be expressed by the following equation.

Equation 65

$$\dot{G}_{ref} = \rho\dot{G} = (1 - \varepsilon_{st})\varepsilon_{hs}\sigma A_{hs}F_{hs-st}T_{hsu}{}^4$$

The amount of radiation which is absorbed can also be expressed as the difference between the amount of incident radiation and the amount of reflected radiation.

Equation 66

$$\dot{G}_{abs} = \dot{G} - \dot{G}_{ref} = \varepsilon_{hs}\sigma A_{hs}F_{hs-st}T_{hsu}{}^4 - (1 - \varepsilon_{st})\varepsilon_{hs}\sigma A_{hs}F_{hs-st}T_{hsu}{}^4$$

Radiation will also be emitted from the spare tire tub's surface to the surroundings.

Equation 67

$$\dot{Q}_{rad\ emit} = \varepsilon_{st}\sigma A_{st}T_{st}{}^4$$

Substituting the convection and radiation terms into the energy balance, Equation 61, yields the following.

Equation 68

$$m_{st}c_{st}\frac{dT_{st}}{dt} = \dot{Q}_{conv} + \dot{G}_{abs} - \dot{Q}_{rad\ emit}$$

Substituting the equations for convection, conduction, radiation emitted, and radiation absorbed provides the equation below.

Equation 69

$$m_{st}c_{st}\frac{dT_{st}}{dt} = h_{st}A_{st}(T_{ast} - T_{st}) + \varepsilon_{hs}\sigma A_{hs}F_{hs-st}T_{hsu}{}^4$$

$$- (1 - \varepsilon_{st})\varepsilon_{hs}\sigma A_{hs}F_{hs-st}T_{hsu}{}^4 - \varepsilon_{st}\sigma A_{st}T_{st}{}^4$$

Substituting the surface areas of the heat shield and spare tire tub, mass of the spare tire tub, and view factor from the heat shield to the spare tire tub with geometric and material properties resulted in the equation shown below:

44

Equation 70

$$\rho_{st} L_{st} W_{st} t_{st} c_{st} \frac{dT_{st}}{dt}$$

$$= h_{st}(L_{st}W_{st})\left(T_{a_{st}} - T_{st}\right)$$

$$+ \varepsilon_{hs}\sigma(L_{hs}W_{hs})\left(\frac{2}{\pi\frac{L_{hs}}{L_{hs\_st}}\frac{W_{hs}}{L_{hs\_st}}}\left\{ln\left[\frac{(1+L_{hs}^2)(1+W_{hs}^2)}{1+L_{hs}^2+W_{hs}^2}\right]^{\frac{1}{2}}\right.\right.$$

$$+ L_{hs}(1+W_{hs}^2)^{\frac{1}{2}}tan^{-1}\frac{L_{hs}}{(1+W_{hs}^2)^{\frac{1}{2}}}$$

$$+ W_{hs}(1+L_{hs}^2)^{\frac{1}{2}}tan^{-1}\frac{W_{hs}}{(1+L_{hs}^2)^{\frac{1}{2}}} - (L_{hs})tan^{-1}(L_{hs})$$

$$\left.\left.- (W_{hs})tan^{-1}(W_{hs})\right\}\right)T_{hsu}^4$$

$$- (1-\varepsilon_{st})\varepsilon_{hs}\sigma(L_{hs}W_{hs})\left(\frac{2}{\pi\frac{L_{hs}}{L_{hs\_st}}\frac{W_{hs}}{L_{hs\_st}}}\left\{ln\left[\frac{(1+L_{hs}^2)(1+W_{hs}^2)}{1+L_{hs}^2+W_{hs}^2}\right]^{1/2}\right.\right.$$

$$+ L_{hs}(1+W_{hs}^2)^{\frac{1}{2}}tan^{-1}\frac{L_{hs}}{(1+W_{hs}^2)^{\frac{1}{2}}}$$

$$+ W_{hs}(1+L_{hs}^2)^{\frac{1}{2}}tan^{-1}\frac{W_{hs}}{(1+L_{hs}^2)^{\frac{1}{2}}} - (L_{hs})tan^{-1}(L_{hs})$$

$$\left.\left.- (W_{hs})tan^{-1}(W_{hs})\right\}\right)T_{hsu}^4 - \varepsilon_{st}\sigma(L_{st}W_{st})T_{st}^4$$

Approximation of Nominal Values of Input Parameters

Convection Heat Transfer Coefficients

The convection heat transfer coefficients were calculated by the RadTherm software

package with the "Automatic Convection Type". This method was applied so that the

results can be directly compared to the subsequent DFSS analysis of the underbody

system completed using RadTherm.

RadTherm calculated the convection heat transfer coefficients using the equations for

parallel flow over a flat plate. The typical Reynolds number used for the transition point

is 500,000. However, RadTherm assumes that the flow transitions from laminar to

turbulent at a Reynolds value of 100,000 to account for the fact that the surface and the

airflow is not completely smooth (ThermoAnalytics, 2014).

An average Nusselt number was calculated to take into account forced convection,

natural horizontal plate convection, and natural vertical plate convection. In RadTherm,

the convection coefficients are calculated for each individual element. For this analysis,

the average convection heat transfer coefficient for the part was used.

Temperatures

Muffler Surface

The muffler surface was assumed to have a uniform surface temperature. The vehicle was

modelled based on NAFTA Davis Dam conditions and a muffler average surface

temperature of 600 K was deemed appropriate. This temperature will vary based on

driving conditions which presents another source of uncertainty to be analyzed by the

FAST method.

Air Flow over Heat Shield Upper Surface and Lower Surface

The temperatures used for this specific analysis were determined based on the NAFTA

Davis Dam conditions but it is important to consider other driving conditions as well. The

temperature of the air flowing over the heat shield depends on environmental conditions

and can vary greatly depending on the location that the vehicle is being used. This

presents another interesting source of uncertainty to be analyzed by the FAST method.

The temperature of the air closer to the muffler is higher than the air above the heat shield

because the heat shield creates a barrier between the air and the muffler. For this analysis,

the air flowing over the lower surface of the heat shield was approximated as 330 K and

the air flowing on the upper surface of the heat shield was approximated as 320 K.

Air Flow over Spare Tire Tub

As the distance from the muffler increases, the temperature is expected to decrease. The

air flowing over the spare tire tub is at the greatest distance from the muffler and was

approximated as 315 K which is a slightly lower temperature than the air flowing over

the heat shield.

Emissivities

Muffler

For this model, the muffler was assumed to have a clean and smooth surface; thus, a low

emissivity of 0.2. This represents the condition of the muffler when it is first installed on

the vehicle. However, as the surface of the muffler oxidizes it becomes darker and the

emissivity can increase drastically. Consequently, the muffler will emit greater amounts

of energy to the surrounding components and increase the component temperatures. It is

important to take this effect in to account when designing the components to ensure that they have the ability to withstand higher thermal loads over time. This is an interesting source of uncertainty which will be analyzed by the FAST method.

Spare Tire Tub

The same considerations which were taken for the muffler emissivity must be applied to the spare tire tub emissivity. However, the spare tire tub emissivity typically begins at 0.9 and the maximum emissivity, for a black body, is 1. Thus, the spare tire tub presents less potential variation as the vehicle is used. This uncertainty will still be considered by the FAST method but it is expected to have less influence on the temperature of the spare tire tub.

Heat Shield

The heat shield emissivity typically begins at approximately 0.45; thus, there is some potential for this value to increase over time. This uncertainty will be analyzed by the FAST method.

Densities

Spare Tire Tub

The spare tire tub was assumed to be made of steel with a density of approximately 7700 kg/m^3.

Heat Shield

The heat shield was modeled as a three-layer heat shield consisting of two aluminum layers surrounding a layer of fiberglass. The aluminum was assumed to have a density of 2800 kg/m^3 and the fiberglass was assumed to have a density of 1300 kg/m^3.

Specific Heat Capacities

Spare Tire Tub

The spare tire tub was assumed to be made of steel with a specific heat capacity of approximately 461 $\frac{J}{kg\ K}$.

Heat Shield

The outer layers of the heat shield were assumed to be made of aluminum with a specific heat capacity of approximately 884 $\frac{J}{kg\ K}$.

Effects of Uncertainty on Thermal Performance

The first investigation using the FAST method was to study the overall effect of varying degrees of uncertainty on the thermal performance of the spare tire tub. Three cases were investigated in which each parameter was assigned the same percentage of uncertainty around the nominal value. The first case was for low uncertainty, in which each parameter was assigned an uncertainty of +/- 1%. In the second case, each parameter was assigned an uncertainty of +/- 10%. In the third case, which represented a situation in which there is high uncertainty, each parameter was assigned an uncertainty of +/- 30%.

The results from this investigation are shown in Figure 6. The parameters along the x-axis correspond to those shown in Table 1 on page 22.
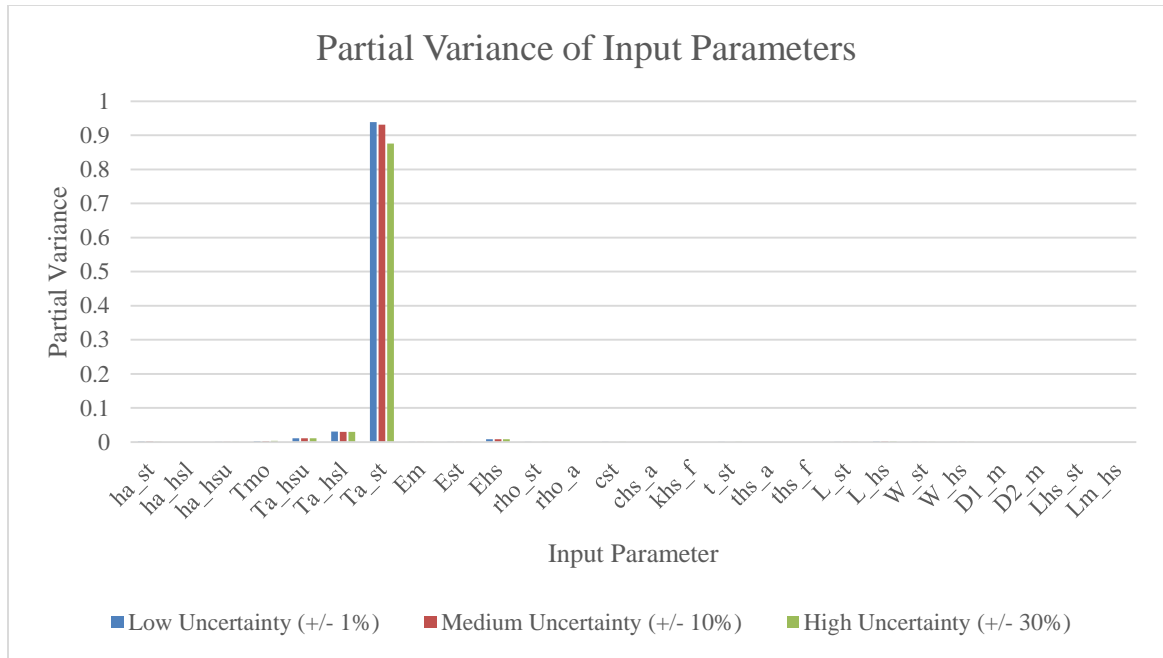
Figure 6 - Partial Variance of Input Parameters for Low, Medium, and High Uncertainty

The temperature of the air flow over the spare tire tub is responsible for the majority of the variation of the spare tire tub temperature. The second most influential parameter is the temperature of the airflow over the lower surface of the heat shield. These results are reasonable but may not help to improve the design because the temperature of the air cannot be easily manipulated. These parameters depend mainly on the environmental conditions which are out of the designer's control without employing an expensive and impractical solution. It can be noted from this investigation that increasing the uncertainty of all the parameters caused the partial variance of the temperature of the airflow over the spare tire tub to decrease. This may suggest that this temperature becomes less significant as the uncertainty of the design rises.

To produce a more meaningful result, the input parameters were separated into control factors, noise factors, and input factors. Control factors are the parameters which can be

controlled under normal operating conditions whereas noise factors are the parameters which the designer is incapable or unwilling to control under normal operating conditions (Czitrom & Spagon, 1997).

The input signal for this system was considered to be the temperature of the muffler surface. This parameter is the result of the exhaust gas temperature which is an output from the engine. The exhaust system must be adequately designed to handle this input.

The temperature of the air was considered as a noise factor. The air temperature depends mainly on the environment and is difficult to control. The heat transfer coefficients were also considered as noise factors because they depend on the characteristics of the air flow which are difficult to manipulate.

The emissivities of the muffler, heat shield, and spare tire tub were considered as control factors because there are possible design solutions which can control the emissivity of these surfaces such as corrosion resistant coatings. The densities, specific heat capacities, and thermal conductivities were considered as control factors because they can be easily changed by using a different material. The thicknesses, lengths, widths, diameters, and clearances were also considered as control factors because they are determined by the designer.

The results from the FAST analysis, considering the control factors, is shown in Figure 7.
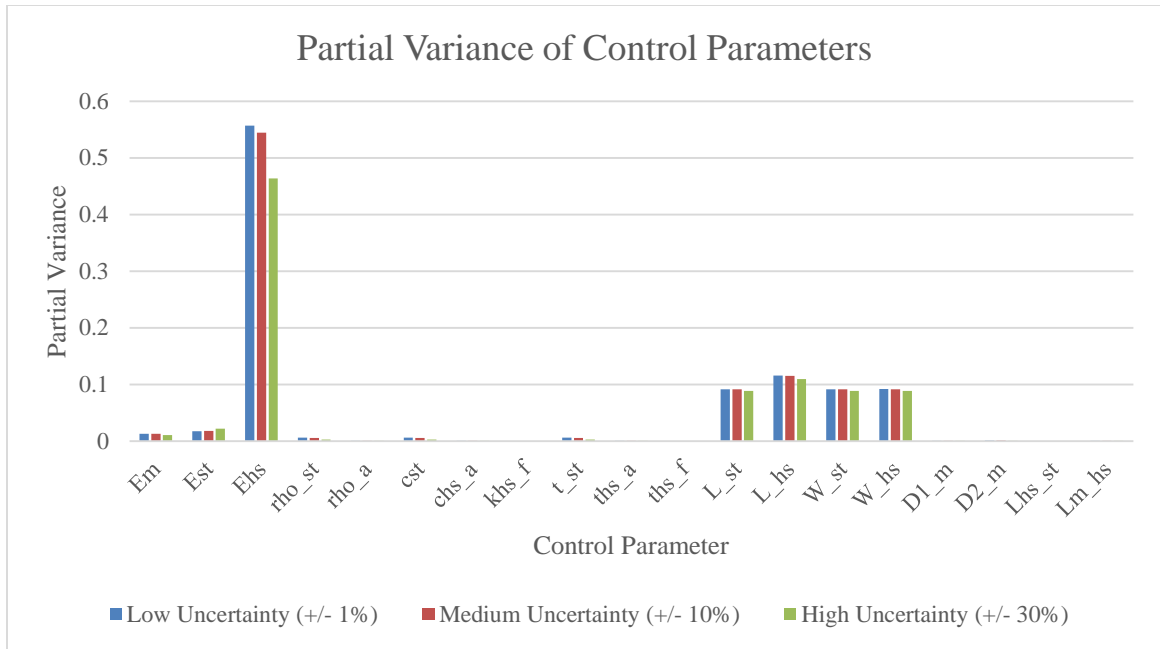
Figure 7 - Partial Variance of Control Parameters at Low, Medium, and High

Uncertainty

By focusing on the control factors, it is possible to see that the highest partial variance is attributed to the emissivity of the heat shield. The second highest partial variance is credited to the length of the heat shield which is the longitudinal dimension of the heat shield. The length and width of the spare tire tub, and the width of the heat shield have approximately the same partial variance. There are five other parameters which have very low partial variance; emissivity of the spare tire tub, emissivity of the muffler, density of the spare tire tub, thickness of the spare tire tub, and specific heat capacity of the spare tire tub. The rest of the parameters have negligible partial variance. At high uncertainty, the parameters with the highest partial variance exhibit a slight reduction in partial variance whereas the parameters that begin with very low partial variance show a slight rise in partial variance.

This study identified the emissivity of the heat shield, the length and width of the spare tire tub, and the length and width of the heat shield as the most influential parameters on the uncertainty of the parameter of interest. However, a further study must be conducted because, in reality, the uncertainty of each input parameter is not equal. For example, the thickness of the heat shield has relatively low uncertainty because it only varies based on manufacturing tolerances. By contrast, the temperature of the air may vary greatly depending on the environmental conditions. Thus, an evaluation of the amount of uncertainty in each parameter is required based on how the nominal value was obtained and/or how much the nominal value is known to vary in the customer environment. Through this study, it is possible to understand the effect of each parameter's uncertainty on the thermal performance on the spare tire tub.

Evaluation of Uncertainty of Input Parameters

Convection Heat Transfer Coefficients

The convection heat transfer coefficients have a high amount of uncertainty and it is difficult to estimate. This uncertainty arises because the heat transfer coefficients are calculated based on many uncertain measured parameters. These include the fluid properties (dynamic viscosity, thermal conductivity, density, and specific heat capacity) as well as the fluid velocity (Cengel & Ghajar, 2014). For this application, the fluid velocity can vary significantly as the vehicle is driven at different speeds and in different environments. To determine a suitable uncertainty range, it is helpful to examine the non-dimensional form of the parameter, the Nusselt number.

$$Nu = \frac{hL_c}{k}$$

The expression for the Nusselt number depends on the flow regime. Thus, the critical

distance "x_{cr}" at which the flow becomes turbulent must be calculated and compared to

the actual length. As mentioned earlier, the critical Reynolds number was taken as

100,000 to account for the fact that the surface and the airflow is not completely smooth

(ThermoAnalytics, 2014).

Approximating the air flow over the heat shield and spare tire tub as a parallel flow over

a flat plate, the critical distance can be calculated using the following equations taken

from "*Heat and Mass Transfer: Fundamentals and Applications*" (Cengel & Ghajar,

2014). First, the calculation for the lower surface of the heat shield are shown. This

calculation is followed by the calculation of the uncertainty in the heat transfer

coefficient for the lower surface of the heat shield. The calculations for the upper heat

shield and the spare tire tub can be found in Appendix A on page 110.

Heat Transfer Coefficient for Airflow over Lower Surface of Heat Shield

Critical Distance, "x_{cr}", for Air Flow over Lower Surface of Heat Shield

$$Re_{cr} = \frac{\rho V x_{cr}}{\mu} = 100{,}000$$

Each of these parameters (density, velocity, and dynamic viscosity) must be estimated to

determine the flow regime. For the airflow over the lower surface of the heat shield, the

density can be determined based on the nominal value of the air temperature which is estimated as 330 K. From the *"Engineering Toolbox"* (Engineering Toolbox, n.d.), the air density was found to be 1.075 $\frac{kg}{m^3}$. The dynamic viscosity was found from the same source, based on the air temperature, to be 1.985 x 10^{-5} $\frac{kg}{m\,s}$. The velocity of the air was assumed to be 4.5 $\frac{m}{s}$ to take into account the underbody components closer to the front of the vehicle which will reduce the airflow which is able to reach the rear underbody components. Thus, the critical distance was calculated as follows.

Equation 73

$$x_{cr} = \frac{Re_{cr}\mu}{\rho V} = \frac{(100{,}000)(1.985 \text{ x } 10^{-5}\,\frac{kg}{m\,s})}{(1.075\frac{kg}{m^3})(4.5\,\frac{m}{s})} = 0.41\ m$$

The critical distance at which the flow transitions from laminar to turbulent is less than the entire length of the heat shield in this model; therefore, the flow will be considered to transition to turbulent before reaching the end of the heat shield. Therefore, the appropriate Nusselt correlation to use, from "*Heat and Mass Transfer: Fundamentals and Applications*" (Cengel & Ghajar, 2014), is shown below:

Equation 74

$$Nu = (0.037Re_L{}^{0.8} - 871)Pr^{1/3}$$

Thus, the equation for the convection heat transfer coefficient for the airflow over the lower surface of the heat shield is obtained as:

Equation 75

$$h = \frac{(0.037Re_L{}^{0.8} - 871)Pr^{1/3}k}{L_c}$$

Now that the equation has been determined, the formula for error propagation can be applied to investigate how the uncertainty of the Reynolds number, Prandtl number, thermal conductivity, and characteristic length contribute to the uncertainty of the convection heat transfer coefficient. As presented earlier, the equation proposed by Kline and McClintock (Kline & McClintock, Mechanical Engineering), shown below, will be used to determine the uncertainty in the heat transfer coefficient.

Equation 76

$$\partial F = \sqrt{\left(\frac{\partial F}{\partial x_1}\partial x_1\right)^2 + \left(\frac{\partial F}{\partial x_2}\partial x_2\right)^2 + \left(\frac{\partial F}{\partial x_3}\partial x_3\right)^2 + \cdots}$$

Substituting the parameters involved in the convection heat transfer coefficient formula provides the formula below.

Equation 77

$$\delta h = \sqrt{\left(\frac{\partial h}{\partial Re_L}\delta Re_L\right)^2 + \left(\frac{\partial h}{\partial Pr}\delta Pr\right)^2 + \left(\frac{\partial h}{\partial k}\delta k\right)^2 + \left(\frac{\partial h}{\partial L_c}\delta L_c\right)^2}$$

To solve for the uncertainty in the heat transfer coefficient, each of the partial derivatives must be computed and a value must be defined for the uncertainty of each parameter.

Heat Transfer Coefficient (for Airflow over Lower Surface of Heat Shield) Partial

Derivative With Respect to Reynolds Number

The partial derivative which is solved below is that of the heat transfer coefficient with

respect to the local Reynolds number. In this case, the partial derivative can be easily

found based on the heat transfer coefficient equation determined earlier (Equation 75).

Equation 78

$$\frac{\partial h}{\partial Re_L} = \frac{0.037(0.8)Re^{-0.2}Pr^{1/3}k}{L_c}$$

The local Reynolds number at the trailing edge of the heat shield is calculated below in

Equation 79. The density, velocity, and dynamic viscosity were determined in the

previous section. The distance to the trailing edge, x, was estimated to be 0.45 m. These

values were used to calculate the Reynolds number, as shown below.

Equation 79

$$Re_L = \frac{\rho V x}{\mu} = \frac{\left(1.075 \ \frac{kg}{m^3}\right)\left(4.5 \ \frac{m}{s}\right)(0.45 \ m)}{\left(1.985 \ x \ 10^{-5} \frac{kg}{m \ s}\right)} = 109666$$

The Prandtl number and thermal conductivity for the air were found from the

"Engineering Toolbox" for a temperature of 330 K to be 0.709 and 0.0279 $\frac{W}{m \ K}$,

respectively. For a flat plate, the characteristic length, L_c, is the distance from the leading

edge which, for this model, is 0.45 m. Substituting these values in to Equation 80

provides the value for this partial derivative:

Equation 80

$$\frac{\partial h}{\partial Re_L} = \frac{(0.037)(0.8)(109666)^{-0.2}(0.709)^{1/3}\left(0.0279\ \frac{W}{m\ K}\right)}{(0.45\ m)} = 0.000161\ \frac{W}{m^2\ K}$$

Heat Transfer Coefficient (for Airflow over Lower Surface of Heat Shield) Partial

Derivative With Respect to Prandtl Number

The next partial derivative to be calculated is the heat transfer coefficient with respect to

the Prandtl number. The derivate is shown below in Equation 81.

Equation 81

$$\frac{\partial h}{\partial Pr} = \frac{0.037 Re_L{}^{0.8}\left(\frac{1}{3}\right)Pr^{-2/3}k}{L_c} - \frac{871\left(\frac{1}{3}\right)Pr^{-\frac{2}{3}}k}{L_c}$$

$$= \frac{0.037(109666)^{0.8}\left(\frac{1}{3}\right)(0.709)^{-\frac{2}{3}}\left(0.0279\ \frac{W}{m\ K}\right)}{(0.45\ m)}$$

$$- \frac{871\left(\frac{1}{3}\right)(0.709)^{-\frac{2}{3}}\left(0.0279\ \frac{W}{m\ K}\right)}{(0.45\ m)} = -12.285\ \frac{W}{m^2\ K}$$

Heat Transfer Coefficient (for Airflow over Lower Surface of Heat Shield) Partial

Derivative With Respect to Thermal Conductivity

The next partial derivative to be calculated is the heat transfer coefficient with respect to

the thermal conductivity.

Equation 82

$$\frac{\partial h}{\partial k} = \frac{(0.037 Re_L{}^{0.8} - 871)Pr^{1/3}}{L_c} = \frac{((0.037)(109666)^{0.8} - 871)(0.709)^{1/3}}{(0.45\ m)}$$

$$= -936.585 \frac{1}{m}$$

Heat Transfer Coefficient (for Airflow over Lower Surface of Heat Shield) Partial

Derivative With Respect to Characteristic Length

The final partial derivative to be calculated is the heat transfer coefficient with respect to

the characteristic length.

Equation 83

$$\frac{\partial h}{\partial L_c} = \frac{-(0.037 Re_L{}^{0.8} - 871)Pr^{1/3} k}{(L_c{}^2)}$$

$$= \frac{(-(0.037)(109666)^{0.8} - 871)(0.709)^{\frac{1}{3}}(0.0279\ \frac{W}{m\ K})}{(0.45\ m)^2}$$

$$= 58.068\ \frac{W}{m^3\ K}$$

The next step is to determine the appropriate value of uncertainty for the Reynolds

number, Prandtl number, thermal conductivity, and characteristic length.

Reynolds Number (for Airflow over Lower Surface of Heat Shield) Uncertainty

Analysis

The error propagation equation was applied to the Reynolds number to determine the

uncertainty in the Reynolds number.

Equation 84

$$\delta Re = \sqrt{\left(\frac{\partial Re}{\partial \rho}\delta\rho\right)^2 + \left(\frac{\partial Re}{\partial V}\delta V\right)^2 + \left(\frac{\partial Re}{\partial L}\delta L\right)^2 + \left(\frac{\partial Re}{\partial \mu}\delta\mu\right)^2}$$

Reynolds Number Partial Derivative With Respect to Density

Equation 85

$$\frac{\partial Re}{\partial \rho} = \frac{VL}{\mu} = \frac{(4.5\,\frac{m}{s})(0.45\,m)}{(1.985\ x\ 10^{-5}\,\frac{kg}{m\,s})} = 102015.113\,\frac{m^3}{kg}$$

Reynolds Number Partial Derivative With Respect to Air Velocity

Equation 86

$$\frac{\partial Re}{\partial V} = \frac{\rho L}{\mu} = \frac{(1.075\,\frac{kg}{m^3})(0.45\,m)}{(1.985\ x\ 10^{-5}\,\frac{kg}{m\,s})} = 24370.277\,\frac{s}{m}$$

Reynolds Number Partial Derivative With Respect to Length

Equation 87

$$\frac{\partial Re}{\partial L} = \frac{\rho V}{\mu} = \frac{(1.075\,\frac{kg}{m^3})(4.5\,\frac{m}{s})}{(1.985\ x\ 10^{-5}\,\frac{kg}{m\,s})} = 243702.771\,\frac{1}{m}$$

Reynolds Number Partial Derivative With Respect to Dynamic Viscosity

Equation 88

$$\frac{\partial Re}{\partial \mu} = \frac{-\rho VL}{\mu^2} = \frac{-(1.075\,\frac{kg}{m^3})(4.5\,\frac{m}{s})(0.45\,m)}{(1.985\ x\ 10^{-5}\,\frac{kg}{m\,s})^2} = -5524747949\,\frac{m\,s}{kg}$$

The next step to evaluate the uncertainty in the Reynolds number is to evaluate the uncertainty in the air density, velocity, dynamic viscosity, and the length of the heat shield.

Air Density Uncertainty

The air density has uncertainty which is related to the variation in air temperature depending on the location of the driven vehicle and the environment. A temperature uncertainty range, defined in Section "Temperatures" on page 65, of 299 K to 366 K was utilized. Examining the variation in air density over this temperature range, the "*Engineering Toolbox*" (Engineering Toolbox, n.d.) shows that the density may vary from $1.18 \frac{kg}{m^3}$ at low air temperatures to $1.05 \frac{kg}{m^3}$ at high air temperatures. This represents a 10% increase in air density above the nominal value and a -10% decrease below the nominal value. Thus, an uncertainty range will be used for this analysis of +/-10%; thus, $\delta\rho$ is equal to $0.111 \frac{kg}{m^3}$.

Air Velocity Uncertainty

Air velocity is another parameter which varies because of environmental conditions but also depends greatly on the speed of the driven vehicle; therefore, some assumptions must be made. Supposing that this vehicle may be at standstill or driven on the highway and can also be located in an area with calm to stormy conditions, it will be assumed that the air velocity may vary +/-50% around the nominal value of 4.5 m/s. Thus, δV is equal to 2.25 m/s. This results in a potential variation of air velocity between 2.25 m/s to 6.75 m/s. According to the Beaufort scale (Beaufort, 2015), this corresponds to the variation between a light breeze and a moderate breeze. This may not appear to be enough

variation, but it must also be noted that there are underbody components near the front of the vehicle which block the air flow from reaching the rear underbody components being investigated.

Heat Shield Length Uncertainty

The uncertainty in the length of the heat shield arises from the manufacturing process and depends on the tolerances of the process. The nominal value for the length of the heat shield is 0.45 m. Assuming a variation of +/- 0.0002 m around this nominal value will result in a potential length variation between 0.4498 m and 0.4502 m. In this case, δL is equal to 0.0002 m.

Dynamic Viscosity Uncertainty

The uncertainty in the dynamic viscosity can be determined by the same approach used for the air density uncertainty. The air temperature is assumed to range from 299 K to 366 K. Therefore, the dynamic viscosity, read from the "Engineering Toolbox" (Engineering Toolbox, n.d.), may range between $1.846 \; x \; 10^{-5} \frac{kg}{m \, s}$ to $2.181 \; x \; 10^{-5} \frac{kg}{m \, s}$. This corresponds to an increase of 10% above the nominal value and a decrease of 7% below the nominal value. Therefore, an uncertainty of +/- 9% was assumed. Thus, $\delta \mu$ is equal to $0.1787 \; x \; 10^{-5}$.

Substituting the partial derivatives and uncertainty values in to the error propagation equation (Equation 89), an estimate of the uncertainty in the Reynolds number was found.

Equation 89

δRe

$$
= \sqrt{\begin{aligned} &\left(\left(102015.113\,\frac{m^3}{kg}\right)\left(0.111\,\frac{kg}{m^3}\right)\right)^2 + \left(\left(24370.277\,\frac{s}{m}\right)\left(2.25\,\frac{m}{s}\right)\right)^2 \\ &+ \left(\left(243702.771\,\frac{1}{m}\right)(0.0002\,m)\right)^2 + \left(\left(-5524747949\,\frac{m\,s}{kg}\right)\left(0.1787\,x\,10^{-5}\,\frac{kg}{m\,s}\right)\right)^2 \end{aligned}}
$$

$= 56854$

This value is extremely high; however, it is meant to represent the variation in the Reynolds number over all possible operating conditions and environments. With this consideration, it seems appropriate for this value to be high.

Referring back to Equation 77, the uncertainty in the Prandtl number and thermal conductivity must be estimated. The uncertainty in the length of the heat shield has already been estimated to calculate the uncertainty in the Reynolds number.

Prandtl Number of Air Uncertainty

The Prandtl number of the air depends on the air temperature. Following the same considerations as for air density and dynamic viscosity, an approximate uncertainty range may be developed. The air temperature range was determined to be 299 K to 366 K. Therefore, from the *"Engineering Toolbox"* (Engineering Toolbox, n.d.) the Prandtl number may vary between 0.713 at low air temperatures to 0.703 at high air temperatures. These values correspond to an increase of 0.6% above the nominal value and a 0.8% decrease below the nominal value. For simplicity, a symmetric uncertainty of +/-0.7% was applied. Therefore, δPr is equal to 0.00496.

Thermal Conductivity of Air Uncertainty

The thermal conductivity of the air depends on the air temperature. The air temperature range was assumed to be 299 K to 366 K. Thus, from the *"Engineering Toolbox"* (Engineering Toolbox, n.d.)*,* the thermal conductivity may vary between $0.0257 \frac{W}{m\,K}$ and $0.0314 \frac{W}{m\,K}$. This corresponds to an increase of 13% above the nominal value and a decrease of 8% below the nominal value. For simplicity, a symmetric uncertainty of +/- 10% was assumed. Thus, δk is equal to 0.00279.

Finally, the partial derivatives and uncertainty values can be substituted into Equation 76 to find the uncertainty in the heat transfer coefficient.

Equation 90

$$\delta h = \sqrt{\left(\frac{\partial h}{\partial Re_L}\delta Re_L\right)^2 + \left(\frac{\partial h}{\partial Pr}\delta Pr\right)^2 + \left(\frac{\partial h}{\partial k}\delta k\right)^2 + \left(\frac{\partial h}{\partial L_c}\delta L_c\right)^2}$$

$$= \sqrt{\begin{array}{l}\left((0.000161\frac{W}{m^2\,K})(56854)\right)^2 + \left(\left(-12.285\frac{W}{m^2\,K}\right)(0.00496)\right)^2 \\ + \left(\left(-936.585\frac{1}{m}\right)(0.00279\frac{W}{m\,K})\right)^2 + \left(\left(58.068\frac{W}{m^3\,K}\right)(0.0002\,m)\right)^2\end{array}}$$

$$= 10\frac{W}{m^2\,K}$$

Thus, the uncertainty in the heat transfer coefficient for the airflow over the lower surface of heat shield is +/- $10\frac{W}{m^2\,K}$. As the nominal value for this coefficient was $13\frac{W}{m^2\,K}$, the potential range for this parameter is $3\frac{W}{m^2\,K}$ to $23\frac{W}{m^2\,K}$.

The same method was used to calculate the uncertainty range for the heat transfer coefficients over the upper surface of the heat shield and the spare tire tub. For the upper surface of the heat shield, the uncertainty range was found to be $+/- 2 \frac{W}{m^2\,K}$. In this case, the nominal value was $7 \frac{W}{m^2\,K}$ so the potential range for this parameter is $5 \frac{W}{m^2\,K}$ to $9 \frac{W}{m^2\,K}$. For the heat transfer coefficient for the airflow over the spare tire tub, the uncertainty range was calculated to be $+/- 3 \frac{W}{m^2\,K}$. The nominal value for this coefficient was $10 \frac{W}{m^2\,K}$. Therefore, the potential range for this parameter is $7 \frac{W}{m^2\,K}$ to $13 \frac{W}{m^2\,K}$. The calculations for these uncertainty ranges are shown in Appendix A.

Temperatures

Assigning an uncertainty range for the airflow temperature is difficult because it depends on the location where the vehicle is being driven. In any case, it is very important that the vehicle is designed to withstand the temperatures which it will be exposed to. Assuming that the vehicle will be driven in the United States of America, it is possible to examine previous climate records to determine a suitable range. The highest temperature ever recorded in the USA was 134 °F (329.8 K) in Death Valley, California on July 10, 1913 (Thompson, 2011). The lowest temperature ever recorded in the USA was -79.8 °F (211.0 K) at the Prospect Creek Camp in the Endicott Mountains of northern Alaska on February 3, 1947 (Weather Temperature Extremes in the United States, 2007). To consider this entire temperature range would be impractical and unnecessary because these extreme temperatures are especially rare. Also, it must be noted that the temperature being considered is that of the air flowing over the muffler; therefore, the temperature will be elevated from ambient conditions. For this analysis, it was decided to assign an

uncertainty of +/- 10% around the nominal value. As an example, for the airflow over the lower surface of the heat shield, this amount of uncertainty results in a range of 299 K (78.5 °F) and 366 K (199.1 °F).

Emissivities

A blackbody is defined as a surface which emits and absorbs the highest amount of radiation of any surface at a defined temperature. Emissivity is the ratio between the radiation emitted by a surface and the radiation emitted by a blackbody at the same temperature (Cengel & Ghajar, 2014).

Equation 91

$$\varepsilon = \frac{Radiation\ Emitted\ by\ a\ Surface}{Radiation\ Emitted\ by\ a\ Blackbody}$$

Based on this definition, the emissivity of a surface must be a value between zero and one. As described in "*Heat and Mass Transfer: Fundamentals and Applications",* the uncertainty of the emissivity of a surface is significant because it is dependent on the surface condition. The surface condition will change due to factors such as cleanliness, oxidation, roughness, and type of finish (Cengel & Ghajar, 2014). Also, the emissivity of metals depends on temperature. Both of these sources of uncertainty are of high importance for this invesitgation of underbody components which are subject to high temperature variations and environmental wear and ageing.

Muffler Emissivity

The nominal value of muffler emissivity is 0.2. This value represents the newly installed muffler which is clean and smooth. However, the muffler is installed on the underbody of

the vehicle where it is exposed to oxidation. For this investigation, it is assumed that the emissivity of the muffler will increase from the nominal value of 0.2 up to a maximum value of 0.9.

Spare Tire Tub Emissivity

The spare tire tub is made of steel and the same considerations which were taken for the muffler should be applied. However, the emissivity of the spare tire tub begins at 0.9 and, as discussed earlier, the maximum emissivity is one. There is not much potential for the emissivity of the spare tire tub to increase. Thus, this uncertainty will be considered as negligible.

Heat Shield Emissivity

The outer surfaces of the heat shield are made of aluminum and there is potential for oxidation to occur. The emissivity of these surfaces have a nominal value of 0.45. Through the same considerations taken for the muffler surface, it was assumed that the heat shield emissivity may increase up to a maximum value of 0.9.

Densities

The nominal value for the densities of the spare tire tub and heat shield were found from the RadTherm library values for density of mild steel and aluminum. The library values are unlikely to be the exact values for the actual components; therefore, there is some uncertainty in these values. For this investigation, an uncertainty of +/-7% was assumed.

Specific Heat Capacities

The specific heat capacity of the spare tire tub and the heat shield nominal values were based on the RadTherm library. However, these values may not be exact representations

of the material of the component which produces some uncertainty. Therefore, the uncertainty for the specific heat capacity is estimated to be +/-7%.

Thermal Conductivities

The thermal conductivity of the fiberglass layer of the heat shield was found from the RadTherm library. This value does not perfectly represent the actual component material and therefore there is some uncertainty in this parameter. The uncertainty for thermal conductivity is estimated to be +/-7%.

Thicknesses

The thicknesses being considered are the thicknesses of the aluminum and fiberglass layers in the heat shield and the thickness of the spare tire tub. These thicknesses are important because they affect the conduction heat transfer through the heat shield as well as the mass of the components. As for all dimensional parameters in this investigation, an uncertainty of +/-0.0002 m was considered. This represents the variation due to manufacturing tolerances. Therefore, the thickness of the aluminum layers of the heat shield may vary from 0.000045 m to 0.000445 m and the thickness of the fiberglass layer of the heat shield may vary between 0.0038 m and 0.0042 m. The thickness of the spare tire tub may vary between 0.0013 m and 0.0017 m.

Lengths, Widths, and Diameters

The length and width of the spare tire tub and heat shield and the diameters of the muffler were assumed to have an uncertainty of +/- 0.0002 m based on manufacturing tolerances.

Clearances

The clearance between the components can vary due to errors in the manufacturing process. An uncertainty of +/-0.0002 m is assumed for this parameter.

Partial Variance Using Estimated Uncertainties

Using the estimated uncertainties for each parameter, the partial variance was calculated using the FAST method and plotted below in Figure 8. The parameter numbers along the x-axis correspond to those depicted in Table 1.Table 1
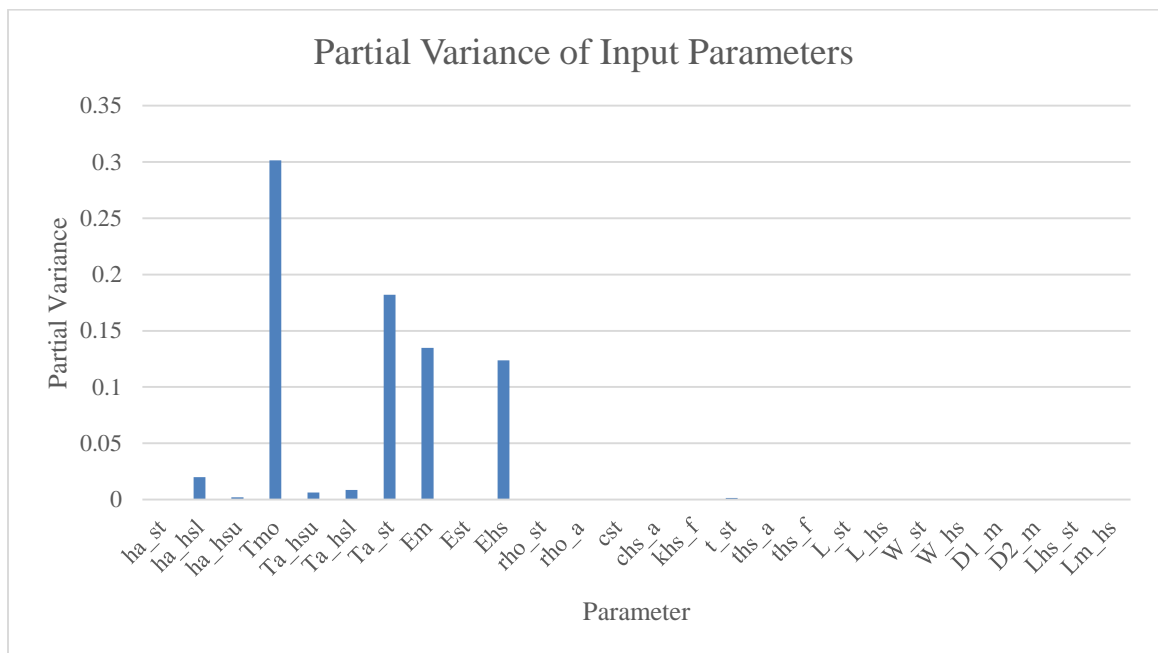
Figure 8 - Partial Variance of Input Parameters Using Estimated Uncertainty for Each Input Parameter

The temperature of the outer surface of the muffler is responsible for the majority of the variation of the spare tire tub temperature. The next most influential parameters were found to be the temperature of the air flowing over the spare tire tub as well as the emissivity of the muffler. A better understanding of the effect of the control factors can

be gained by removing the temperature of the muffler, the air temperatures, and the heat transfer coefficients from the FAST analysis, as shown below in Figure 9.
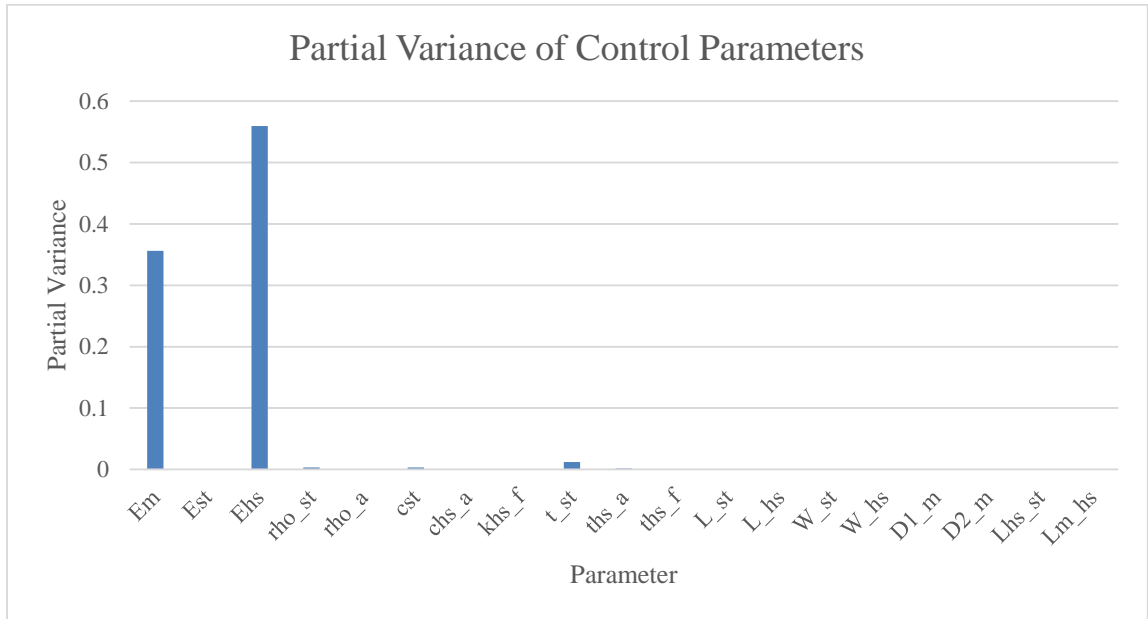
Figure 9 - Partial Variance of Control Parameters Using Estimated Uncertainty for Each

Input Parameter

Figure 9 shows the results from the FAST analysis applied to the control factors.

The top six most influential parameters on the variation of the spare tire tub temperature are listed below:

1) Emissivity of the heat shield

2) Emissivity of the muffler

3) Thickness of the spare tire tub

4) Density of the spare tire tub

5) Specific heat capacity of the spare tire tub

6) Thickness of the outer layers of the heat shield

These six control parameters are represented below in a pie chart to give a visual representation of each parameter's contribution to the total variance in the spare tire tub temperature. It is clear that the emissivity of the heat shield has a significant impact.

Partial Variance of Control Parameters

■ Em ■ Ehs ■ rho_st ■ cst ■ t_st ■ ths_a
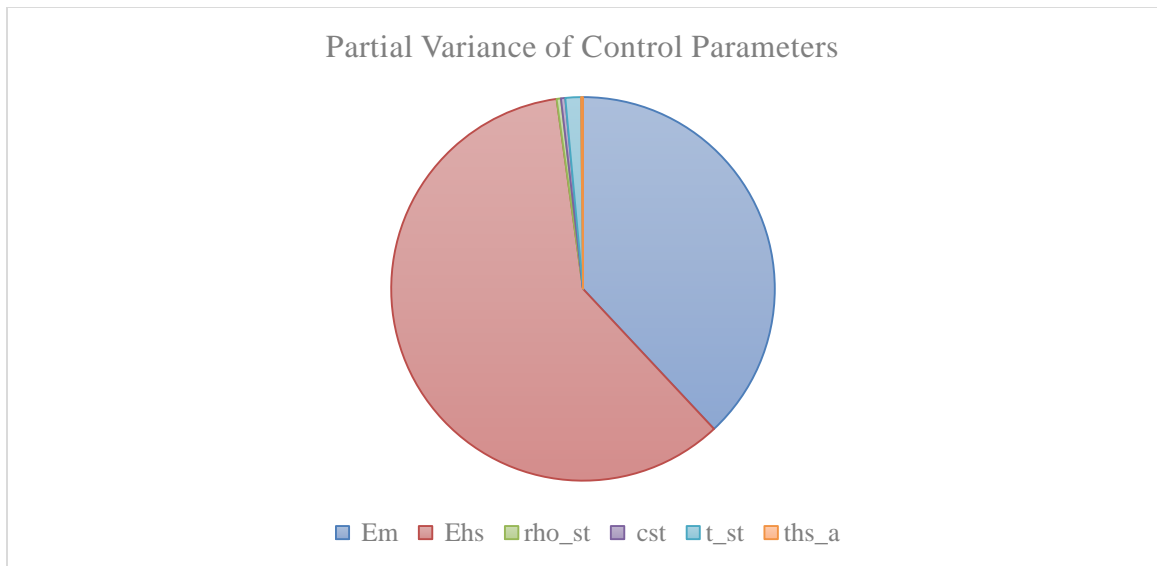
Figure 10 - Partial Variance of Control factors Using Estimated Uncertainty for Each Input Parameter

The FAST analysis has clearly defined the parameters which are the most influential on the system robustness. These control factors are studied further, in the next section, using DFSS. The DFSS study will distinguish the best settings for each of these important parameters to reduce the variability of the spare tire tub temperature and improve the thermal system robustness. The main advantage of this process is to form a robust design

71

early in the design process so that changes do not need to be made when the vehicle is near the production phase.

CHAPTER 5

DEVELOPMENT OF A METHOD TO INTERFACE THE RESULTS FROM FAST WITH DESIGN FOR SIX SIGMA (DFSS) TO ACHIEVE ROBUST DESIGN FOR THERMAL PROTECTION

As suggested by El-Sharkawy, to accomplish a robust design of thermal protection plans, the thermal analysis process should be coupled with techniques for robust design such as Design for Six Sigma (DFSS) (El-Sharkawy A. , Sensitivity and Uncertainty Analysis in Computational Thermal Models, 2014).

The application of DFSS to the underbody system surrounding the spare tire tub began with IOV (Identify opportunity, Optimize, Verify).

Step 1 – Identify Opportunity

An underbody system design is required to maintain spare tire tub temperature within a range that is acceptable for durability and performance of underbody components. The goal of this work is to create a robust process for development of underbody systems to meet spare tire tub temperature requirements.

In this system, the exhaust gases travel through the exhaust system at highly elevated temperatures. As a consequence of the second law of thermodynamics, heat is spontaneously transferred to the cooler surrounding components and the environment. In an ideal system, the heat would be transferred solely to the environment and the

surrounding components would be thermally protected. In the figure shown below, the energy emitted to the environment is plotted against the energy emitted from the muffler for an ideal design as well as an approximation of the current design. Ideally, the energy transferred to the environment is always equal to the energy emitted from the muffler resulting in a line with a slope of one. In this design, the performance is not ideal; consequently; the slope of this line is somewhere below one.
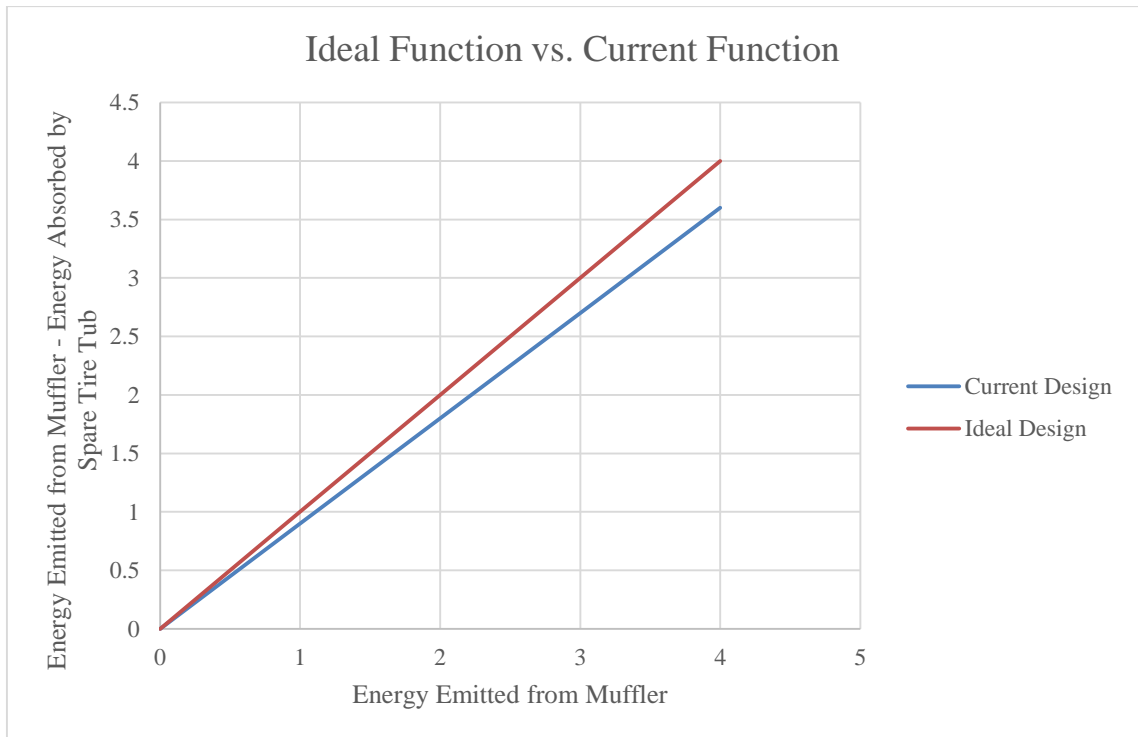
Figure 11 - Comparison between the Current Design and the Ideal Design

The difference between the current design and the ideal design presents an opportunity for improvement. As the design is improved, the energy emitted from the muffler will be emitted to the environment rather than the surrounding components including the spare tire tub.

Step 2 – Robust Optimization

The Signal-to-Noise Ratio is an indicator of robustness. A greater Signal-to-Noise ratio indicates higher robustness.

Equation 92

$$\frac{S}{N} = \frac{Efficiency}{Variability}$$

For this analysis, a dynamic analysis was utilized to calculate the signal-to-noise ratio. Thus, the following equation was applied to calculate the dynamic signal-to-noise ratio:

Equation 93

$$\frac{S}{N} = 10\log\left(\left(\frac{1}{r}\right)\left(\frac{(S_\beta - V_e)}{V_e}\right)\right)$$

Where:

r is the sum of squares of the input signal factor levels. In this case, the signal factor levels are the four surface temperatures of the muffler used in the simulations.

Equation 94

$$r = \sum_{i=1}^{n} M_i{}^2$$

S_β is the sum of squares of distance between zero and the least square best fit line (forced through zero) for each data point, also known as the power of the linear slope. A value of zero for this parameter, S_β, indicates that there is no response generated by the signal, M. S_β is calculated using the following formula.

Equation 95

$$S_\beta = \frac{(\sum_{i=1}^{n} M_i y_i)^2}{r}$$

Where:

M_i is the input signal (muffler surface temperature)

y_i is the output response (spare tire tub temperature)

V_e is the variance of the data points. This parameter is estimated by the formula below.

Equation 96

$$V_e = \frac{S_e}{n-1}$$

Where:

n is the number of data points. In this analysis, the number of data points is equal to four because each design was simulated four times.

S_e is the sum of squares of distance between individual data point to the least square best fit line. This parameter is also known as the power of noise and non-linearity. As this value increases, the variability due to noise also increases. S_e is calculated by the formula given below.

Equation 97

$$S_e = S_T - S_\beta$$

Where:

S_T is the total sum of squares of distance between zero to each data point. S_T is calculated as shown in the formula below.

Equation 98

$$S_T = \sum_{i=1}^{n} y_i{}^2$$

As discussed earlier in Section, "Analytical Model Development" on page 20, an analytical model was established which takes into account the heat transfer between the muffler, heat shield, and spare tire tub. This model determines the temperature of the spare tire tub. DFSS is used to determine the most effective combination of control factors to improve the robustness of the spare tire tub temperature.

Based on the analytical model developed, the input parameters were separated into control factors which are easily manipulated and the noise factors which are not possible to control and/or too expensive to control. The input signal for this analysis in the temperature of the muffler and the output is the temperature of the spare tire tub. The DFSS P-Diagram, shown in Figure 12, clearly displays this information.

Control Factors
Emissivity of Heat Shield
Emissivity of Muffler
Density of Spare Tire Tub Material
Specific Heat Capacity of Spare Tire Tub Material
Thickness of Spare Tire Tub
Thickness of Outer Layers of Heat Shield

Input Signal	System	Output Response
M: Muffler Temp.	Spare Tire Tub	y: Spare Tire Tub Temp.

Noise Factors
Temperature of Air Flow over Heat Shield and Spare Tire Tub
Heat Transfer Coefficients of Air Flow over Heat Shield and Spare Tire Tub

Figure 12 - DFSS P-Diagram (Parametric Diagram)

To improve the robustness of the spare tire tub temperature, the combination of control

factors which will allow the spare tire tub temperature to remain consistent during

variation in the noise factors and input signal must be determined. It is desirable to obtain

a design which will perform consistently and independently of the sources of noise. To

determine this set of control factors, an analysis was conducted using RadTherm software

package. This software is capable of simulating the temperature distribution over

complex component systems. A model of the rear underbody system, which was

previously studied analytically, was utilized. Thus, variations in the most influential

control factors could be made and the effect of these variations on the spare tire tub temperature could be observed.

One method to find the settings for the control factors which will lead to a robust design is to apply a full factorial design. By this method, every possible combination of the control factors is simulated and the set of parameters which led to the most robust design would be selected. However, this type of method requires a high number of simulations. For example, to simulate the eight control factors, with three settings for each, would require 6561 simulations.

To reduce the number of required simulations, an orthogonal array was used. To demonstrate the meaning of an orthogonal array, a simple example is given. If a test requires three control factors to be run using two different settings (i.e. two levels) each, then a full factorial design would require 27 simulations total. Rather, an orthogonal array, like the one shown below, may be used. In this table, the control factors are listed along the top row. Below each control parameter, the number represents the level for that control parameter for that specific simulation. Accordingly, for the first simulation, the three control factors are each set at their first level.

Table 2 - L4 Orthogonal Array

Simulation No.	Control Parameter 1	Control Parameter 2	Control Parameter 3
1	1	1	1
2	1	2	2
3	2	1	2
4	2	2	1

The orthogonal array is able to reduce the number of simulations from 27 to 4 because the columns are balanced. This means that within each control parameter column, the number of level 1's is equal to the number of level 2's. In the case shown above, there are two level 1's and two level 2's in each column. Also, comparing sets of columns, it is found that the combinations of control factors are present the same number of times. This means that between column 1 and 2, there is a combination of two level 1's, two combinations of level 1 and level 2, and one combination of two level 2's. There is an equal distribution of combinations between column 1 and 3 as well as column 2 and 3.

Based on the balance of the array, the effect of each control factor on the output can be found by taking an average of the simulations in which the control factor is at each level. For example, the result of control factor 1 at level 1 is equal to the average result of simulation 1 and 2. Since the other parameters exist an equal number of times at an equal number of levels within simulation 1 and 2, their effect is negated and the result is solely the effect of control factor 1.

To apply Dr. Taguchi's orthogonal array method to the underbody system case study, the levels for each control factor had to be decided. These levels allow the engineer to study potential design variations that he/she is interested in implementing. When applying the DFSS method, the feasibility and cost of each level must also be taken in to account. As a general rule suggested in Taguchi's Handbook, for every X dB which is gained through DFSS, one should spend X/2 dB to reduce costs or improve productivity (Taguchi, Chowdhury, & Wu, 2005). In this investigation, the levels were selected to demonstrate the process without considering implementation costs because this was out of the scope of the project.

Settings for each level were created to represent the "worst-case scenario" and the "best-case scenario" so that the control factors which allow the system to perform consistently well in both scenarios can be identified.

In the following tables, the "worst-case scenario" is denoted with the number "1". This means that the noise which will cause the system to perform poorly is written as "N1". The input signal which causes the system to perform poorly is given as "M1". In contrast, the "best-case scenario" is written as "2". Therefore, the noise and input signals which would cause the system to perform better are written as "N2" and "M2", respectively.

The sources of noise within the control parameters fall in to three categories including outer noise, inner noise, and between noise. Outer noise is due to environmental conditions, inner noise is due to age and deterioration, and between noise is due to variation in the manufacturing process.

Control Factors and Levels

Control Factor 1 - Emissivity of the Heat Shield

The first control factor is the emissivity of the heat shield. This control factor was assigned three levels. The first level represents the current design in which the emissivity begins at 0.45 and may increase, due to wear and ageing, up to 0.8. Therefore, this variation can be classified as inner noise. When the emissivity of the heat shield is high, it will emit more radiation to the surrounding components such as the spare tire tub. Therefore, the N1 condition was set at an emissivity of 0.8. The best-case scenario, the N2 condition, was set as an emissivity of 0.45 to represent a newly installed heat shield.

A second level for this factor was created to represent a heat shield with a corrosion resistant coating which reduces the amount by which the muffler emissivity increases to 0.55. Therefore, the worst-case scenario, N1, is a heat shield emissivity of 0.55. The N2 condition was the same as the best-case scenario for the first level which is a heat shield with an emissivity of 0.45.

A third level for this factor was created to represent a heat shield which has a dark coating applied to its surface. In this case, the emissivity of the heat shield would be high even when it is first installed on the vehicle. Oxidation of the surface of the heat shield would have no impact on the emissivity. Thus, the worst-case scenario and best-case scenario are both a heat shield with an emissivity of 0.99. These levels are displayed in the table below.

Table 3 - Levels of the Emissivity of the Heat Shield

Control Factors	Level	Nominal Value	Unit	Design Modification	Uncertainty	N1 (Worst Case)	N2 (Best Case)	Noise Type
Emissivity of Heat Shield	1	0.45	-	Current Design	-	0.8	0.45	Inner
	2	0.45	-	Corrosion Resistant Coating	-	0.55	0.45	
	3	0.99	-	Black Coating	-	0.99	0.99	

Control Factor 2 – Emissivity of the Muffler

The second control factor is the emissivity of the muffler. The three levels used for this control factor are the same as for the first control factor; current design, corrosion resistant coating, and black coating. However, the emissivity of the muffler is lower than the emissivity of the heat shield when it is first installed on the vehicle. Therefore, the best-case scenario is a lower emissivity of 0.2. Over time, the emissivity of the surface

will increase due to oxidation and may reach the same level as the emissivity of the heat shield. Therefore, the worst-case scenario for each of this control factors levels are the same as for the previous control factor. These levels are shown in the table below.

Table 4 - Levels of the Emissivity of the Muffler

Control Factors	Level	Nominal Value	Unit	Design Modification	Uncertainty	N1 (Worst Case)	N2 (Best Case)	Noise Type
Emissivity of Heat Shield	1	0.2	-	Current Design	-	0.8	0.2	Inner
	2	0.2	-	Corrosion Resistant Coating	-	0.3	0.2	
	3	0.99	-	Black Coating	-	0.99	0.99	

Control Factor 3 – Density of the Spare Tire Tub

The third control factor is the density of the spare tire tub. This control factor was assigned three levels. The first level represents the current design in which the spare tire tub is made of mild steel and has a nominal density of 7769 $\frac{kg}{m^3}$. The uncertainty in this value occurs for two reasons. The first reason is that the nominal value was read from a library in the RadTherm software package and may not perfectly represent the actual material. Also, the manufacturer of the spare tire tub may not always supply components with the exact same density. This is especially true for factors which are not tested to meet certain specifications.

The second level for this factor is used to represent the possibility of constructing a spare tire tub out of plastic. In this case, the density would have a lower nominal value but the uncertainty would remain the same. A third level represents a spare tire tub made of aluminum.

Table 5 - Levels of the Density of the Heat Shield

Control Factors	Level	Nominal Value	Unit	Design Modification	Uncertainty	N1 (Worst Case)	N2 (Best Case)	Noise Type
Density of Spare Tire Tub	1	7769	kg/m^3	Current Design - Mild Steel	7%	7225	8312	Between
	2	908	kg/m^3	Plastic	7%	844	971	
	3	2770	kg/m^3	Aluminum	7%	2576	2964	

Control Factor 4 – Specific Heat Capacity of the Spare Tire Tub

The fourth control factor is the specific heat capacity of the spare tire tub. The first level for this factor is the specific heat capacity of the spare tire tub in the current design (mild steel with a specific heat capacity of $460.97 \frac{J}{kg\ K}$). The second level for this control factor represents a spare tire tub made of plastic with a specific heat capacity of $1882.8 \frac{J}{kg\ K}$. The third level for this control factor is for a spare tire tub made of aluminum with a specific heat capacity of $884.25 \frac{J}{kg\ K}$. Each of these levels was assigned a +/-7% uncertainty around the nominal value to account for the uncertainty in the RadTherm material library as well as variation in manufacturing processes.

Table 6 - Levels of the Specific Heat Capacity of the Spare Tire Tub

Control Factors	Level	Nominal Value	Unit	Design Modification	Uncertainty	N1 (Worst Case)	N2 (Best Case)	Noise Type
Specific Heat Capacity of Spare Tire Tub	1	460.97	J/(kg K)	Current Design - Mild Steel	7%	428.70	493.23	Between
	2	1882.8	J/(kg K)	Plastic	7%	1751.00	2014.60	
	3	884.25	J/(kg K)	Aluminum	7%	822.35	946.15	

Control Factor 5 – Thickness of the Spare Tire Tub

The fifth control factor, the thickness of the spare tire tub, has three levels. The first level is for the current design in which the spare tire tub has a thickness of 0.0015 m. The second level is for a thinner spare tire tub with a thickness of 0.0012 m. The third level is for a thicker spare tire tub of thickness 0.0018 m. The uncertainty in the nominal value corresponds to a variation of +/- 0.0002 m.

Table 7 - Levels of the Thickness of the Spare Tire Tub

Control Factors	Level	Nominal Value	Unit	Design Modification	Uncertainty	N1 (Worst Case)	N2 (Best Case)	Noise Type
Thickness of Spare Tire Tub	1	0.0015	m	Current Design	13%	0.0013	0.0017	Between
	2	0.0012	m	Thinner Spare Tire Tub	17%	0.0010	0.0014	
	3	0.0018	m	Thicker Spare Tire Tub	11%	0.0016	0.0020	

Control Factor 6 – Thickness of the Outer Layers of the Heat Shield

The sixth control factor is the thickness of the outer layers of the heat shield. The current design thickness for these layers is 0.000254 m. The second level for this factor represents narrower layers and the third level represents thicker layers. An uncertainty of +/- 0.0002 m was assumed to exist for each of these three levels.

Table 8 - Levels of the Thickness of the Outer Layers of the Heat Shield

Control Factors	Level	Nominal Value	Unit	Design Modification	Uncertainty	N1 (Worst Case)	N2 (Best Case)	Noise Type
Thickness of Outer Layers of Heat Shield	1	0.000254	m	Current Design	79%	0.000054	0.000454	Between
	2	0.000229	m	Narrower Heat Shield	87%	0.0000286	0.000429	
	3	0.000279	m	Thicker Heat Shield	72%	0.0000794	0.000479	

These six control factors are summarized in the table below.

Table 9 - Control Factors and Levels

Control Factors	Level	Nominal Value	Unit	Design Modification	Uncertainty	N1 (Worst Case)	N2 (Best Case)	Noise Type
Emissivity of Heat Shield	1	0.45	-	Current Design	-	0.8	0.45	Inner
	2	0.45	-	Corrosion Resistant Coating	-	0.55	0.45	
	3	0.99	-	Painted Black	-	0.99	0.99	
Emissivity of Muffler	1	0.2	-	Current Design	-	0.80	0.20	Between
	2	0.2	-	Corrosion Resistant Coating	-	0.30	0.20	
	3	0.99	-	Painted Black	-	0.99	0.99	
Density of Spare Tire Tub Material	1	7768.9	kg/m^3	Current Design - Mild Steel	7%	7225.08	8312.72	Between
	2	908.25	kg/m^3	Plastic	7%	844.67	971.83	
	3	2770.09	kg/m^3	Aluminum	7%	2576.18	2964.00	
Specific Heat Capacity of Spare Tire Tub	1	460.97	J/(kg K)	Current Design - Mild Steel	7%	428.70	493.23	Between
	2	1882.8	J/(kg K)	Plastic	7%	1751.00	2014.60	
	3	884.25	J/(kg K)	Aluminum	7%	822.35	946.15	
Thickness of Spare Tire Tub	1	0.0015	m	Current Design	13%	0.0013	0.0017	Between
	2	0.0012	m	Narrower Spare Tire Tub	17%	0.001	0.0014	
	3	0.0018	m	Wider Spare Tire Tub	11%	0.0016	0.002	
Thickness of Outer Layers of Heat Shield	1	0.000254	m	Current Design - Aluminum Heat Shield Layers	79%	0.000054	0.000454	Between
	2	0.000229	m	Narrower Heat Shield	87%	0.0000286	0.000429	
	3	0.000279	m	Wider Heat Shield	72%	0.0000794	0.000479	

The noise factors for this design include the temperature of the underbody airflow as well as the velocity of the air. As discussed previously, these are the design parameters which the engineers cannot or do not want to control because it would be expensive or impractical to do so. As with the control factors, an N1 "worst-case scenario" and an N2 "best-case scenario" was assigned to each noise factor. These scenarios were evaluated based on the uncertainty ranges developed earlier for each factor. For the temperature of the air, the N1 condition was that the temperature rises 20% above the nominal value and the N2 condition was that the temperature dropped 20% below the nominal value. For the velocity of air, the N1 condition was that the air was travelling 50% slower than the nominal condition and the N2 condition was that the air was travelling 50% faster than the nominal condition. The table below shows the noise factors and their corresponding N1 and N2 conditions.

Table 10 - Noise Factors

Noise Factors	Component(s)	Nominal Value	Unit	Uncertainty	N1 (Worst Case)	N2 (Best Case)
Air Temperature	Air Flow Over Heat Shield Upper Surface	319.6	K	10%	351.6	287.6
	Air Flow Over Heat Shield Lower Surface	332.8	K	10%	366.1	299.5
	Air Flow Over Spare Tire Tub	317.0	K	10%	348.7	285.3
Air Velocity	Air to Spare Tire Tub	2.74	m/s	50%	1.37	4.11
	Air to Heat Shield Lower Surface (FRONT)	4.57	m/s	50%	2.28	6.85
	Air to Heat Shield Upper Surface (BACK)	2.64	m/s	50%	1.32	3.96

The input signal to the system is the surface temperature of the muffler. In reality, the surface temperature of the muffler varies drastically from one location to another. For this DFSS study, it was assumed that the muffler surface is isothermal at the average surface temperature. The worst-case scenario, M1 condition, is if the entire muffler surface raised to the temperature at the hottest location on the muffler surface. The M2 condition represents the entire muffler at the temperature at the coldest location on the muffler surface. These temperatures are shown in the table below.

Table 11 - Input Signal

Input Signal	Component(s)	Nominal Value	Unit	Uncertainty	M1 (Worst Case)	M2 (Best Case)
Muffler Surface Temperature	Muffler Surface	602.9	K	-	794.261	438.706

The next step in the application of DFSS was to place the control factors and corresponding levels into orthogonal arrays. Four arrays were required to represent four different noise and input signal conditions. The first condition is for worst-case input signal and worst-case noise (M1 & N1). The second condition is for worst-case input signal and best-case noise (M1 & N2). The third condition is best-case input signal and worst-case noise (M2 & N1). The fourth condition is best-case input signal and best-case noise (M2 & N2). As discussed earlier, this DFSS study will identify which control factor levels result in the most consistent spare tire tub temperature as the input signal and noise factors vary between best and worst case conditions.

Each orthogonal array requires 18 simulations. In this case, four orthogonal arrays were utilized (one for each of the noise and input signal conditions). Therefore, a total of 72 simulations was required. These orthogonal arrays are given below.

The first orthogonal array is for the N1 & M1 condition. For simulations 1 through 18:

- Each level of each control factor is set to the worst-case scenario (N1)

- Underbody air flow temperature is set to the worst-case scenario (N1)

- Underbody air velocity is set to the worst-case scenario (N1)

- Muffler surface temperature is set to the worst-case scenario (M1)

Table 12 - Orthogonal Array for N1 (Worst-Case Noise) and M1 (Worst-Case Input Signal) Condition

Run No.	A	B	C	D	E	F	Emissivity of Heat Shield	Emissivity of Muffler	Density of Spare Tire Tub Material	Specific Heat Capacity of Spare Tire Tub	Thickness of Spare Tire Tub	Thickness of Aluminum Layers of Heat Shield
1	1	1	1	1	1	1	0.8	0.8	7225.077	428.699	0.0013	0.000054
2	1	2	2	2	2	2	0.8	0.3	844.672	1751.004	0.001	0.0000286
3	1	3	3	3	3	3	0.8	0.99	2576.183	822.354	0.0016	0.0000794
4	2	1	1	2	2	3	0.55	0.8	7225.077	1751.004	0.001	0.0000794
5	2	2	2	3	3	1	0.55	0.3	844.672	822.354	0.0016	0.000054
6	2	3	3	1	1	2	0.55	0.99	2576.183	428.699	0.0013	0.0000286
7	3	1	2	1	3	2	0.99	0.8	844.672	428.699	0.0016	0.0000286
8	3	2	3	2	1	3	0.99	0.3	2576.183	1751.004	0.0013	0.0000794
9	3	3	1	3	2	1	0.99	0.99	7225.077	822.354	0.001	0.000054
10	1	1	3	3	2	2	0.8	0.8	2576.183	822.354	0.001	0.0000286
11	1	2	1	1	3	3	0.8	0.3	7225.077	428.699	0.0016	0.0000794
12	1	3	2	2	1	1	0.8	0.99	844.672	1751.004	0.0013	0.000054
13	2	1	2	3	1	3	0.55	0.8	844.672	822.354	0.0013	0.0000794
14	2	2	3	1	2	1	0.55	0.3	2576.183	428.699	0.001	0.000054
15	2	3	1	2	3	2	0.55	0.99	7225.077	1751.004	0.0016	0.0000286
16	3	1	3	2	3	1	0.99	0.8	2576.183	1751.004	0.0016	0.000054
17	3	2	1	3	1	2	0.99	0.3	7225.077	822.354	0.0013	0.0000286
18	3	3	2	1	2	3	0.99	0.99	844.672	428.699	0.001	0.0000794

The second orthogonal array is for the N1 & M2 condition. For simulations 19 through

36:

- Each level of each control factor is set to the worst-case scenario (N1)

- Underbody air flow temperature is set to the worst-case scenario (N1)

- Underbody air velocity is set to the worst-case scenario (N1)

- Muffler surface temperature is set to the best-case scenario (M2)

Table 13 - Orthogonal Array for N1 (Worst-Case Noise) and M2 (Best-Case Input Signal) Condition

Run No.	A	B	C	D	E	F	Emissivity of Heat Shield	Emissivity of Muffler	Density of Spare Tire Tub Material	Specific Heat Capacity of Spare Tire Tub	Thickness of Spare Tire Tub	Thickness of Aluminum Layers of Heat Shield
19	1	1	1	1	1	1	0.8	0.8	7225.077	428.699	0.0013	0.000054
20	1	2	2	2	2	2	0.8	0.3	844.672	1751.004	0.001	0.0000286
21	1	3	3	3	3	3	0.8	0.99	2576.183	822.354	0.0016	0.0000794
22	2	1	1	2	2	3	0.55	0.8	7225.077	1751.004	0.001	0.0000794
23	2	2	2	3	3	1	0.55	0.3	844.672	822.354	0.0016	0.000054
24	2	3	3	1	1	2	0.55	0.99	2576.183	428.699	0.0013	0.0000286
25	3	1	2	1	3	2	0.99	0.8	844.672	428.699	0.0016	0.0000286
26	3	2	3	2	1	3	0.99	0.3	2576.183	1751.004	0.0013	0.0000794
27	3	3	1	3	2	1	0.99	0.99	7225.077	822.354	0.001	0.000054
28	1	1	3	3	2	2	0.8	0.8	2576.183	822.354	0.001	0.0000286
29	1	2	1	1	3	3	0.8	0.3	7225.077	428.699	0.0016	0.0000794
30	1	3	2	2	1	1	0.8	0.99	844.672	1751.004	0.0013	0.000054
31	2	1	2	3	1	3	0.55	0.8	844.672	822.354	0.0013	0.0000794
32	2	2	3	1	2	1	0.55	0.3	2576.183	428.699	0.001	0.000054
33	2	3	1	2	3	2	0.55	0.99	7225.077	1751.004	0.0016	0.0000286
34	3	1	3	2	3	1	0.99	0.8	2576.183	1751.004	0.0016	0.000054
35	3	2	1	3	1	2	0.99	0.3	7225.077	822.354	0.0013	0.0000286
36	3	3	2	1	2	3	0.99	0.99	844.672	428.699	0.001	0.0000794

The third orthogonal array is for the N2 & M1 condition. For simulations 37 through 54:

- Each level of each control factor is set to the best-case scenario (N2)

- Underbody air flow temperature is set to the best-case scenario (N2)

- Underbody air velocity is set to the best-case scenario (N2)

- Muffler surface temperature is set to the worst-case scenario (M1)

Table 14 - Orthogonal Array for N2 (Best-Case Noise) and M1 (Worst-Case Input Signal) Condition

Run No.	A	B	C	D	E	F	Emissivity of Heat Shield	Emissivity of Muffler	Density of Spare Tire Tub Material	Specific Heat Capacity of Spare Tire Tub	Thickness of Spare Tire Tub	Thickness of Aluminum Layers of Heat Shield
37	1	1	1	1	1	1	0.45	0.2	8312.72	493.23	0.0017	0.000454
38	1	2	2	2	2	2	0.45	0.2	971.83	2014.6	0.0014	0.0004286
39	1	3	3	3	3	3	0.45	0.99	2964	946.15	0.002	0.0004794
40	2	1	1	2	2	3	0.45	0.2	8312.72	2014.6	0.0014	0.0004794
41	2	2	2	3	3	1	0.45	0.2	971.83	946.15	0.002	0.000454
42	2	3	3	1	1	2	0.45	0.99	2964	493.23	0.0017	0.0004286
43	3	1	2	1	3	2	0.99	0.2	971.83	493.23	0.002	0.0004286
44	3	2	3	2	1	3	0.99	0.2	2964	2014.6	0.0017	0.0004794
45	3	3	1	3	2	1	0.99	0.99	8312.72	946.15	0.0014	0.000454
46	1	1	3	3	2	2	0.45	0.2	2964	946.15	0.0014	0.0004286
47	1	2	1	1	3	3	0.45	0.2	8312.72	493.23	0.002	0.0004794
48	1	3	2	2	1	1	0.45	0.99	971.83	2014.6	0.0017	0.000454
49	2	1	2	3	1	3	0.45	0.2	971.83	946.15	0.0017	0.0004794
50	2	2	3	1	2	1	0.45	0.2	2964	493.23	0.0014	0.000454
51	2	3	1	2	3	2	0.45	0.99	8312.72	2014.6	0.002	0.0004286
52	3	1	3	2	3	1	0.99	0.2	2964	2014.6	0.002	0.000454
53	3	2	1	3	1	2	0.99	0.2	8312.72	946.15	0.0017	0.0004286
54	3	3	2	1	2	3	0.99	0.99	971.83	493.23	0.0014	0.0004794

The fourth orthogonal array is for the N2 & M2 condition. For simulations 55 through 72:

- Each level of each control factor is set to the best-case scenario (N2)

- Underbody air flow temperature is set to the best-case scenario (N2)

- Underbody air velocity is set to the best-case scenario (N2)

- Muffler surface temperature is set to the best-case scenario (M2)

Table 15 - Orthogonal Array for N2 (Best-Case Noise) and M2 (Best-Case Input Signal) Condition

Run No.	A	B	C	D	E	F	Emissivity of Heat Shield	Emissivity of Muffler	Density of Spare Tire Tub Material	Specific Heat Capacity of Spare Tire Tub	Thickness of Spare Tire Tub	Thickness of Aluminum Layers of Heat Shield
55	1	1	1	1	1	1	0.45	0.2	8312.72	493.23	0.0017	0.000454
56	1	2	2	2	2	2	0.45	0.2	971.83	2014.6	0.0014	0.0004286
57	1	3	3	3	3	3	0.45	0.99	2964	946.15	0.002	0.0004794
58	2	1	1	2	2	3	0.45	0.2	8312.72	2014.6	0.0014	0.0004794
59	2	2	2	3	3	1	0.45	0.2	971.83	946.15	0.002	0.000454
60	2	3	3	1	1	2	0.45	0.99	2964	493.23	0.0017	0.0004286
61	3	1	2	1	3	2	0.99	0.2	971.83	493.23	0.002	0.0004286
62	3	2	3	2	1	3	0.99	0.2	2964	2014.6	0.0017	0.0004794
63	3	3	1	3	2	1	0.99	0.99	8312.72	946.15	0.0014	0.000454
64	1	1	3	3	2	2	0.45	0.2	2964	946.15	0.0014	0.0004286
65	1	2	1	1	3	3	0.45	0.2	8312.72	493.23	0.002	0.0004794
66	1	3	2	2	1	1	0.45	0.99	971.83	2014.6	0.0017	0.000454
67	2	1	2	3	1	3	0.45	0.2	971.83	946.15	0.0017	0.0004794
68	2	2	3	1	2	1	0.45	0.2	2964	493.23	0.0014	0.000454
69	2	3	1	2	3	2	0.45	0.99	8312.72	2014.6	0.002	0.0004286
70	3	1	3	2	3	1	0.99	0.2	2964	2014.6	0.002	0.000454
71	3	2	1	3	1	2	0.99	0.2	8312.72	946.15	0.0017	0.0004286
72	3	3	2	1	2	3	0.99	0.99	971.83	493.23	0.0014	0.0004794

ModeFrontier software package was used to run these 72 simulations without manual

input. A workflow was created to automatically change the necessary design parameters.

This workflow is shown in

Appendix B - ModeFrontier Workflow.

Optimization Results

After the seventy-two simulations were completed, the maximum spare tire temperature

for each design and noise condition was known. In this analysis, the ideal design is

measured as a system which allows the difference between the muffler temperature and

the spare tire tub temperature to be equal to the muffler temperature. In this way, the

spare tire tub temperature is minimized. To accomplish this type of analysis, the data for

the temperature of the spare tire tub was first subtracted from the muffler temperature.

For each of the eighteen designs, S_T, S_β, and V_e of the muffler temperature less the

maximum spare tire tub temperature was calculated between the four noise conditions.

With these three values, the signal-to-noise ratio (S/N) could be calculated for each

design using the dynamic signal-to-noise equation, given below.

Equation 99

$$\frac{S}{N} = 10\log\left(\left(\frac{1}{r}\right)\left(\frac{(S_\beta - V_e)}{V_e}\right)\right)$$

The maximum temperature of the spare tire tub, determined from the seventy-two

simulations on RadTherm, are given in the table below. The results from the first

eighteen simulations, which were run under N1 and M1 conditions, are given in the first

blue column. The results from simulations nineteen through thirty-six are written under

the second blue column for N2 and M1 conditions. The results from simulations thirty-

seven through fifty-four are given in the third blue column for N1 and M2 conditions.

Finally, the results from simulations fifty-five through seventy-two are given in the fourth

blue column for N2 and M2 conditions.

S_T, S_β, and V_e were calculated for each design as shown in the table below. These values were used to calculate the dynamic signal-to-noise ratio (S/N) and the slope of best-fit line (β).

Table 16 - Dynamic Signal-to-Noise Ratio (S/N) and Slope of Best-Fit Line (ß)

							M1	M1	M2	M2					
							794.3	794.3	438.7	438.7					
							N1	N2	N1	N2	ST	Sβ	Ve	S/N	β
Run	A	B	C	D	E	F									
1	1	1	1	1	1	1	627	722	387	388	1214123	1209255	1623	-33.4	0.857
2	2	2	2	2	2	2	684	724	385	388	1290264	1289447	272	-25.4	0.885
3	3	3	3	3	3	3	586	722	306	388	1108375	1095536	4279	-38.1	0.816
4	1	1	2	2	3	3	627	722	385	388	1212932	1208198	1578	-33.3	0.857
5	2	2	3	3	1	1	693	726	387	388	1307206	1306643	188	-23.7	0.891
6	3	3	1	1	2	2	591	722	299	388	1109640	1096637	4334	-38.2	0.816
7	1	2	1	3	2	3	623	722	385	388	1208834	1203581	1751	-33.8	0.855
8	2	3	2	1	3	1	688	724	383	388	1295311	1294607	235	-24.8	0.887
9	3	1	3	2	1	2	570	720	285	388	1073945	1056718	5742	-39.5	0.801
10	1	3	3	2	2	1	620	721	384	388	1201946	1196396	1850	-34.1	0.852
11	2	1	1	3	3	2	689	725	388	388	1302259	1301606	218	-24.4	0.889
12	3	2	2	1	1	3	581	721	299	388	1097553	1083485	4689	-38.5	0.811
13	1	2	3	1	3	2	638	722	387	388	1229009	1225235	1258	-32.3	0.863
14	2	3	1	2	1	3	687	724	384	388	1294595	1293874	240	-24.9	0.886
15	3	1	2	3	2	1	599	722	304	388	1123208	1111563	3882	-37.6	0.822
16	1	3	2	3	1	2	622	722	386	388	1208101	1202708	1798	-33.9	0.855
17	2	1	3	1	2	3	689	724	384	388	1297818	1297169	216	-24.4	0.888
18	3	2	1	2	3	1	570	720	285	388	1074644	1057487	5719	-39.5	0.801
												AVE.		-32.215	0.8517

As can be seen in the table above, the data in the column for the signal-to-noise ratio (S/N) is highlighted green, yellow, or red. Green represents the high signal-to-noise ratios which were found, yellow represents the moderate signal-to-noise ratios, and red represents the lowest signal-to-noise ratios. As mentioned previously, a higher signal-to-noise ratio is preferred.

Out of the eighteen designs simulated, the design which provided the highest S/N ratio was Design #5. In this design, control factor A was at level 2, control factor B was at level 2, control factor C was at level 3, control factor D was at level 3, control factor E was at level 1, and control factor F was at level 1. The graph below demonstrates the improvement to the design between the current design and Design #5.
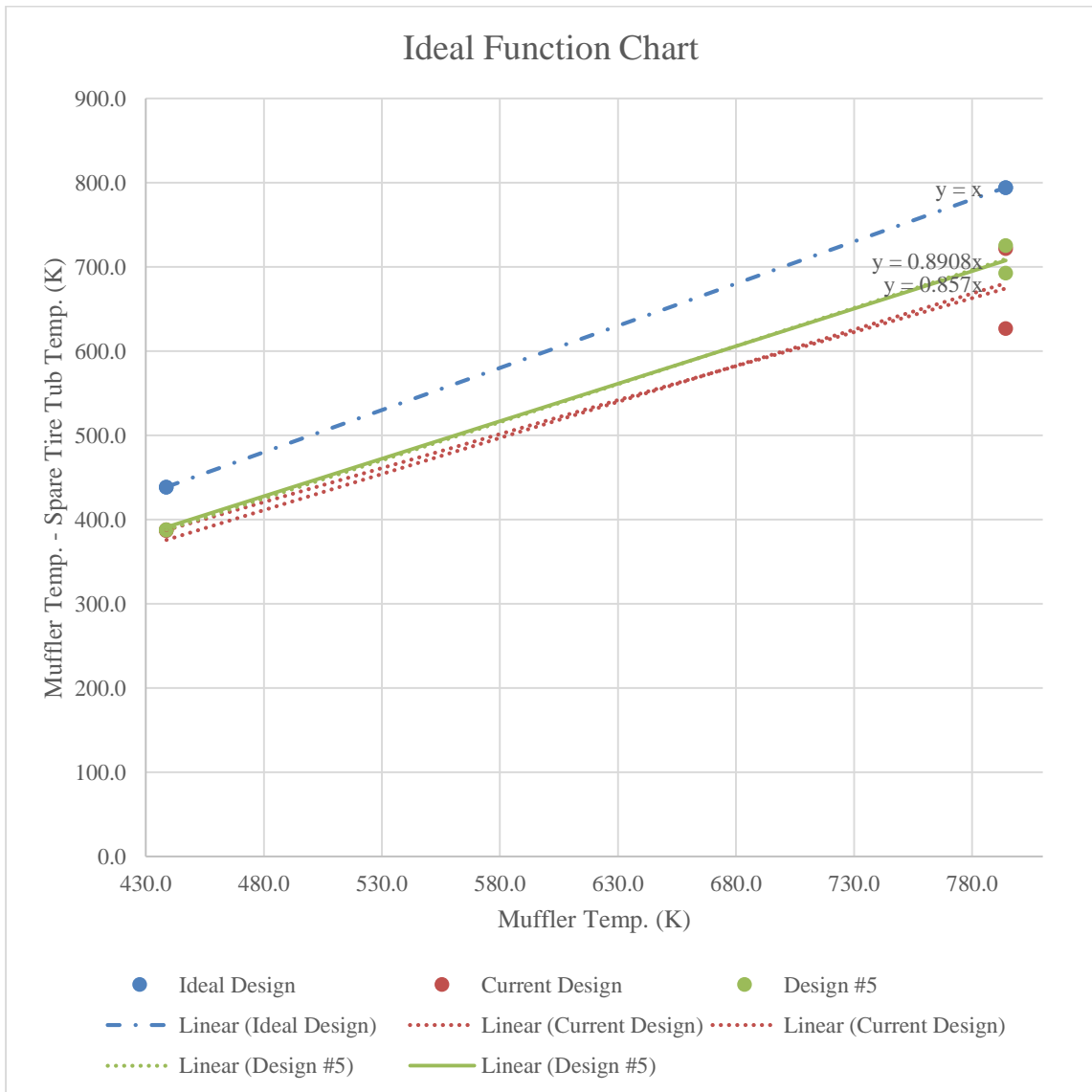

Figure 13 - Ideal Function Chart with Ideal Design, Current Design, and Design #5 (Highest S/N Ratio of the L18)

As shown in the Figure above, Design #5 is closer to the Ideal Design than the Current Design. This design was selected out of the eighteen simulations because the S/N ratio was the highest meaning that this design will perform the most consistently in various noise and signal conditions. The slope of the best-fit line, β, was also improved from the current design from 0.857 to 0.891. As mentioned earlier, the ideal slope is equal to one because this means that the spare tire tub temperature is minimized. Therefore, the design changes made in Design #5 have the potential to improve the robustness of the spare tire tub temperature, rendering the system less sensitive to noise.

It was determined that the fifth design was the best design of the eighteen designs which were simulated. However, there may be a better combination of control factors which was not simulated. Therefore, the next step is to predict the optimal design by calculating the average S/N ratio and β for each control factor and each level. Once the optimal design is determined it will be simulated to confirm the prediction.

Prediction of Optimal Design

Signal-to-Noise Ratio for Each Control Factor at Each Level

To understand the influence of each control factor at each level, the average signal-to-noise ratio was calculated for each design in which a control factor was at a specific level. For example, to find the influence of control factor A at level 1, the average was computed of the signal-to-noise ratios found for each design in which control factor A was set at level 1. As discussed earlier, the orthogonality of the matrix ensures that the influence of the other factors will be negated. The average signal-to-noise ratios for each control factor at each level is given in the table below. The row which is bolded, **Δ**, states the greatest change in signal-to-noise ratio for a specific control factor between its levels.

The final row, RANK, ranks the control factors in order, from largest to smallest, based on the Δ value. A high Δ value indicates that changing that control factor has a significant impact on the robustness of the system.

Table 17 - Signal-to-Noise Ratios Calculated for Each Control Factor at Each Level

	A	B	C	D	E	F
1	-33.48	-32.12	-32.36	-31.930	-32.34	-32.19
2	-24.59	-32.22	-32.26	-32.787	-32.24	-32.29
3	-38.58	-32.31	-32.02	-31.929	-32.07	-32.17
Δ	13.99	0.19	0.34	0.86	0.28	0.11
RANK	1	5	3	2	4	6

The first objective of this analysis is to determine the level for each control factor which maximizes the signal-to-noise ratio for the muffler temperature less the maximum spare tire temperature. These values are highlighted in green in the table above. Therefore, the optimal settings for robustness are: control factor A at level 2, control factor B at level 1, control factor C at level 2, control factor D at level 3, control factor E at level 3, and control factor F at level 3.

It was determined that the design changes made to control factor A, the emissivity of the heat shield, had the highest impact on the system robustness. The Δ value from this control factor was significantly higher than the rest and this suggests that making a design change to this factor may produce great benefits for the robustness of the spare tire tub maximum temperature.

Slope of the Best-Fit Line, β, for the Muffler Temperature Less the Maximum

Temperature of Spare Tire Tub for Each Control Factor at Each Level

The slope of the best-fit line, β, is also very important to this analysis. An ideal design would have a slope of one. As with the signal-to-noise ratio, the average value of β for the muffler temperature less the maximum spare tire tub temperature was calculated for the designs in which each control factor was set at each level. The results are shown in the table below. Once again, the Δ row represents the greatest change between the three levels and the RANK row places the control factors in order based on the Δ value.

	A	B	C	D	E	F
1	0.856	0.8522	0.851	0.8535	0.850	0.8516
2	0.888	0.8510	0.853	0.8471	0.8529	0.8514
3	0.811	0.8520	0.852	0.8545	0.8520	0.8521
Δ	0.076	0.001	0.002	0.007	0.003	0.001
RANK	1	5	4	2	3	6

Figure 14 - Slope of Best-Fit Line, β, Calculated for Each Control Factor at Each Level

The optimal levels for each control factor for S/N ratio are highlighted in green. In cases where the optimal level for improving β is different from the optimal level for the S/N ratio, the value is highlighted in yellow. The optimal settings for slope are: control factor A at level 2, control factor B at level 1, control factor C at level 2, control factor D at level 3, control factor E at level 2, and control factor F at level 3.

To clearly visualize the variation in the signal-to-noise ratio between the levels of each control factor, the tabulated values are placed into a graph, as shown below.
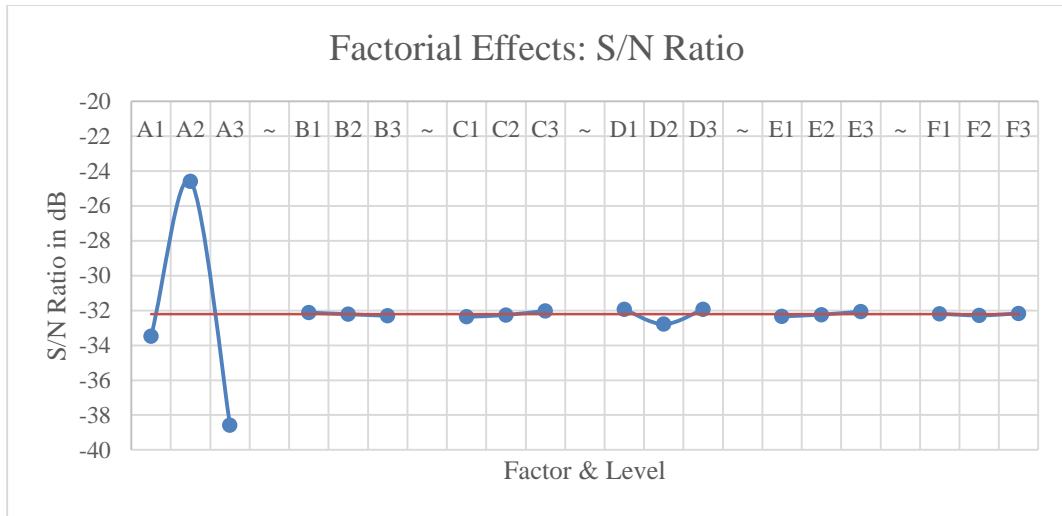
Figure 15 - Signal-to-Noise Ratio Response Graph

Level one for each control factor represents what is used in the current design. Each

control factor except for control factor B showed improvement from the suggested design

changes. Factor A, the emissivity of the heat shield, showed the most potential for
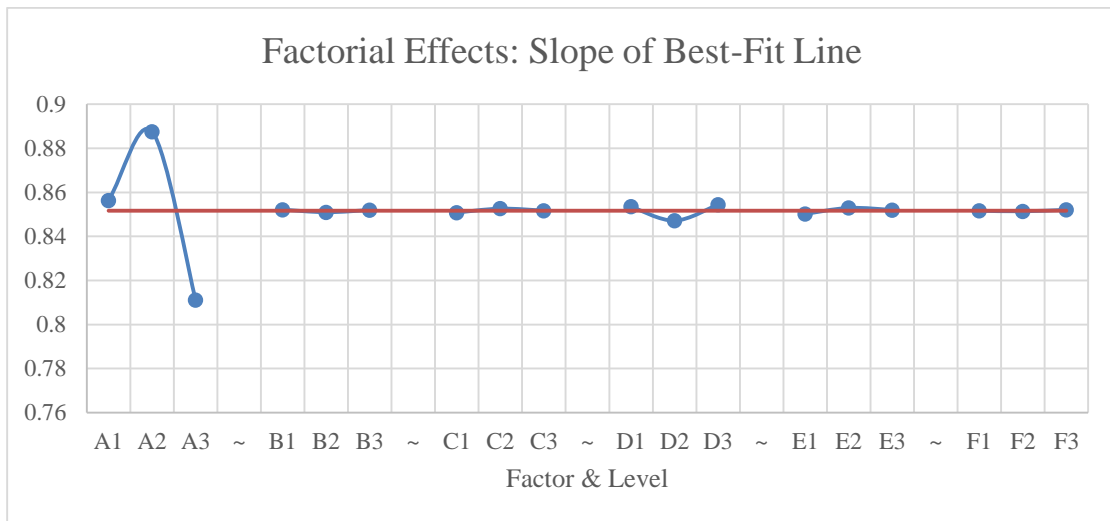
improvement to the S/N ratio.

Figure 16 – Slope of Best-Fit Line Response Graph

99

Each control factor showed improved slope of best-fit line when the design changes were applied except for control factor B. The greatest improvement to slope was accomplished by changing control factor A to level 2.

A prediction of the S/N ratio and β for the optimized design for S/N ratio was made using the formulas below. For the optimized design for β, the same formulas were utilized by substituting the appropriate control factor levels.

Equation 100

$$S/N_{opt} = S/N_{ave} + (\overline{A_2} - S/N_{ave}) + (\overline{B_1} - S/N_{ave}) + (\overline{C_2} - S/N_{ave})$$
$$+ (\overline{D_3} - S/N_{ave}) + (\overline{E_3} - S/N_{ave}) + (\overline{F_3} - S/N_{ave})$$

Equation 101

$$\beta_{opt} = S/N_{ave} + (\overline{A_2} - \beta_{ave}) + (\overline{B_1} - \beta_{ave}) + (\overline{C_2} - \beta_{ave}) + (\overline{D_3} - \beta_{ave})$$
$$+ (\overline{E_3} - \beta_{ave}) + (\overline{F_3} - \beta_{ave})$$

For the design which optimized the S/N ratio, the S/N ratio was calculated to be -23.82 and β was found to be 0.891. For the design which optimized β, the S/N ratio was calculated to be -24.24 and β was found to be 0.893. These results seem quite similar, however, it is important to note that the formula to calculate the S/N ratio is logarithmic. Therefore, a small change in S/N ratio can actually result in a significant improvement to the robustness of the design.

Step 3 – Confirmation of DFSS Optimal Design Predictions

The optimal design for improving S/N ratio was predicted to be control factor A at level 2, control factor B at level 1, and control factors C through F at level 3. This design was simulated under the four noise and signal combinations that were used for the previous

simulations (N1 & M1, N1 & M2, N2 & M1, N2 & M2). The S/N ratio and slope of best-fit line, β, were then calculated and compared to the prediction. The same process was applied to the predicted optimal design for improving the slope of best-fit line, β. The results are given in the table below. Note that the values given are for the muffler temperature less the maximum spare tire tub temperature.

Table 18 - Confirmation Runs for Optimal S/N Ratio and Optimal Slope of Best-Fit Line

						M1	M1	M2	M2					
						794.3	794.3	438.7	438.7					
						N1	N2	N1	N2	ST	Sβ	Ve	S/N	β
A	B	C	D	E	F									
2	1	3	3	3	3	690.9	724.6	388.2	389.0	1304520	1303944	191.9	-23.84	0.889
2	1	2	3	2	3	692.9	726.8	386.4	390.6	1310376	1309774	200.5	-24.01	0.892

Finally, the simulated S/N and β were compared to the predicted S/N and β to confirm the predictions. These values are summarized in the table below.

Table 19 - Summary of Confirmations

	Predictions		Confirmation	
	S/N	β	S/N	β
Run 1 A1,B1,C1,D1,E1,F1	-33.34	0.856	-33.449	0.857
Predicted Highest S/N A2,B1,C3,D3,E3,F3	-23.82	0.891	-23.845	0.890
Gain	9.52	0.035	9.604	0.033

	S/N	β	S/N	β
Highest Predicted Beta Design A2,B1,C2,D3,E2,F3	-24.24	0.893	-24.0	0.892
Gain (Highest Beta to Highest S/N)	-0.41	0.002	-0.2	0.002

The first conclusion to note from this table is that the predicted values are close to the confirmed values. As a rule of thumb used in DFSS, the process is considered validated as long as the predicted values are within 25% of the confirmed values. In this analysis, the predicted values are well within 25% of the confirmed values; thus, the process to calculate the optimal S/N ratio and β is validated. The next important observation is that a gain of 9.6 in the S/N ratio was accomplished through the predicted optimal design for S/N ratio. However, the predicted optimal design for β provided minimal further improvement to the S/N ratio or β. Therefore, this DFSS study determined that the design which will allow for optimal robustness of the spare tire tub temperature is the optimal S/N ratio design in which control factor A is at level 2, control factor B is at level 1, and control factors C through F are at level 3. To visualize the improvement to the design created by these changes, the Ideal Function Chart is given below.
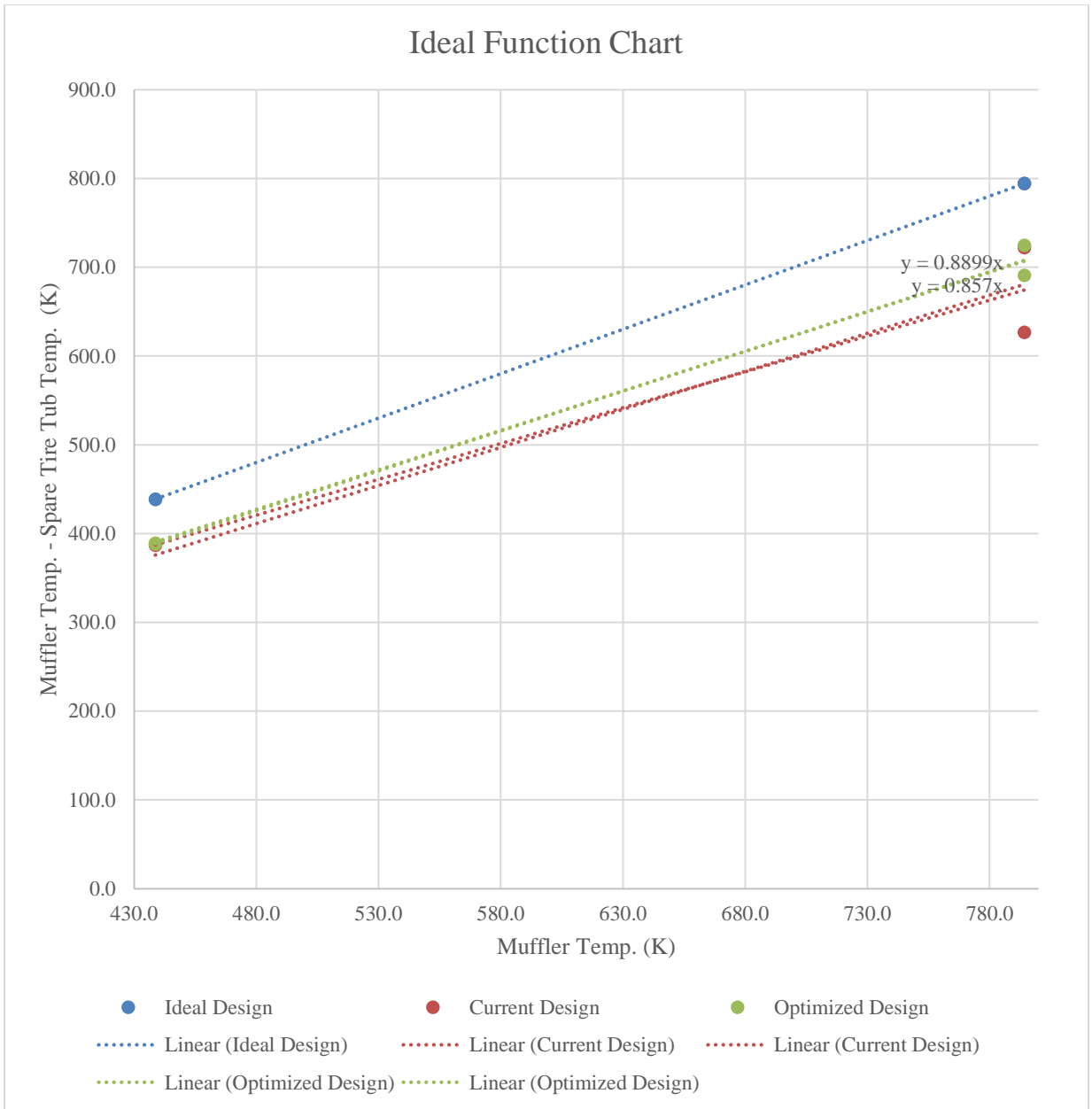
Figure 17 - Ideal Function Chart with Ideal Design, Current Design, and Optimized Design

As shown in the figure above, the optimized design is closer to the ideal design when

compared to the current design. This result will cause the design to perform more

consistently under various noise and signal conditions which may occur in the customer

environment. Overall, these design changes will allow for an improved system robustness of the spare tire tub temperature.

CHAPTER 6

CONCLUSIONS

This investigation has established a process for analyzing the effects of uncertainty in design parameters on system performance. The FAST method was successfully implemented on the specific case study, the spare tire tub, to determine the parameters whose uncertainty was the most influential on the uncertainty of the design target, the maximum temperature.

The first investigation used the Fourier Amplitude Sensitivity Test (FAST) to calculate the partial variance of each input parameter on the temperature of the spare tire tub using a consistent amount of uncertainty for each input parameter. Before the analysis could be conducted, the relevant input parameters were identified through the development of a simple analytical model of the system. To understand the effects of a low, medium, and high amount of design uncertainty, the uncertainty of each of the parameters was set at 1%, 10%, and then 30%. With an equal amount of uncertainty assigned to each input parameter, it was found that the temperature of the air flowing over the spare tire tub was the most influential input parameter followed by the temperature of the air flowing over the lower surface of the heat shield. This result was consistent for the low, medium, and high uncertainty cases. Considering that the air temperature is not a parameter which can be easily manipulated, the input parameters were separated into control, noise, and input parameters. The control factors are those which can be feasibly controlled and the noise

factors are those which are too difficult or expensive to control. The input parameter is the one providing the input signal to the system and which the system must be designed to handle. Repeating the analysis, using only the control factors, allowed for the determination of the most influential control parameters. The top five parameters were found to be the emissivity of the heat shield, the longitudinal and lateral dimensions of the heat shield, and the longitudinal and lateral dimensions of the spare tire tub. This initial investigation successfully determined the design parameters with the highest partial variance with the assumption that the uncertainty in every design parameter is equal.

The second investigation also utilized the FAST method to determine the partial variance of the input parameters. However, this study applied more accurate uncertainty ranges for each input parameter to obtain an improved evaluation of the influence of each parameter. These uncertainty ranges were based on the knowledge of experienced engineers as well as the application of the error propagation formula. Through this study, an approximate value of uncertainty range was formed for each input parameter. As in the first investigation, the FAST method was first applied using all of the input parameters. The most influential parameters were found to be the temperature of the muffler, the temperature of the air flowing over the spare tire tub, and the emissivity of the muffler. Based on the same considerations taken in the first investigation, the parameters were separated into control, noise, and input factors. In this case, the top six influential design parameters were determined to be the emissivity of the heat shield, the emissivity of the muffler, the thickness of the spare tire tub, the density of the spare tire

tub, the specific heat capacity of the spare tire tub, and the thickness of the outer layers of the heat shield.

The next step in this investigation was to develop a method to interface the results from uncertainty analysis with Design for Six Sigma (DFSS).

The DFSS analysis identified several design improvements which could increase the robustness of the spare tire tub maximum temperature as well as reduce the average temperature. To improve the robustness of the spare tire tub maximum temperature, the design changes which were identified were:

1) Add a corrosion resistance coating to the muffler

2) Reduce the density of the spare tire tub by using a different material such as plastic or aluminum

3) Increase the specific heat capacity of the spare tire tub by using a different material such as plastic or aluminum

4) Increase the thickness of the spare tire tub from 1.5 mm to 1.8 mm.

5) Increase the thickness of the outer layers of the heat shield from 0.25 mm to 0.28 mm.

It is important to take into account that these design changes are suggested based solely on their improvement to robustness. To actually employ these changes, further investigation must be conducted to determine the costs and feasibility for the actual design. This process was meant only to demonstrate how to apply DFSS analysis to investigate potential design changes to the most critical design parameters as determined by the FAST process.

This method allowed for the determination of the best settings for the most influential design parameters to improve system robustness. In this specific case study, the goal was to improve thermal performance of vehicle components which are exposed to high thermal loads. In the future, this methodology may be applied to other systems to improve robustness in the early design stages. The main advantage of this developed process is that it can be used to pinpoint potential issues and determine optimal solutions prior to experimental testing.

REFERENCES/BIBLIOGRAPHY

Beaufort, S. F. (2015, March 24). *Beaufort Wind Scale.* Retrieved from Storm Prediction Center: www.spc.noaa.gov

Cengel, Y., & Ghajar, A. (2014). *Heat and Mass Transfer: Fundamentals and Applications.* McGraw-Hill Science/Engineering/Math.

Chowdhury, S. (2003). *Design for Six Sigma: The Revolutionary Process for Achieving Extraordinary Profits.* Pearson Education Limited.

Churchill , S., & Chu, H. (1975). Correlating Equations for Laminar and Turbulent Free Convection from a Vertical Plate. *International Journal of Heat Mass Transfer*, 1323-1329.

Coleman, H. W., & Steele, W. G. (1999). *Experimentation and Uncertainty Analysis for Engineers.* John Wiley & Sons.

Cukier, R. I., Levine, H. B., & Shuler, K. E. (1974). *Nonlinear Sensitivity Analysis of Multi-Parameter Model Systems.* San Diego: Defense Technical Information Center.

Czitrom, V., & Spagon, P. D. (1997). *Statistical Case Studies for Industrial Process Improvement.* Philadelphia: Society for Industrial and Applied Mathematics.

El-Sharkawy, A. (2007). Reliability Analysis of Dynamometer Loading Parameters during Vehicle Cell Testing. *SAE Technical Paper Series*.

El-Sharkawy, A. (2014). Sensitivity and Uncertainty Analysis in Computational Thermal Models. *SAE International*.

El-Sharkawy, A. E. (2001). Sensitivity/Uncertainty Analysis of Automotive Heat Exchanger Designs. *SAE Technical Paper Series*.

El-Sharkawy, A. E. (2008). Analysis of Thermocouple Temperature Response under Actual Vehicle Test Conditons. *SAE International*.

El-Sharkawy, A., & Kamrad, J. (2012). Sensitivity/Uncertainty Analysis of Material Thermal Degradation Models. *SAE International*.

El-Sharkawy, A., & Uddin, A. (2014). Development of Transient Thermal Models Based on Theoretical Analysis and Vehicle Test Data. *SAE International*.

El-Sharkawy, A., Salahuddin, A., & Komarisky, B. (2014). Design for Six Sigma (DFSS) for Optimization of Automotive Heat Exchanger and Underhood Air Temperature. *SAE International*.

El-Sharkawy, A., Salahuddin, A., & Komarisky, B. (n.d.). *Application of DFSS for Design of Heat Exchangers.* Chrysler Group LLC.

Engineering Toolbox. (n.d.). *Air - Density and Specific Weight*. Retrieved from Engineering Toolbox: www.engineeringtoolbox.com

Holman, J. (1981). *Heat Transfer.* McGraw-Hill International Book Company.

Khanna, A. S. (2002). *Introduction to High Temperature Oxidation and Corrosion.* ASM International.

Kline, S. J., & McClintock, F. A. (Mechanical Engineering). *Describing Uncertainties in Single-Sample Experiments.*

Knaust, H. (2013, December). *Taylor Series*. Retrieved from SOS Math: www.sosmath.com/calculus/tayser/tayser01/tayser01.html

Leuenberger, H., & Person, A. (1994). Compilation of Radiation Shape Factors. *The American Society of Mechanical Engineers*.

McRae, G. J., Tilden, J. W., & Seinfeld, J. H. (1982). Global Sensitivity Analysis - A Computational Implementation of the Fourier Amplitude Sensitivity Test (FAST). *Computers & Chemical Engineering*.

Rathakrishnan, E. (2005). *Fundamentals of Engineering Thermodynamics.* PHI Learning Pvt. Ltd.

Taguchi, G., Chowdhury, S., & Wu, Y. (2005). *Taguchi's Quality Engineering Handbook.* Wiley.

ThermoAnalytics. (2014). *RadTherm User Manual Version 11.3.0.*

Thompson, A. (2011, July 08). *What's the Highest Temperature Ever Recorded in the U.S.?* Retrieved from Live Science: m.livescience.com

Weather Temperature Extremes in the United States. (2007). Retrieved from InfoPlease: www.infoplease.com

APPENDICES

Heat Transfer Coefficient for Airflow over Upper Surface of Heat Shield

The heat transfer coefficient for the airflow over the upper surface of the heat shield was calculated by the same method for lower surface of the heat shield. The difference between the two heat transfer coefficients arises because of a difference in airflow velocity which increases the critical distance at which the flow becomes turbulent, as depicted in the following section.

Critical Distance, "x_{cr}", for Air Flow over Upper Surface of Heat Shield:

For the airflow over the upper surface of the heat shield, the density can be determined based on the nominal value of the air temperature which, in this location, is 320 K. As before, the density was read from the *"Engineering Toolbox"* (Engineering Toolbox, n.d.) and was found to be $1.115 \frac{kg}{m^3}$. The dynamic viscosity was found from the same source, based on the air temperature, to be $1.939 \times 10^{-5} \frac{kg}{m\,s}$. The velocity of the air was assumed to be $2 \frac{m}{s}$ to take into account the underbody components closer to the front of the vehicle which will reduce the airflow which is able to reach the rear underbody components. Thus, the critical distance was calculated as follows.

Equation 102

$$x_{cr} = \frac{Re_{cr}\mu}{\rho V} = \frac{(100{,}000)(1.939 \times 10^{-5} \frac{kg}{m\,s})}{(1.115 \frac{kg}{m^3})(2 \frac{m}{s})} = 0.87\ m$$

Since the critical distance was found to be greater than the length of the heat shield in the direction of the airflow, it can be assumed that the flow will be laminar in this region. Based on this assumption, the Nusselt correlation was obtained from "*Heat and Mass Transfer: Fundamentals and Applications*" (Cengel & Ghajar, 2014):

Equation 103

$$Nu = 0.664 Re_L{}^{0.5} Pr^{1/3}$$

Thus, the equation to apply the uncertainty analysis to is obtained:

Equation 104

$$h = \frac{0.664 Re_L{}^{0.5} Pr^{1/3} k}{L_c}$$

Therefore, the uncertainty in the heat transfer coefficient can be expressed as a function of the uncertainty in the Reynolds number, Prandtl number, thermal conductivity, and characteristic length.

Equation 105

$$\delta h = \sqrt{\left(\frac{\partial h}{\partial Re_L} \delta Re_L\right)^2 + \left(\frac{\partial h}{\partial Pr} \delta Pr\right)^2 + \left(\frac{\partial h}{\partial k} \delta k\right)^2 + \left(\frac{\partial h}{\partial L_c} \delta L_c\right)^2}$$

As was shown for the calculation of the uncertainty in the heat transfer coefficient for the airflow over the lower surface of the heat shield, the partial derivatives and uncertainties in each parameter must be evaluated.

Heat Transfer Coefficient (for Airflow over Upper Surface of Heat Shield) Partial

Derivative With Respect to Reynolds number

Equation 106

$$\frac{\partial h}{\partial Re_L} = \frac{0.664(0.5)Re_L^{-0.5}Pr^{1/3}k}{L_c}$$

The local Reynolds number at the trailing edge of the heat shield is calculated below in

Equation 107. The density, velocity, and dynamic viscosity were determined in the

previous section. The distance to the trailing edge, x, was estimated to be 0.45 m. These

values were used to calculate the Reynolds number, as shown below.

Equation 107

$$Re_L = \frac{\rho V x}{\mu} = \frac{\left(1.115 \ \frac{kg}{m^3}\right)\left(2 \ \frac{m}{s}\right)(0.45 \ m)}{\left(1.939 \ x \ 10^{-5} \ \frac{kg}{m \ s}\right)} = 51753$$

The Prandtl number and thermal conductivity for the air were found from the

"Engineering Toolbox" for a temperature of 320 K to be 0.710 and $0.0276 \ \frac{W}{m \ K}$,

respectively. For a flat plate, the characteristic length, L_c, is the distance from the leading

edge which, for this model, is 0.45 m. Substituting these values in to Equation 106

provides the value for this partial derivative:

Equation 108

$$\frac{\partial h}{\partial Re_L} = \frac{(0.664)(0.5)(51753)^{-0.5}(0.710)^{1/3} \ (0.0276 \ \frac{W}{m \ K})}{(0.45 \ m)} = 0.000079852 \ \frac{W}{m^2 \ K}$$

Heat Transfer Coefficient (for Airflow over Upper Surface of Heat Shield) Partial

Derivative With Respect to Prandtl Number

The next partial derivative to be calculated is the heat transfer coefficient with respect to

the Prandtl number. The derivate is shown below in Equation 81.

Equation 109

$$\frac{\partial h}{\partial Pr} = \frac{0.664 Re_L^{0.5}(\frac{1}{3})Pr^{-2/3}k}{L_c} = \frac{0.664(51753)^{0.5}\left(\frac{1}{3}\right)(0.710)^{-\frac{2}{3}}(0.0276\frac{W}{m\,K})}{(0.45\,m)}$$

$$= 3.880\frac{W}{m^2\,K}$$

Heat Transfer Coefficient (for Airflow over Upper Surface of Heat Shield) Partial

Derivative With Respect to Thermal Conductivity

The next partial derivative to be calculated is the heat transfer coefficient with respect to

the thermal conductivity.

Equation 110

$$\frac{\partial h}{\partial k} = \frac{0.664 Re_L^{0.5}Pr^{1/3}}{L_c} = \frac{(0.664)(51753)^{0.5}(0.710)^{1/3}}{(0.45\,m)} = 299.463\frac{1}{m}$$

Heat Transfer Coefficient (for Airflow over Upper Surface of Heat Shield) Partial

Derivative With Respect to Characteristic Length

The final partial derivative to be calculated is the heat transfer coefficient with respect to

the characteristic length.

Equation 111

$$\frac{\partial h}{\partial L_c} = \frac{-0.664 Re_L{}^{0.5} Pr^{1/3} k}{(L_c{}^2)} = \frac{(-0.664)(51753)^{0.5}(0.710)^{\frac{1}{3}}(0.0276 \frac{W}{m\,K})}{(0.45\,m)^2}$$

$$= -18.367 \frac{W}{m^3\,K}$$

The next step is to determine the appropriate value of uncertainty for the Reynolds number, Prandtl number, thermal conductivity, and characteristic length.

Reynolds Number (for Airflow over Upper Surface of Heat Shield) Uncertainty Analysis

By the same method used for the airflow over the lower surface of the heat shield, the error propagation equation was applied to the Reynolds number to determine the uncertainty in the Reynolds number.

Equation 112

$$\delta Re = \sqrt{\left(\frac{\partial Re}{\partial \rho}\delta\rho\right)^2 + \left(\frac{\partial Re}{\partial V}\delta V\right)^2 + \left(\frac{\partial Re}{\partial L}\delta L\right)^2 + \left(\frac{\partial Re}{\partial \mu}\delta\mu\right)^2}$$

Reynolds Number Partial Derivative With Respect to Density

Equation 113

$$\frac{\partial Re}{\partial \rho} = \frac{VL}{\mu} = \frac{(2\frac{m}{s})(0.45\,m)}{(1.939\,x\,10^{-5}\frac{kg}{m\,s})} = 46416 \frac{m^3}{kg}$$

Reynolds Number Partial Derivative With Respect to Air Velocity

Equation 114

$$\frac{\partial Re}{\partial V} = \frac{\rho L}{\mu} = \frac{(1.115\ \frac{kg}{m^3})(0.45\ m)}{(1.939\ x\ 10^{-5}\ \frac{kg}{m\ s})} = 25877\ \frac{s}{m}$$

Reynolds Number Partial Derivative With Respect to Length

Equation 115

$$\frac{\partial Re}{\partial L} = \frac{\rho V}{\mu} = \frac{(1.115\ \frac{kg}{m^3})(2\ \frac{m}{s})}{(1.939\ x\ 10^{-5}\ \frac{kg}{m\ s})} = 115008\ \frac{1}{m}$$

Reynolds Number Partial Derivative With Respect to Dynamic Viscosity

Equation 116

$$\frac{\partial Re}{\partial \mu} = \frac{-\rho V L}{\mu^2} = \frac{-(1.115\ \frac{kg}{m^3})(2\ \frac{m}{s})(0.45\ m)}{(1.939\ x\ 10^{-5}\ \frac{kg}{m\ s})^2} = -2669081030\ \frac{m\ s}{kg}$$

The next step required to evaluate the uncertainty in the Reynolds number is to evaluate
the uncertainty in the air density, velocity, dynamic viscosity, and the length of the heat
shield.

Air Density Uncertainty

The air density has uncertainty which is related to the variation in air temperature
depending on the location of the driven vehicle and the environment. A temperature
uncertainty range, defined in , of +/-10% the nominal value is applied. Examining the
variation in air density over this temperature range, the "*Engineering Toolbox*"

(Engineering Toolbox, n.d.) shows that the density may vary from $1.225 \frac{kg}{m^3}$ at low air temperatures to $0.999 \frac{kg}{m^3}$ at high air temperatures. This represents a 10% increase in air density above the nominal value and a -10% decrease below the nominal value. Therefore, the uncertainty range used for this analysis is +/-10%. Therefore, $\delta\rho$ is equal to $0.1115 \frac{kg}{m^3}$.

Air Velocity Uncertainty

Air velocity is another parameter which varies because of environmental conditions but also depends greatly on the speed of the driven vehicle; therefore, some assumptions must be made. Supposing that this vehicle may be at standstill or driven on the highway and can also be located in an area with calm to stormy conditions, it will be assumed that the air velocity may vary +/-50% around the nominal value of 2 m/s. Therefore, δV is equal to 1 m/s.

 This results in a potential variation of air velocity between 1 m/s to 3 m/s. According to the Beaufort scale (Beaufort, 2015), this corresponds to the variation between light air and a light breeze. This may not appear to be enough variation, but it must also be noted that there are underbody components near the front of the vehicle which block the air flow from reaching the rear underbody components being investigated. Also, the clearance between the upper surface of the heat shield and the spare tire tub is small and will reduce the airflow to this area.

Heat Shield Length Uncertainty

As discussed in Section "Lengths, Widths, and Diameters" on page 68, the uncertainty in the length of the heat shield is assumed to be +/- 0.0002 m. Therefore, δL is equal to 0.0002 m.

Dynamic Viscosity Uncertainty

The uncertainty in the dynamic viscosity can be determined by the same approach used for the air density uncertainty. The air temperature is assumed to range from 288 K to 352 K. Therefore, the dynamic viscosity, read from the "Engineering Toolbox" (Engineering Toolbox, n.d.), may range between $1.846 \ x \ 10^{-5} \frac{kg}{m \ s}$ to $2.075 \ x \ 10^{-5} \frac{kg}{m \ s}$. This corresponds to an increase of 7% above the nominal value and a decrease of 5% below the nominal value. Therefore, an uncertainty of +/- 6% was assumed. Therefore, $\delta \mu$ is equal to $0.1163 \ x \ 10^{-5} \frac{kg}{m \ s}$.

Substituting the partial derivatives and uncertainty values in to the error propagation equation (Equation 117), an estimate of the uncertainty in the Reynolds number was found.

Equation 117

δRe

$$= \sqrt{ \left(\left(46416 \ \frac{m^3}{kg} \right) \left(0.1115 \ \frac{kg}{m^3} \right) \right)^2 + \left(\left(25877 \ \frac{s}{m} \right) \left(1 \ \frac{m}{s} \right) \right)^2 + \left(\left(115008 \ \frac{1}{m} \right) (0.0002 \ m) \right)^2 + \left(\left(-2669081030 \ \frac{m \ s}{kg} \right) (0.1163 \ x \ 10^{-5} \frac{kg}{m \ s}) \right)^2 }$$

$= 26571$

117

This value is extremely high; however, it is meant to represent the variation in the Reynolds number over all possible operating conditions and environments. With this consideration, this value seems appropriate.

Referring back to Equation 105, the uncertainty in the Prandtl number and thermal conductivity must be estimated. The uncertainty in the length of the heat shield has already been estimated to calculate the uncertainty in the Reynolds number.

Prandtl Number of Air Uncertainty

The Prandtl number of the air depends on the air temperature. Following the same considerations used for air density and dynamic viscosity, an approximate uncertainty range may be developed. The air temperature range was determined to be 288 K to 352 K. Therefore, from the *"Engineering Toolbox"* (Engineering Toolbox, n.d.) the Prandtl number may vary between 0.707 at low air temperatures to 0.697 at high air temperatures. These values correspond to an increase of 1% above the nominal value and a 1% decrease below the nominal value. Thus, an uncertainty of +/-1% was applied. Therefore, δPr is equal to 0.00701.

Thermal Conductivity of Air Uncertainty

The thermal conductivity of the air depends on the air temperature. The air temperature range was assumed to be 288 K to 352 K. Thus, from the *"Engineering Toolbox"* (Engineering Toolbox, n.d.), the thermal conductivity may vary between $0.02624 \frac{W}{m\,K}$ and $0.03003 \frac{W}{m\,K}$. This corresponds to an increase of 9% above the nominal value and a decrease of 5% below the nominal value. For simplicity, a symmetric uncertainty of +/-7% was assumed. Thus, δk is equal to $0.001932 \frac{W}{m\,K}$.

Finally, the partial derivatives and uncertainty values can be substituted into Equation 105 to find the uncertainty in the heat transfer coefficient.

Equation 118

$$\delta h = \sqrt{\left(\frac{\partial h}{\partial Re_L}\delta Re_L\right)^2 + \left(\frac{\partial h}{\partial Pr}\delta Pr\right)^2 + \left(\frac{\partial h}{\partial k}\delta k\right)^2 + \left(\frac{\partial h}{\partial L_c}\delta L_c\right)^2}$$

$$= \sqrt{\begin{array}{l}\left((0.0000799\,\frac{W}{m^2\,K})(26571))\right)^2 + \left(\left(3.880\,\frac{W}{m^2\,K}\right)(0.00701)\right)^2 + \\ \left((299.463\,\frac{1}{m})(0.001932\,\frac{W}{m\,K})\right)^2 + \left(\left(-18.367\,\frac{W}{m^3\,K}\right)(0.0002\,m)\right)^2\end{array}} = 2\,\frac{W}{m^2\,K}$$

Thus, the uncertainty in the heat transfer coefficient for the airflow over the upper surface of the heat shield is +/- 2 $\frac{W}{m^2\,K}$. This uncertainty is slightly lower that the uncertainty which was calculated for the heat transfer coefficient of the airflow over the lower surface of the heat shield. This result is according to expectation because the airflow in this location is more laminar and predictable.

Heat Transfer Coefficient for Airflow over Spare Tire Tub

The heat transfer coefficient for the airflow over the spare tire tub was calculated by the same method for upper and lower surface of the heat shield.

Critical Distance, "x_{cr}", for Air Flow over Spare Tire Tub:

For the airflow over the spare tire tub, the density can be determined based on the nominal value of the air temperature which, in this location, is 315 K. As before, the density was read from the *"Engineering Toolbox"* (Engineering Toolbox, n.d.) and was found to be 1.123 $\frac{kg}{m^3}$. The dynamic viscosity was found from the same source, based on

the air temperature, to be 1.916 x 10^{-5} $\frac{kg}{m\,s}$. The velocity of the air was assumed to be 2.74

$\frac{m}{s}$ to take into account the underbody components closer to the front of the vehicle which

will reduce the airflow which is able to reach the rear underbody components. Thus, the

critical distance was calculated as follows.

Equation 119

$$x_{cr} = \frac{Re_{cr}\mu}{\rho V} = \frac{(100{,}000)(1.916 \text{ x } 10^{-5}\ \frac{kg}{m\,s})}{(1.123\frac{kg}{m^3})(2.74\ \frac{m}{s})} = 0.62\ m$$

Since the critical distance was found to be greater than the length of the heat shield in the

direction of the airflow, it can be assumed that the flow will be laminar in this region.

Based on this assumption, the Nusselt correlation was obtained from "*Heat and Mass*

Transfer: Fundamentals and Applications" (Cengel & Ghajar, 2014):

Equation 120

$$Nu = 0.664 Re_L{}^{0.5} Pr^{1/3}$$

Thus, the equation to apply the uncertainty analysis to is obtained:

Equation 121

$$h = \frac{0.664 Re_L{}^{0.5} Pr^{1/3} k}{L_c}$$

Therefore, the uncertainty in the heat transfer coefficient can be expressed as a function

of the uncertainty in the Reynolds number, Prandtl number, thermal conductivity, and

characteristic length.

Equation 122

$$\delta h = \sqrt{\left(\frac{\partial h}{\partial Re_L}\delta Re_L\right)^2 + \left(\frac{\partial h}{\partial Pr}\delta Pr\right)^2 + \left(\frac{\partial h}{\partial k}\delta k\right)^2 + \left(\frac{\partial h}{\partial L_c}\delta L_c\right)^2}$$

As was shown for the calculation of the uncertainty in the heat transfer coefficient for the airflow over the heat shield, the partial derivatives and uncertainties in each parameter must be evaluated.

Heat Transfer Coefficient (for Airflow over Spare Tire Tub) Partial Derivative With Respect to Reynolds number

Equation 123

$$\frac{\partial h}{\partial Re_L} = \frac{0.664(0.5)Re_L^{-0.5}Pr^{1/3}k}{L_c}$$

The local Reynolds number at the trailing edge of the heat shield is calculated below in Equation 124. The density, velocity, and dynamic viscosity were determined in the previous section. The distance to the trailing edge, x, was estimated to be 0.45 m. These values were used to calculate the Reynolds number, as shown below.

Equation 124

$$Re_L = \frac{\rho V x}{\mu} = \frac{\left(1.123\,\frac{kg}{m^3}\right)\left(2.74\,\frac{m}{s}\right)(0.45\,m)}{\left(1.916\,x\,10^{-5}\,\frac{kg}{m\,s}\right)} = 72268$$

The Prandtl number and thermal conductivity for the air were found from the

"Engineering Toolbox" for a temperature of 315 K to be 0.703 and 0.0274 $\frac{W}{m\,K}$,

respectively. For a flat plate, the characteristic length, L_c, is the distance from the leading edge which, for this model, is 0.45 m. Substituting these values in to Equation 125 provides the value for this partial derivative:

Equation 125

$$\frac{\partial h}{\partial Re_L} = \frac{(0.664)(0.5)(72268)^{-0.5}(0.703)^{1/3}\left(0.0274\,\frac{W}{m\,K}\right)}{(0.45\,m)} = 0.00006686\,\frac{W}{m^2\,K}$$

Heat Transfer Coefficient (for Airflow over Spare Tire Tub) Partial Derivative With Respect to Prandtl Number

The next partial derivative to be calculated is the heat transfer coefficient with respect to the Prandtl number. The derivate is shown below in Equation 126.

Equation 126

$$\frac{\partial h}{\partial Pr} = \frac{0.664Re_L^{0.5}\left(\frac{1}{3}\right)Pr^{-2/3}k}{L_c} = \frac{0.664(72268)^{0.5}\left(\frac{1}{3}\right)(0.703)^{-\frac{2}{3}}\left(0.0274\,\frac{W}{m\,K}\right)}{(0.45\,m)}$$

$$= 4.582\,\frac{W}{m^2\,K}$$

Heat Transfer Coefficient (for Airflow over Spare Tire Tub) Partial Derivative With Respect to Thermal Conductivity

The next partial derivative to be calculated is the heat transfer coefficient with respect to the thermal conductivity.

Equation 127

$$\frac{\partial h}{\partial k} = \frac{0.664Re_L^{0.5}Pr^{1/3}}{L_c} = \frac{(0.664)(72268)^{0.5}(0.703)^{1/3}}{(0.45\,m)} = 352.71\,\frac{1}{m}$$

Heat Transfer Coefficient (for Airflow over Spare Tire Tub) Partial Derivative With Respect to Characteristic Length

The final partial derivative to be calculated is the heat transfer coefficient with respect to the characteristic length.

Equation 128

$$\frac{\partial h}{\partial L_c} = \frac{-0.664 Re_L{}^{0.5} Pr^{1/3} k}{(L_c{}^2)} = \frac{(-0.664)(72268)^{0.5}(0.703)^{\frac{1}{3}}(0.0274\ \frac{W}{m\ K})}{(0.45\ m)^2}$$

$$= -21.476\ \frac{W}{m^3\ K}$$

The next step is to determine the appropriate value of uncertainty for the Reynolds number, Prandtl number, thermal conductivity, and characteristic length.

Reynolds Number (for Airflow over Spare Tire Tub) Uncertainty Analysis

By the same method used for the airflow over the heat shield, the error propagation equation was applied to the Reynolds number to determine the uncertainty in the Reynolds number.

Equation 129

$$\delta Re = \sqrt{\left(\frac{\partial Re}{\partial \rho} \delta\rho\right)^2 + \left(\frac{\partial Re}{\partial V} \delta V\right)^2 + \left(\frac{\partial Re}{\partial L} \delta L\right)^2 + \left(\frac{\partial Re}{\partial \mu} \delta\mu\right)^2}$$

Reynolds Number Partial Derivative With Respect to Density

Equation 130

$$\frac{\partial Re}{\partial \rho} = \frac{VL}{\mu} = \frac{(2.74\ \frac{m}{s})(0.45\ m)}{(1.916\ x\ 10^{-5}\ \frac{kg}{m\ s})} = 64353\ \frac{m^3}{kg}$$

Reynolds Number Partial Derivative With Respect to Air Velocity

Equation 131

$$\frac{\partial Re}{\partial V} = \frac{\rho L}{\mu} = \frac{(1.123\ \frac{kg}{m^3})(0.45\ m)}{(1.916\ x\ 10^{-5}\ \frac{kg}{m\ s})} = 26375\ \frac{s}{m}$$

Reynolds Number Partial Derivative With Respect to Length

Equation 132

$$\frac{\partial Re}{\partial L} = \frac{\rho V}{\mu} = \frac{(1.123\ \frac{kg}{m^3})(2.74\ \frac{m}{s})}{(1.916\ x\ 10^{-5}\ \frac{kg}{m\ s})} = 160596\ \frac{1}{m}$$

Reynolds Number Partial Derivative With Respect to Dynamic Viscosity

Equation 133

$$\frac{\partial Re}{\partial \mu} = \frac{-\rho VL}{\mu^2} = \frac{-(1.123\ \frac{kg}{m^3})(2.74\ \frac{m}{s})(0.45\ m)}{(1.916\ x\ 10^{-5}\ \frac{kg}{m\ s})^2} = -3771827507\ \frac{m\ s}{kg}$$

The next step required to evaluate the uncertainty in the Reynolds number is to evaluate

the uncertainty in the air density, velocity, dynamic viscosity, and the length of the heat

shield.

Air Density Uncertainty

The temperature uncertainty range, defined in Section "Temperatures" on page 65, of +/-

10% the nominal value was used to determine an air density uncertainty range.

Examining the variation in air density over this temperature range, the "*Engineering*

Toolbox" (Engineering Toolbox, n.d.) shows that the density may vary from $1.247 \frac{kg}{m^3}$ at

low air temperatures to $0.999 \frac{kg}{m^3}$ at high air temperatures. This represents a 11% increase

in air density above the nominal value and a 11% decrease below the nominal value.

Thus, an uncertainty of +/-11% is used in this analysis. Therefore, $\delta\rho$ is equal to 0.124

$\frac{kg}{m^3}$.

Air Velocity Uncertainty

Air velocity is another parameter which varies because of environmental conditions but

also depends greatly on the speed of the driven vehicle; therefore, some assumptions

must be made. Supposing that this vehicle may be at standstill or driven on the highway

and can also be located in an area with calm to stormy conditions, it will be assumed that

the air velocity may vary +/-50% around the nominal value of 2.74 m/s. This results in a

potential variation of air velocity between 1.37 m/s to 4.11 m/s. Thus, δV is equal to 1.37

m/s.

According to the Beaufort scale (Beaufort, 2015), this corresponds to the variation

between light air and a gentle breeze. As discussed before, this may not appear to be

enough variation. However, it must also be considered that there are underbody

components near the front of the vehicle which block the air flow from reaching the rear

underbody components being investigated. Also, the clearance between the upper surface

of the heat shield and the spare tire tub is small and will reduce the airflow to this area.

Heat Shield Length Uncertainty

As discussed in Section "Lengths, Widths, and Diameters" on page 68, the uncertainty in

the length of the heat shield is assumed to be +/- 0.0002 m. Therefore, δL is equal to

0.0002 m.

Dynamic Viscosity Uncertainty

The uncertainty in the dynamic viscosity can be determined by the same approach used

for the air density uncertainty. The air temperature is assumed to range from 285 K to

349 K. Therefore, the dynamic viscosity, read from the "Engineering Toolbox"

(Engineering Toolbox, n.d.), may range between $1.725 \ x \ 10^{-5} \frac{kg}{m \ s}$ to $2.075 \ x \ 10^{-5} \frac{kg}{m \ s}$.

This corresponds to an increase of 11% above the nominal value and a decrease of 8%

below the nominal value. Therefore, an uncertainty of +/- 10% was assumed. Thus, $\delta \mu$ is

equal to $0.1916 \ x \ 10^{-5} \frac{kg}{m \ s}$.

Substituting the partial derivatives and uncertainty values in to the error propagation

equation (Equation 134), an estimate of the uncertainty in the Reynolds number was

found.

Equation 134

δRe

$$= \sqrt{\begin{array}{c}\left(\left(64353\,\frac{m^3}{kg}\right)\left(0.124\,\frac{kg}{m^3}\right)\right)^2 + \left(\left(26375\,\frac{s}{m}\right)\left(1.37\,\frac{m}{s}\right)\right)^2 + \left(\left(160596\,\frac{1}{m}\right)(0.0002\,m)\right)^2 + \\ \left((-3771827507\,\frac{m\,s}{kg})(0.1916\,x\,10^{-5}\,\frac{kg}{m\,s})\right)^2\end{array}}$$

$= 37703$

This value is extremely high; however, it is meant to represent the variation in the Reynolds number over all possible operating conditions and environments. With this consideration, this value seems appropriate.

Referring back to Equation 122, the uncertainty in the Prandtl number and thermal conductivity must be estimated. The uncertainty in the length of the heat shield has already been estimated to calculate the uncertainty in the Reynolds number.

Prandtl Number of Air Uncertainty

The Prandtl number of the air depends on the air temperature. Following the same considerations used for air density and dynamic viscosity, an approximate uncertainty range may be developed. The air temperature range was determined to be 285 K to 349 K. Therefore, from the *"Engineering Toolbox"* (Engineering Toolbox, n.d.) the Prandtl number may vary between 0.713 at low air temperatures to 0.697 at high air temperatures. These values correspond to an increase of 1.4% above the nominal value and a 0.9% decrease below the nominal value. For simplicity, a symmetric uncertainty of +/-1% was applied. Therefore, δPr is equal to 0.00703.

Thermal Conductivity of Air Uncertainty

The thermal conductivity of the air depends on the air temperature. The air temperature

range in this area was assumed to be 285 K to 349 K. Thus, from the *"Engineering*

Toolbox" (Engineering Toolbox, n.d.)*,* the thermal conductivity may vary between

$0.02428 \frac{W}{m\,K}$ and $0.03003 \frac{W}{m\,K}$. This corresponds to an increase of 10% above the nominal

value and a decrease of 11% below the nominal value. For simplicity, a symmetric

uncertainty of +/- 10% was assumed. Therefore, δk is equal to $0.00274 \frac{W}{m\,K}$.

Finally, the partial derivatives and uncertainty values can be substituted into Equation

122 to find the uncertainty in the heat transfer coefficient.

Equation 135

$$\delta h = \sqrt{\left(\frac{\partial h}{\partial Re_L}\delta Re_L\right)^2 + \left(\frac{\partial h}{\partial Pr}\delta Pr\right)^2 + \left(\frac{\partial h}{\partial k}\delta k\right)^2 + \left(\frac{\partial h}{\partial L_c}\delta L_c\right)^2}$$

$$= \sqrt{\begin{array}{l}\left((0.00006686\,\frac{W}{m^2\,K})(37703)\right)^2 + \left(\left(4.582\,\frac{W}{m^2\,K}\right)(0.005624)\right)^2 + \\ \left((352.71\,\frac{1}{m})(0.00274\,\frac{W}{m\,K})\right)^2 + \left(\left(-21.476\,\frac{W}{m^3\,K}\right)(0.0002\,m)\right)^2\end{array}} = 3\,\frac{W}{m^2\,K}$$

Thus, the uncertainty in the heat transfer coefficient for the airflow over the spare tire tub

is +/-3 $\frac{W}{m^2\,K}$. This uncertainty is higher than the uncertainty in the heat transfer coefficient

for the airflow over the upper surface of the heat shield but lower than the uncertainty in

the heat transfer coefficient for the airflow over the lower surface of the heat shield.
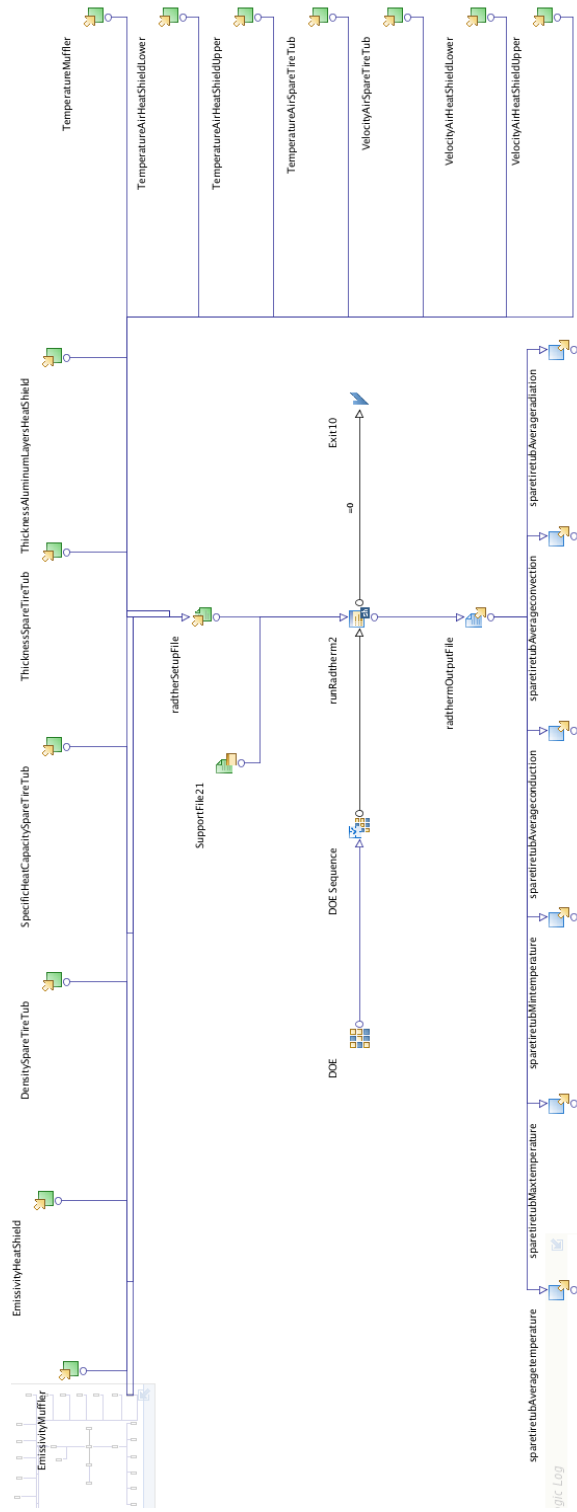
VITA AUCTORIS

NAME: Ashley Lehman

PLACE OF BIRTH: Calgary, AB

YEAR OF BIRTH: 1991

EDUCATION: Vincent Massey Secondary School, Windsor, ON, 2009

                            University of Windsor, B.ASc., Windsor, ON, 2013

                            University of Windsor, M.ASc., Windsor, ON, 2015

                            Politecnico di Torino, Laurea Magistrale, Torino, Italy, 2015